

# **Implementation of Machine Learning Models for Transmission Grid Monitoring and Blackout Prevention.**

Zur Erlangung des akademischen Grades eines

**Doktors der Ingenieurwissenschaften (Dr.-Ing.)**

von der KIT-Fakultät für  
Elektrotechnik und Informationstechnik,  
des Karlsruher Instituts für Technologie (KIT)

genehmigte

**DISSERTATION**

von

**M.Sc. Dejenie Birile Gemed**

geb. in Arsi, Ethiopia

Tag der mündlichen Prüfung:

12.03.2024

Hauptreferent:

Prof. Dr.rer.nat. Wilhelm Stork

Korreferent:

Assoc. Prof. Dr. Kinde Anlay Fante



# Zusammenfassung

Nachhaltige Energie ist eines der wichtigsten Systeme in der modernen Gesellschaft. Um das Ziel einer nachhaltigen Energieversorgung zu erreichen, hat Äthiopien in den letzten Jahrzehnten erhebliche Investitionen in erneuerbare Energiere Ressourcen getätigt, was zu einem erheblichen Anstieg der Stromerzeugung geführt hat. Die wachsende Nachfrage nach Strom und die ungleiche räumliche Verteilung von Erzeugungs- und Verbrauchszentren haben jedoch zu Überlastungen des Stromnetzes und häufigen Stromausfällen geführt. Diese lokalen Ausfälle können zu weitreichenden Stromausfällen im ganzen Land eskalieren. Lösungen hierfür können die Modernisierung und der Bau neuer Leitungen sein, die erhebliche Investitionen erfordern und für eine sich entwickelnde Wirtschaft zusätzlich zu den laufenden großen Erzeugungsprojekten eine Herausforderung darstellen. Ein alternativer Ansatz besteht darin, die Nutzung bestehender Übertragungsleitungen und Infrastrukturen durch den Einsatz von Echtzeit-Überwachungssystemen zu optimieren. In dieser Dissertation wird eine Echtzeit-Überwachung der Stromtragfähigkeit (oder Strombelastbarkeit) vorgestellt, die als Dynamic Line Rating (DLR) bezeichnet wird. DLR beinhaltet die kontinuierliche Überwachung von Freileitungen unter Berücksichtigung der umgebenden Wetterbedingungen. Bei dieser Methode werden die meteorologischen Vorhersagen an die lokalen Wetterbedingungen entlang der Freileitung angepasst. Außerdem kann die Platzierung der Wetterstationen optimiert werden, um Bereiche oder Stellen zu überwachen, an denen die Freileitung ihre höchsten Temperaturen erreichen könnte. Das DLR-System bietet den Vorteil, die Strombelastbarkeit in Notfällen oder bei plötzlichen Lastschwankungen zu erhöhen und damit die Sicherheit des Stromnetzes (z. B. bei Stromausfällen) zu verbessern.

Das DLR nutzt ein maschinelles Lernmodell, um die Übertragungsnetzbetreiber (ÜNB) beim Engpass- und Überlastmanagement in Verbindung mit der Überwachung von Netzfrequenzabweichungen zum Ausgleich von Angebot und Nachfrage zu unterstützen. Dies trägt erheblich zur Verbesserung des Netzbetriebs, der Netzsteuerung und der Netzplanung bei. Die Analyse von Mechanismen zur Risikovermeidung bei der Ampazitätsvorhersage ist für Netzbetreiber jedoch von entscheidender Bedeutung. Die meisten bestehenden DLR-Ampazitätsvorhersagetechniken basierten auf einem deterministischen Vorhersagemechanismus, der fehleranfällig ist. In dieser Dissertation wird die probabilistische DLR-Prognose (Quantile regression forest, QRF) für die OHTL-Ampazitätsprognose verwendet. QRF ist gut geeignet für kurzfristige Vorhersagen wie Minuten bis Stunden bei der Stauüberwachung. Die vorgestellten Rahmenbedingungen für die Bestimmung der DLR auf der Grundlage probabilistischer Prognosen zeigen, dass niedrige Quantile das Risiko für die Entscheidungsträger reduzieren, Überschätzungen vermeiden und Verluste im Vergleich zur deterministischen DLR-Prognose minimieren können.

Die Aufrechterhaltung des Frequenzgleichgewichts ist von entscheidender Bedeutung für eine effektive Überwachung von Leitungsüberlastungen und die Gewährleistung der Sicherheit des Stromnetzes (d. h. die Vermeidung von Stromausfällen). Die Kombination der DLR-Überwachung mit der Vorhersage von Frequenzabweichungen kann Stromunterbrechungen durch die Aufrechterhaltung einer konstanten Stromnachfrage-Stromversorgungskette reduzieren. Abweichungen von der Referenzfrequenz von 50 Hz (wie in Äthiopien) entstehen durch Ungleichgewichte zwischen Stromangebot und -nachfrage aufgrund von Lastschwankungen. Dies erfordert ein leistungsfähiges Echtzeit-Überwachungssystem für den Ausgleich von Angebot und Nachfrage zusätzlich zur Überwachung von Überlastungen in den Übertragungsleitungen. Im äthiopischen Netz wird die Stromerzeugung in der Regel lastabhängig geplant. Bei starken Lastschwankungen und Unwägbarkeiten muss schnell reagiert werden, und es sind rasche Anpassungen erforderlich, um mögliche Stromausfälle und kaskadenartige Blackouts zu verhindern. Um die Frequenzstabilität in einem derart komplexen und unsicheren Umfeld zu gewährleisten, überwachen die ÜNB das System intensiv und setzen

teure Regelreserven ein. Ein besseres Verständnis der Frequenzdynamik, der Leitungsüberlastung und ihrer Wechselwirkung mit dem Ungleichgewicht zwischen Stromnachfrage und -angebot könnte die Kontrollbemühungen erheblich erleichtern und zur Stabilität des Stromsystems beitragen.

In dieser Dissertation wird ein kosteneffizientes drahtloses Sensornetzwerk vorgestellt, das sich für den Einsatz in Äthiopien und anderen Entwicklungsländern eignet. Die Studie konzentriert sich auf die Schaffung energieeffizienter drahtloser Maschennetzwerke unter Verwendung der LoRa-Modulationstechnologie (mit großer Reichweite) von Semtech. Das Netzwerk ist für die Überwachung von Stromnetzinfrastrukturen gedacht, die sich über Dutzende bis Hunderte von Kilometern erstrecken. Das Hauptziel ist es, Daten aus den Netzen zu sammeln, um ein für DLR-Zwecke implementiertes Machine-Learning-Modell zu unterstützen. Die Leistung des vorgeschlagenen Protokolls wird zunächst durch Simulation und dann mit einem Demonstrationsnetz auf dem Universitätsgelände analysiert. Die Ergebnisse zeigen, dass das vorgeschlagene Netzwerk eine ausreichend hohe Paketübertragungsrate erreicht, um die Überwachung von statischen Infrastrukturen über geografische Gebiete hinweg zu ermöglichen.

Schließlich wurde ein webbasiertes Tool zur Visualisierung von Echtzeit- Erzeugungsdaten, Übertragungsnetz- und Lastdaten, Wetterdaten und der voraussichtlichen Kapazität der Übertragungsleitungen entwickelt, sobald das System in Betrieb ist (d. h. sobald es installiert ist und läuft). Dieses Tool führt auch Leistungsfluss- und Transientenanalysen durch, um zu beurteilen, ob vorübergehende Engpässe bewältigt werden können, ohne dass die maximalen Leitertemperaturen überschritten werden. Es schlägt eine Lösung zur Unterstützung eines flexiblen Stromnetzes für einen Kurzzeitplan vor, der eine entscheidende Komponente für die optimale Nutzung der bestehenden Infrastruktur und einen erfolgreichen Energiewendeplan darstellt.



# Abstract

Sustainable energy is one of the most important systems in modern society. To achieve the sustainable energy provision goal, Ethiopia has made significant investments in renewable energy resources in the last decades, resulting in a substantial increase in power generation. However, the growing demand for power consumption and uneven spatial distribution of generation and consumption centers have caused electrical network overloads and frequent power outages. These local outages can potentially escalate into widespread blackouts across the country. Solutions for this may be upgrading and construction of new lines, which require substantial investments, and are challenging for a developing economy in addition to ongoing big generation projects. An alternative approach involves optimizing the use of existing transmission lines and infrastructure through the implementation of real-time monitoring systems. This dissertation introduces a real-time current carrying capacity (or ampacity) monitoring known as dynamic line rating (DLR). DLR involves continuously monitoring overhead transmission lines (OHTLs) by taking into account surrounding weather conditions. The method involves adjusting meteorological forecasts to the local weather conditions along the transmission line. Furthermore, weather station placement can be optimized to monitor areas or spots where the transmission line might reach its highest temperatures. The DLR system offers the benefit of increasing ampacity during emergencies or sudden load fluctuations, thus improving power system security (i.e., blackouts).

DLR utilizes a machine learning model to assist transmission system operators (TSOs) in congestion and overload management in coupling with grid frequency deviation monitoring for supply and demand balancing. This contributes significant improvement to grid operation, control, and planning. However, analyzing

risk avoidance mechanisms in ampacity prediction is essential for grid operators. Most existing DLR ampacity forecasting techniques were based on a deterministic forecasting mechanism, which is prone to errors. In this dissertation, Quantile regression forest (QRF) probabilistic DLR forecasting is used for OHTL ampacity forecasting. QRF is well-suited for short-term predictions like minutes to hours in congestion monitoring. The presented frameworks for determining DLR based on probabilistic forecasts demonstrate that low quantiles can reduce the risk for decision-makers, avoiding overestimation and minimizing losses compared to deterministic DLR forecasting.

Maintaining frequency balance is crucial for effective line congestion monitoring and ensuring power system security (i.e., avoiding blackouts). Combining DLR monitoring with frequency deviation prediction can reduce power interruption by maintaining a constant demand-supply power chain. Deviations from the reference frequency of 50Hz (case in Ethiopia), result from imbalances in power supply and demand due to fluctuations in load patterns. This needs a strong real-time monitoring system for demand-supply balancing in addition to transmission line congestion monitoring. In the Ethiopian grid system, the generation scheduling response is usually load following. During high load variation and contingencies, it needs a fast response and requires rapid adjustments to prevent potential power outages and cascading blackouts. To guarantee frequency stability in such a complex and uncertain environment, TSOs intensively monitor the system and allocate expensive control reserves. An improved understanding of the frequency dynamics, line congestion, and its interaction with power demand-supply imbalance could greatly facilitate control efforts and contribute to power system stability.

This dissertation presented a cost-effective wireless sensor network design suitable for implementation in Ethiopia and other developing nations. The study focuses on creating energy-efficient wireless mesh networks (LPWMNs) utilizing Semtech's LoRa (long-range) modulation technology. The network is intended for monitoring power grid infrastructures that span tens to hundreds of kilometers. The key objective is to gather data from the grids to support a machine-learning model implemented for DLR purposes. The performance of the proposed protocol is analyzed first by simulation and then with a demonstrator network on the

university campus. The findings indicated that the proposed network achieves a sufficiently high packet delivery ratio (PDR) to enable the monitoring of static infrastructures extended over geographical areas.

Lastly, a web-based tool was created to visualize real-time generation data, transmission grid and load data, weather data, and transmission lines predicted capacity once the system is operational (i.e., once installed and running). This tool also conducts power flow and transient analyses to assess whether temporary congestion can be managed without exceeding maximum conductor temperatures. It proposes a solution to support a flexible electrical grid for a short-duration plan, which is a crucial component for the optimal utilization of existing infrastructure and a successful energy transition plan.



# Acknowledgements

First and foremost, I would like to express my heartfelt gratitude and appreciation to my supervisor Prof. Dr.rer.nat. Wilhelm Stork for his continuous supervision and patience throughout all my journey, for his invaluable advice, continuous support, and autonomy he has provided throughout my Ph.D. journey. His immense knowledge and plentiful experience have encouraged me in all the time of my academic research.

Furthermore, I would like to extend my sincere thanks to Assoc. Prof. Kinde Anlay Fante for serving me as the second reviewer for my dissertation. I am truly grateful for his willingness to contribute his expertise to the evaluation process.

I am extremely grateful for the opportunity to work alongside the most incredible colleagues at ITIV. A special mention also to my friends Gabriela, Markus, Con, Toni, Marius, Simon, Nana, Xiang, and Anqi for their cheerful attitude and relaxing moments at ITIV.

I would also like to extend my heartfelt thanks to all my teachers, professors, friends, and individuals in Ethiopia, Germany, and beyond who have been a source of inspiration and imparted valuable lessons to me. Your guidance and support have played a significant role in shaping who I am today.

My gratitude towards my parents knows no bounds. Dear Dad, you were my first source of inspiration and shaped me where I am today. I appreciate your valuing of education. Words fail to express how grateful I am for everything you sacrificed and provided me with.

Finally, I would like to express my gratitude to my wife Addis Dereje, and my kids Fenet Dejenie and Ribka Dejenie. Without their tremendous understanding

and encouragement over the past few years, it would have been impossible for me to complete my study.

# Contents

<b>Zusammenfassung</b> . . . . .	<b>i</b>
<b>Abstract</b> . . . . .	<b>v</b>
<b>Acknowledgements</b> . . . . .	<b>ix</b>
<b>Acronyms and symbols</b> . . . . .	<b>xvii</b>
<b>1 Introduction</b> . . . . .	<b>1</b>
1.1 Background . . . . .	1
1.2 Motivation . . . . .	2
1.3 Research objectives . . . . .	5
1.4 Dissertation structure organization . . . . .	7
<b>2 Developing Countries Grid Infrastructure - The Case of Ethiopia</b> . . . . .	<b>9</b>
2.1 Access to electricity and grid infrastructure in developing countries . . . . .	9
2.2 The Current and future states of Ethiopia's energy sector . . . . .	11
2.3 Transmission and substation network . . . . .	16
2.4 Assessment of distribution grid . . . . .	19
2.5 Ten-year strategic development plan of the government of Ethiopia . . . . .	21
<b>3 Power Systems Stability</b> . . . . .	<b>23</b>
3.1 Traditional Power Systems . . . . .	23
3.2 Principles of active power flow control . . . . .	25
3.3 Stability in Power System . . . . .	27
3.4 Frequency stability . . . . .	28
3.5 Cascading blackout event . . . . .	30

3.6	State-of-art transmission expansion strategies . . . . .	32
3.6.1	AC transmission lines reinforcements . . . . .	33
3.6.2	Flexible AC Transmission Systems devices . . . . .	34
3.6.3	High voltage direct current transmission . . . . .	34
3.6.4	Dynamic line rating application . . . . .	35
3.6.5	Cost comparison and evaluation . . . . .	36
<b>4</b>	<b>Case Study – Power outage economic cost . . . . .</b>	<b>39</b>
4.1	Power outage economic cost for households in Ethiopia . . . . .	40
4.2	Power outage economic cost on manufacturing firms . . . . .	43
4.3	Electricity supply and ease of doing business . . . . .	46
<b>5</b>	<b>Artificial Intelligence in Power Grid Monitoring . . . . .</b>	<b>47</b>
5.1	Theoretical concept of Machine Learning . . . . .	48
5.1.1	Learning Methods . . . . .	49
5.1.2	Over- and under-fitting . . . . .	49
5.1.3	Hyperparameter Optimization . . . . .	51
5.2	Time series forecasting . . . . .	52
5.2.1	Univariate time series forecasting . . . . .	53
5.2.2	Multivariate time series forecasting . . . . .	56
5.3	Data preprocessing and engineering . . . . .	57
5.3.1	Missing value handling . . . . .	57
5.3.2	Feature selection . . . . .	58
5.3.3	Data scaling . . . . .	58
5.3.4	Feature engineering . . . . .	60
5.3.5	Learning phase reconstruction . . . . .	60
5.4	Machine learning algorithm . . . . .	62
5.4.1	Artificial Neural Networks . . . . .	62
5.4.2	Recurrent Neural Networks . . . . .	68
5.4.3	Convolutional Neural Networks . . . . .	72
5.4.4	Quantile Regression Forests . . . . .	73
5.4.5	Explainable machine learning . . . . .	75
5.5	Evaluation Metrics . . . . .	77
5.5.1	Mean absolute percentage error . . . . .	77
5.5.2	Mean absolute error . . . . .	78

---

5.5.3	Root mean squared error . . . . .	78
<b>6</b>	<b>Machine Learning for Grid Frequency Deviation Predictions . . . . .</b>	<b>79</b>
6.1	Frequency variation pattern of Ethiopian grid . . . . .	80
6.2	Feature engineering and data reconstruction . . . . .	82
6.2.1	Data preparation . . . . .	83
6.2.2	Feature engineering . . . . .	83
6.2.3	Data Reconstruction and learning phases . . . . .	85
6.3	Determination of deep network structure . . . . .	86
6.4	Model evaluation for frequency forecasting . . . . .	89
6.5	Model prediction explanations . . . . .	91
<b>7</b>	<b>Dynamic Line Rating for Overhead Transmission Line Monitoring . . . . .</b>	<b>97</b>
7.1	Thermal rating of overhead lines . . . . .	99
7.1.1	Joule heating . . . . .	100
7.1.2	Convective cooling . . . . .	100
7.1.3	Radiative cooling . . . . .	101
7.1.4	Solar heating . . . . .	102
7.1.5	Current-carrying capacity . . . . .	102
7.1.6	Dynamic state . . . . .	104
7.2	State-of-art conductor dynamic line rating . . . . .	105
<b>8</b>	<b>A Methodology for Assessing Risk of Dynamic Line Rating Utilization . . . . .</b>	<b>107</b>
8.1	Probability-based dynamic line rating models . . . . .	108
8.2	Dynamic line rating integration into Ethiopian grid . . . . .	111
8.3	Ampacity forecasting models . . . . .	116
8.3.1	Forecasting methodology . . . . .	116
8.3.2	Weather data forecast models . . . . .	118
8.4	Probabilistic ampacity forecast . . . . .	122
<b>9</b>	<b>Intelligent sensors network for Power Grid Monitoring . . . . .</b>	<b>127</b>
9.1	LPWANs and LoRa technology overview . . . . .	127
9.1.1	LPWAN networks . . . . .	127
9.1.2	LoRa and LoRaWAN technology . . . . .	128

- 9.1.3 LoRaWAN Protocol Architecture . . . . . 129
- 9.1.4 LoRa physical layer . . . . . 131
- 9.2 Wireless mesh networks . . . . . 135
- 9.3 Routing . . . . . 136
  - 9.3.1 Flooding . . . . . 137
  - 9.3.2 Data-centric . . . . . 137
  - 9.3.3 Location-based routing . . . . . 138
  - 9.3.4 Routing Protocol for Low-power and Lossy networks - RPL . 139
- 9.4 Combination of LPWAN and WMN . . . . . 140

**10 Wireless Sensor Network Grid Monitoring for**

**Developing Economies . . . . . 141**

- 10.1 Design requirements and design choices . . . . . 142
  - 10.1.1 Design requirements . . . . . 142
  - 10.1.2 Design choices . . . . . 144
- 10.2 Protocol Overview . . . . . 145
  - 10.2.1 Physical Layer (PHY) . . . . . 145
  - 10.2.2 Medium Access Control (MAC) . . . . . 147
  - 10.2.3 Routing . . . . . 147
  - 10.2.4 Transport and Application layer . . . . . 151
  - 10.2.5 Packet structure . . . . . 152
  - 10.2.6 Time synchronization . . . . . 153
- 10.3 Simulation . . . . . 154
  - 10.3.1 Simulation setup . . . . . 155
  - 10.3.2 Simulation result . . . . . 156
- 10.4 Hardware measurement results . . . . . 158
  - 10.4.1 Central node . . . . . 159
  - 10.4.2 Sensor node . . . . . 160
  - 10.4.3 Range testing . . . . . 161
- 10.5 Performance analysis . . . . . 163
- 10.6 Energy consumption . . . . . 165

**11 Intelligent sensors network for Power Grid Monitoring . . . . 167**

- 11.1 Implementation of a distributed sensor network . . . . . 167
- 11.2 Tools for system monitoring . . . . . 170

<b>12 Summary</b> . . . . .	<b>175</b>
12.1 Summary . . . . .	175
12.2 Outlook . . . . .	177
<b>A Appendix</b> . . . . .	<b>179</b>
A.1 Simulation results . . . . .	179
<b>List of Figures</b> . . . . .	<b>181</b>
<b>List of Tables</b> . . . . .	<b>185</b>
<b>Bibliography</b> . . . . .	<b>187</b>
Journal articles . . . . .	209
Conference contributions . . . . .	209



# Acronyms and symbols

## Acronyms

<b>ACSR</b>	Aluminum Conductor Steel-Reinforced
<b>ANN</b>	Artificial Neural Network
<b>CNN</b>	Convolutional Neural Network
<b>DC</b>	Duty Cycle
<b>DLR</b>	Dynamic Line Rating
<b>EEP</b>	Ethiopian Electric Power
<b>EEU</b>	Ethiopian Electric Utility
<b>FFNN</b>	Feedforward Neural Network
<b>GW</b>	Gateway
<b>GD</b>	Gradient Descent
<b>GoE</b>	Government of Ethiopia
<b>GRU</b>	Gated Recurrent Unit
<b>ITIV</b>	Institute for Information Processing and Technology
<b>KIT</b>	Karlsruhe Institute of Technology
<b>LSTM</b>	Long Short-Term Memory

<b>LPWANs</b>	Low Power Wide Area Networks
<b>MAE</b>	Mean Absolute Error
<b>MAPE</b>	Mean Absolute Percentage Error
<b>MAC</b>	Medium Access Control
<b>NID</b>	Node Identifier
<b>OLM</b>	Overhead Line Monitoring
<b>OLMS</b>	Overhead Line Monitoring System
<b>OHTL</b>	Overhead Transmission Line
<b>PDR</b>	Packet Delivery Ratio
<b>PID</b>	Packet Identifier
<b>PHY</b>	Physical Layer
<b>QRF</b>	Quantile Regression Forest
<b>RSSI</b>	Received Signal Strength Indicator
<b>ReLU</b>	Rectified Linear Unit
<b>RES</b>	Renewable Energy Sources
<b>SNR</b>	Signal-to-noise ratio
<b>SF</b>	Spreading Factor
<b>SGD</b>	Stochastic Gradient Descent
<b>SLR</b>	Static Line Rating
<b>TSOs</b>	Transmission system operators
<b>WMN</b>	Wireless Mesh Network

# 1 Introduction

## 1.1 Background

Ethiopia has undergone a significant transformation in its power generation and infrastructure development, with substantial investments in renewable energy leading to a major increase in power generation over the past two decades. The Government's commitment and substantial budget allocations for infrastructure development [1] have led to a remarkable surge in energy production, with ongoing several projects, particularly from wind, solar, hydro, and geothermal sources. This push aligns with the country's efforts to address the mounting energy requirements due to population growth, economic activities, and urbanization [2,3]. Looking ahead, the socio-economic context and population increase imply a continuous rise in electricity demand. Consequently, assessing the current interconnected transmission system's effectiveness becomes crucial, and strategic expansion plans are necessary to cater to the country's future energy needs.

However, the transmission grid expansion has not kept pace with significant changes in power generation. The power transmission grid is crucial for integrating renewable energy sources, transporting electricity to high power consumption areas, facilitating long-distance interconnection, and cross-border energy exchange, thus ensuring power system security (i.e., avoiding blackouts). As a result, there is a growing consensus that the grid will need reinforcement and partial redesign in the coming years.

## 1.2 Motivation

Despite improvements in power generation, the country still faces frequent power outages due to ever-growing load demand, transmission line trips, and distribution network failures. These outages present significant challenges for the manufacturing sectors, leading to high operation costs, reduced productivity, and heavy reliance on imported goods [4,5]. To cope with the unreliable power supply, many manufacturers continue to depend on backup generators, further impacting their profitability.

With the current electricity generation capacity, it is sufficient for grid-connected load needs. However, the primary cause of persistent power outages is the inadequacy of the transmission and distribution networks at high-power consumption centers. This is especially evident during peak demand hours when the existing infrastructure struggles to handle the growing electricity consumption demand. As a result, transmission line trips and transformer overloading failures take place, resulting in local power outages that are prone to power total blackouts. To resolve this problem, there's a need for real-time monitoring of supply-demand power mismatch, and transmission line congestion monitoring. However, the current Ethiopian grid lacks effective mechanisms to tackle these problems.

Recently, Artificial intelligence-based solutions have been introduced in many areas of applications, including the energy sector. Artificial intelligence-assisted real-time management of active power balancing can offer new opportunities with respect to power system operation and control. While the grid frequency is supposed to be a fixed value, for example, 50 Hz in Ethiopia, however, perturbations always exist due to the aforementioned reasons, and the dynamic stability should be maintained. The instability of grid frequency can lead to a higher cost of operation and energy consumption, which means a higher loss for the electric utility.

Monitoring the grid frequency can serve as an indicator of active power balance, and this dissertation introduces a method for predicting frequency perturbations or deviations in the next few minutes to anticipate power imbalances before

outages occur. As demand for electricity continues to grow steadily and generation patterns fluctuate in response to load changes, the need for vigilant real-time monitoring and proactive active power balancing becomes essential to ensure a stable power supply. This can be achieved by continuously tracking power balance discrepancies and alerting decision-makers to potential issues before they happen, to ensure a dependable power supply and minimize frequency deviations from the nominal setting range.

On another hand, the government of Ethiopia is working extremely on generating renewable energy sources from various sources such as wind, solar, hydro, and geothermal sources to supply the growing demand. This has a burden on the existing grid infrastructure by creating congestion on transmission lines, pushing it closer to its thermal stability limits [6, 7]. In this case, the active power control method or frequency deviation prediction alone cannot solve the congestion problem and expansion measures are essential to achieve economic and demand growth targets. This is particularly important, for thermally limited transmission and distribution networks at high-load centers. However, in Ethiopia, it has been observed that the expansion of transmission lines and distribution network capacity has not kept phase in line with power generation efforts.

The reinforcement or expansion of electricity infrastructure is undoubtedly a capital-intensive project and requires the government of Ethiopia (GoE) to prioritize investment options, as a result, the government focuses more on generation buildup, construction of long-distance high power transmission lines for electricity export to neighboring countries, and access rate expansion. On top of that, the distances between the generation and the main consumption points are far apart, and the construction of new transmission lines is necessary to transport electricity to load centers. This requires significant investments in the transmission network to ensure a reliable and efficient power supply to high-load centers. Therefore, the performance of the existing transmission system facilities must be investigated, and appropriate expansion planning may be carried out to supply the growing demand of the country.

This dissertation proposes an alternative grid optimization solution through the implementation of Overhead Line Monitoring Systems before reinforcement and expansion planning, which enable the determination of the conductor's maximum current carrying capacity, also known as ampacity. This approach allows for real-time monitoring of overhead transmission lines also called Dynamic Line Rating (DLR). DLR serves as a cost-effective and short-term investment solution to prioritize investment options for the government at the same time provide real-time transmission line congestion and ampacity monitoring.

In order to take advantage and the functionalities of DLR, we need new algorithms and methods that will be integrated them into the planning and operation of the power system. DLR integration into existing infrastructure enables the efficient exploitation of overhead transmission lines (OHTL). The current carrying capacity of OHTL varies dynamically based on external parameters such as weather conditions and loading history [8]. In contrast, the design time rating method uses static line rating (SLR) based on worst-case weather conditions such as high ambient temperature, total solar radiation, and low wind speed. The use of SLR often underestimates the actual current-carrying capability of overhead conductors. Therefore, fast assessment of OHTL overloading has significant improvement in real-time operation, congestion monitoring, and dispatch monitoring measures [9–11]. It is essential to couple DLR congestion monitoring with grid frequency deviation predictions and existing centralized active power balancing tasks in Ethiopia's grid system.

The majority of DLR systems currently on the market offer real-time estimations of current carrying capacities. However, the decision-making process heavily relies on single-point forecasts for real-time monitoring. This dissertation proposes a solution to address the limitations of existing approaches, presenting a probabilistic current-carrying forecasting tool for transmission line operators' reluctance toward the use of DLR in their systems.

## 1.3 Research objectives

The close connection between economic growth and energy consumption underscores the need for expanding infrastructure and investing in power transmission networks. To ensure the smooth transmission of electricity from new hydropower plants to areas with high demand and consumption, it is essential to invest in constructing new power lines, enhancing existing transmission and distribution grids, and modernizing networks, especially in major consumption hubs. While the construction of new transmission lines demands substantial financial commitment from the Ethiopian government, there is an opportunity to leverage dynamic line rating, particularly for transmission and distribution grids at high-load centers. This approach involves real-time monitoring to make use of existing infrastructure, which often proves more cost-effective than other options. This dissertation's primary goal is to explore and suggest alternate strategies for optimizing the grid, including techniques like active power balancing and Dynamic Line Rating (DLR). These measures aim to alleviate congestion problems and reduce power blackout problems within the Ethiopian grid. Furthermore, the research aims to examine the economic impact of power outages on individual households and industrial firms in Ethiopia.

**Research Objective 1** To analyze the cost of power outages. (Chapter 4)

The World Bank Enterprise Survey data [12] has been utilized to analyze the economic consequences of power outages on households and industrial firms in Ethiopia. By examining the effects of power interruptions on individual households and industrial entities, it becomes evident that these outages can lead to substantial financial, environmental, and health-related losses. Their impact extends across multiple sectors, impeding economic activities and everyday routines. Therefore, it is crucial to evaluate the expenses associated with power outages in order to identify opportunities for enhancement and potential investment avenues.

**Research Objective 2** To develop machine learning models that improve frequency deviation prediction to monitor active power balancing. (Chapter 6)

In order to accomplish this goal, it is necessary to develop a system that can effectively forecast frequency deviation. To address the research question posed in this dissertation, an investigation was conducted to evaluate various machine learning algorithms and their input features. As part of this exploration, the dataset was transformed into an embedding matrix reconstruction and a distinct analysis was conducted (see Section 5.3.5).

**Research Objective 3** To exploit the capacity of existing overhead transmission lines and reduce the risk of overload/congestion in the Ethiopian power grid. (Chapter 8)

The dissertation aimed to address its research objective by conducting an exploration of the quantile regression forest machine learning algorithm and its input feature set (Section 5.4.4). The dataset was divided into two parts: weather observations and predictions. Subsequently, prediction analysis was performed to gain insights from the data (Section 8.3.2).

DLR can be utilized for the efficient exploitation of overhead transmission lines to integrate more RES into existing infrastructure. However, this action itself may create additional planning and operational challenges, it may create overloading and line congestion due to overestimation problems with the point forecast. To avoid the risk of overestimation, quantiles were employed for DLR forecasting (Chapter 8). A probabilistic DLR scheme to avoid risks arising from weather prediction errors and TSO reluctance toward DLR acceptance.

The resulting system relies on comprehensive data collection [13]. Installing sensors at each electrical tower is ideal, but this option is costly for Ethiopia's economy. Hence, the fourth research objective focuses on exploring the implementation of low-cost wireless sensors for data collection, ensuring a simple deployment process that aligns with the country's economic requirements.

**Research Objective 4** To implement a wireless sensor network for overhead transmission line data collection, while maintaining low-cost investment options. (Chapter 10)

In this dissertation work, a LoRa wireless mesh network (WMN) is proposed for wireless sensors that collect data and communicate with monitoring stations. LoRa WMN requires minimal additional investment for grid operators relative to legacy communication infrastructures. Then ML algorithm translates collected sensor data into the current carrying of OHTL and transformers. This offers potential benefits such as increased capacity utilization, improved safety, minimized investments, and enhanced operational efficiency.

## **1.4 Dissertation structure organization**

This dissertation is structured around its contribution and organized as follows.

Chapter 1 lays the foundations by providing context and a comprehensive understanding of the solution development process. In Chapter 2, the current state of the Ethiopian power sector, energy transition plan, and problems with existing energy infrastructures are presented to establish a basis for understanding the Ethiopian energy landscape. Chapter 3 focuses on defining the electrical power system, describing its traditional structure, discussing the challenges posed by frequency perturbations and dynamics due to the increasing integration of renewable energy sources, exploring the mechanism of blackout occurrence, and presenting state-of-the-art transmission line expansion strategies to reduce blackout (security) risk.

Chapter 4 explores the economic costs of power outages for individual households and industrial firms in Ethiopia. In Chapter 5, the machine learning algorithms utilized in this dissertation are explained in detail. Chapter 6 presents the framework of frequency deviation prediction, highlighting its relevance for enabling system operators to take proactive measures in response to contingencies. The study is based on measurement data of the Ethiopian electric grid network.

Chapter 7 provides a general overview of weather-dependent overhead line operation, including the fundamental equations for calculating current-carrying capacity based on weather conditions and an analysis of the current state-of-the-art in this

field. Chapter 8 focuses on probabilistic dynamic line ratings as a means of reducing the risk associated with overestimation errors. The chapter details the development process of current-carrying capacity forecasting models, including a case study and evaluation of machine learning model performance. The study specifically focuses on overhead transmission lines in the Ethiopian electric grid and emphasizes the positioning of weather stations along the lines.

Chapter 9 highlights the importance of wireless sensor network monitoring for grid management in real time. It reviews existing legacy wireless network varieties and low-power wireless technologies, ultimately presenting the LoRa and LoRaWAN systems. Chapter 10 presented the design architecture and requirements of a LoRa wireless mesh network (WMN) and presented the results of simulation and field test results. The chapter also addressed sensor data logging tool. Chapter 11 addressed the integration and positioning of sensor locations along overhead lines and a web-based data grid monitoring and visualization tool.

Lastly, Chapter 12 provides a final summary and a discussion of the dissertation's achievements. It also outlines the next steps required to ensure ongoing growth and support for the energy transition plan in the coming years.

## **2 Developing Countries Grid Infrastructure - The Case of Ethiopia**

This chapter aims to provide a comprehensive overview of electricity access, grid infrastructures, the challenges and opportunities associated with grid development in the context of developing nations, mainly focusing on the Ethiopian case. Also, it examines the current grid infrastructure of Ethiopia to create a foundation for subsequent chapters. a compressive

### **2.1 Access to electricity and grid infrastructure in developing countries**

The United Nations established the 17 Sustainable Development Goals (SDGs) to provide a global framework for guiding actions from 2015 to 2030 [14]. Among these goals, SDG 7 emphasizes the importance of "Ensuring access to affordable, reliable, sustainable and modern energy for all". The key aspects of sustainability, security, and affordability in energy supply are expected to play a pivotal role in the future development of the power sector. Energy infrastructure is a critical concern for achieving Sustainable Development Goals. Yet, the current global energy infrastructure is significantly unequal, leading to varying levels of access and affordability among nations (Figure 2.1).

Access to energy is fundamental for global development. It serves as the cornerstone for economic progress and is a critical concern for all nations. However, the

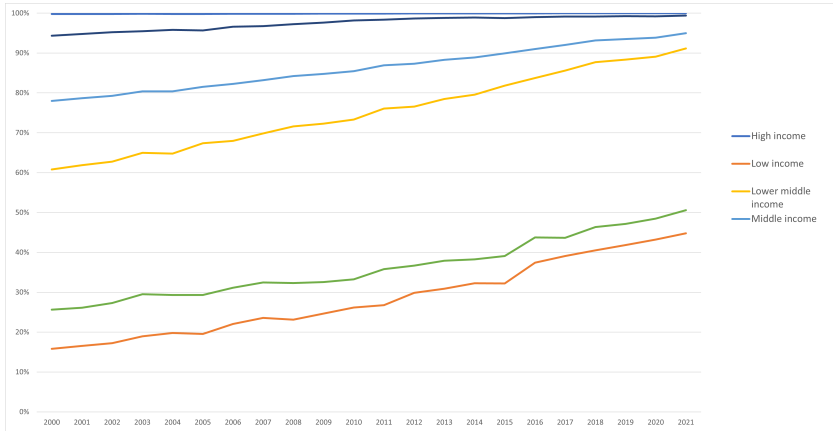


**Figure 2.1:** Significant contrast in electricity accessibility between high-income nations and low-income nations (Data Source: World Bank).

availability of energy resources significantly varies among countries, with approximately two billion people worldwide lacking access to modern energy sources. For those reliant on traditional resources like fuel wood and animal dung, development remains stagnant. Notably, no nation has managed to effectively alleviate poverty without a substantial increase in energy usage, enabling the transition from manual labor to more efficient energy sources.

Energy consumption in developing nations especially Sub-Saharan African countries is highly linked to various social challenges, including poverty reduction, education, healthcare, population growth, employment, communication, urbanization, and gender equality. For instance, using poorly ventilated stoves adversely affects health, while millions spend extensive time gathering firewood and water daily. The absence of electricity leads to inadequate lighting, limited communication, and a lack of access to essential devices and income opportunities. In some cases, mostly in sub-Saharan African countries, urban areas may have a relatively stable power supply, while rural areas might face frequent power outages or have limited access to the grid.

Expanding renewable energies offers a crucial opportunity to address both developmental and social challenges simultaneously due to the increased flexibility and grid responsiveness. In recent years, there has been a significant development of alternative energy technologies, both in terms of performance and cost reduction [15]. Some developing countries are exploring renewable grid generation technologies to improve the efficiency, reliability, and sustainability of their electricity grids. Modernizing grid infrastructure improves energy efficiency, better demand management, reduces losses in transmission and distribution, and enhances the integration of renewable energy sources. These benefits align with the sustainable development objectives of many developing nations.

However, the development of on-grid renewable energy resources demands grid infrastructure expansion. Many sub-Saharan African countries face challenges in expanding and maintaining their existing electricity grids due to factors such as insufficient financial resources, technical constraints, rapid population growth, and rapid urbanization.

Therefore, to tackle financial constraints in the development of renewable energies and smart grid initiatives, effective utilization of the existing grid structure measures before reinforcement has a significant advantage. Effective utilization of existing grid infrastructure is the main core of this dissertation focusing on Ethiopian grid infrastructures. It explores digital communication technologies to enhance grid efficiency, reliability, and resilience, addressing some of the challenges faced by traditional grids.

## **2.2 The Current and future states of Ethiopia's energy sector**

Ethiopia is a large country in the Horn of Africa (see Figure 2.2 [16]), occupying a high plateau characterized by mountain ranges that are separated by the East African rift valley. The country's diverse topography leads to significant variations in climate ranging from desert regions to tropical forests and moderate-temperature

zones, soil types, natural vegetation, and the distribution of settlements. Ethiopia, the second most populous country in Africa, has a multi-ethnic population of approximately 120.3 million people, the majority, about 77% in 2022 [17], reside in rural areas. Projections estimate that the population will reach 130 million by 2030. Despite the predominantly rural population, there is a noticeable trend of urbanization [18], with an annual growth rate of 4.79% [17] and is expected to rise rapidly [19]. Urban areas, particularly the capital city of Addis Ababa and the surrounding areas of Oromia state, are growing more due to economic growth [2,3, 18]. Urbanization is associated with higher energy consumption and can be an indicator of energy inefficiency [20].

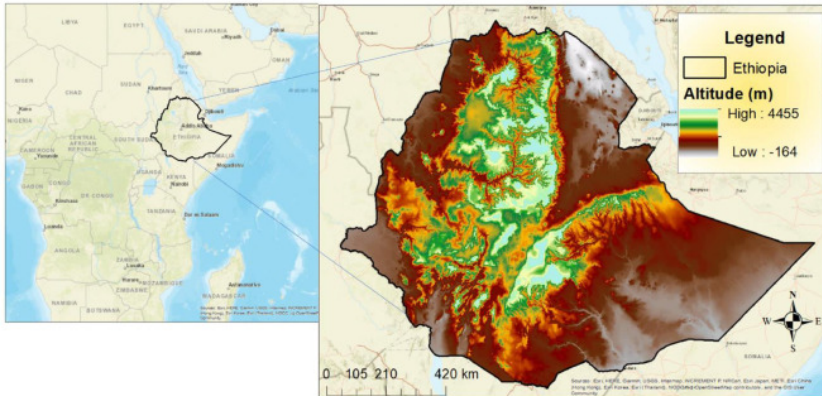


**Figure 2.2:** Geographical location of Ethiopia and study area [16].

Ethiopia has experienced an average annual economic growth of 10.6% for ten consecutive years from 2005/06 to 2015/16, almost double compared to the regional average growth of 5.4% [21]. There are changes in lifestyles and industries, such as increased urbanization and industrialization [22]. As of 2022, Ethiopia’s gross domestic product (GDP) amounted to \$111.27 billion [17]. Figure 2.3 depicts the evolution of Ethiopia’s GDP in recent years [23]. From 2009 to 2011, the growth was stagnant due to a decline in the international balance of payments. However, it rebounded, and in 2012, the growth rate reached approximately 36%.

Subsequently, the GDP continued to rise, with growth rates ranging from approximately 10% to 17%. However, there was a slight slowdown in growth from 2020 to 2022 attributed to the impact of the COVID-19 pandemic and a civil war. As a result, GDP growth fell to 6.1% in 2022 but remained above East Africa's average (4.4% in 2022). Inflation rose to 34% in 2022 from 26.6% in 2021. Both growth and inflation were adversely impacted by internal conflict, drought, and the effects of Russia's invasion of Ukraine on commodity prices [24].

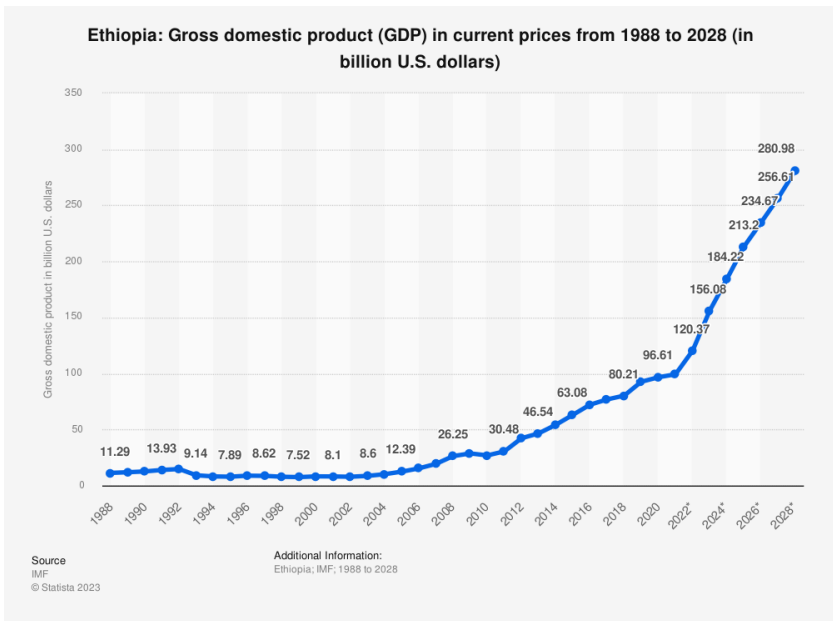


**Figure 2.3:** Trends of Ethiopia's GDP growth from 1988 to 2028: Source, IMF 2023 [23].

Ethiopia is rich in natural resources, including abundant sunlight, water, and wind, which present a potential for renewable energy generation sources. There is significant untapped potential from hydropower and wind power generation. The estimated hydropower potential is around 45 GW, but currently, only 5% of this potential is being exploited. Similarly, the estimated wind potential is

1,350 GW, but the actual utilization is much lower, with less than 1% being harnessed. Additionally, Ethiopia possesses some reserves of natural gas, coal, and biomass [25].

In Ethiopia, energy is primarily sourced from three main categories: biomass, petroleum, and electricity. Among these, only petroleum products are imported. In 2018, the energy supply breakdown showed that biomass contributed 87% of the total, petroleum products made up 10%, coal 1%, and electricity accounted for 2% of the supply (see Figure 2.4 (a)). The sectors consuming the most energy were households, accounting for 88%, and transportation, responsible for 9% of the total energy consumption. The industry and construction sectors combined consumed 2%, followed by the commercial sector with 1% (see Figure 2.4 (b)).

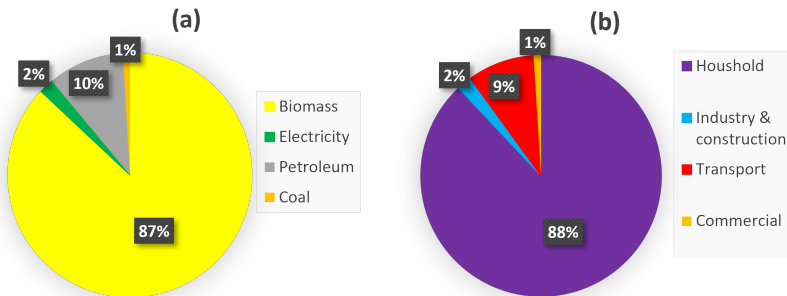


**Figure 2.4:** Energy supply and consumption in Ethiopia by type and sector: (a) Energy supply by type in 2018. (b) Energy consumption by sector in 2018 [26].

The majority of the population in rural areas heavily depends on traditional biomass energy for cooking and heating. Urban areas have almost achieved universal access to electricity, with 96% of the population having access, compared to only 27% in rural regions. The total electricity access rate stands at approximately 47%, with a per capita consumption of 143 kWh [27]. Ethiopia's electricity demand is rising due to factors such as population growth, urbanization, energy export plans, and improving living standards. This increasing demand, coupled with the power system's poor performance, has led to electricity supply insecurity. This low level of electricity consumption in Ethiopia indicates the need for

further development and expansion of energy infrastructure to meet the increasing demands of the population.

In the past decade, Ethiopia's electricity sector has also experienced significant progress. From 2005 to 2022, the coverage of electricity services expanded from 648 towns and rural villages to 7,959, and the number of electricity customers rose from 800,000 to over 4.3 million [28]. Ethiopia's electricity access for 2020 was 51.09%, a 3.03% increase from 2019 [29], with per capita electricity consumption of 118 kWh, where the average for Africa is at 500 kWh and for Germany is 3,113 kWh [30]. The electricity demand is expected to grow at a rate of 13.7% annually, reaching 62,000 GWh by 2030 compared to 13,800 GWh in 2021 [24]. To meet this increasing demand, Ethiopia has plans to enhance its generation capacity to 17.1 GW by 2030 [31]. The rapid growth in the electricity sector has presented significant challenges for the Ethiopian utilities<sup>1</sup>, the utility responsible for power generation and transmission. These constraints can be attributed to several factors:

- The expansion of transmission and distribution infrastructure has not kept up with the increasing demand and generation capacity, even though the government has invested heavily in the construction of new power generation.
- Efforts to increase connectivity and access to electricity services have been inadequate.
- The implementation demands of numerous large-scale projects and operational challenges have strained the resources and capabilities of utilities.

---

<sup>1</sup> In Ethiopia, the electric power utility is solely governed by two state-owned electricity enterprises: (1) the Ethiopian Electric Power Company (EEP), responsible for building generation plants, power transmission and substation, wholesale of electricity, compliance research, design, and survey work; and (2) the Ethiopian Electric Utility (EEU), responsible for power distribution, sales and implementation of the Universal Electricity Access Program (UEAP). In addition, the GoE established a federal electricity sector regulator, the Ethiopian Energy Authority (EEA) [31].

- The low electricity tariff, despite recent revisions, poses a significant constraint to scaling up electricity access. The flat tariff rate, currently at 2.1240 ETB (or US\$0.039/kWh), is one of the lowest in the world [28].

Addressing these challenges often requires a multi-faceted approach that involves policy reforms, investment in infrastructure, improvements in regulatory frameworks, and efforts to diversify and modernize the energy mix. The detailed electricity development plan of the government of Ethiopia was discussed in Section 2.5. Sustainable and reliable electricity is crucial for economic development, and overcoming these obstacles can significantly benefit businesses and the overall development of a country.

## 2.3 Transmission and substation network

Ethiopia's electricity generation is predominantly green electricity, with 90.70% of its installed generation capacity being from hydropower, 6.61% from wind, 2.03% from diesel, 0.15% from biomass and 0.51% from geothermal sources [31]. Figure 2.5 illustrates installed energy share by sources. Geothermal, wind energy, and hydropower are predicted to become increasingly important components of the country's energy mix in the near future [22].

The country has made substantial investments, resulting in a current power production capacity of over 5,330 MW. This capacity is expected to exceed 10,000 MW once the Grand Ethiopian Renaissance Dam (GERD)<sup>2</sup> is completed.

Ethiopian Electric Power (EEP) currently manages an interconnected system consisting of hydroelectric, wind, geothermal, and solid waste power plants [31]. The main high voltage levels of the power transmission lines in the EEP grid are 500 KV, 400 KV, 230 KV, and 132 KV. Among them, the 400 KV and 230 KV

---

<sup>2</sup> The Grand Ethiopian Renaissance Dam (GERD), formerly known as the Millennium Dam, is a 5.15GW hydropower dam that Ethiopia is constructing on the Abbay/Blue Nile River. Ethiopia generates 86% of the Nile flow, with a total average annual flow of 77 billion cubic meters.

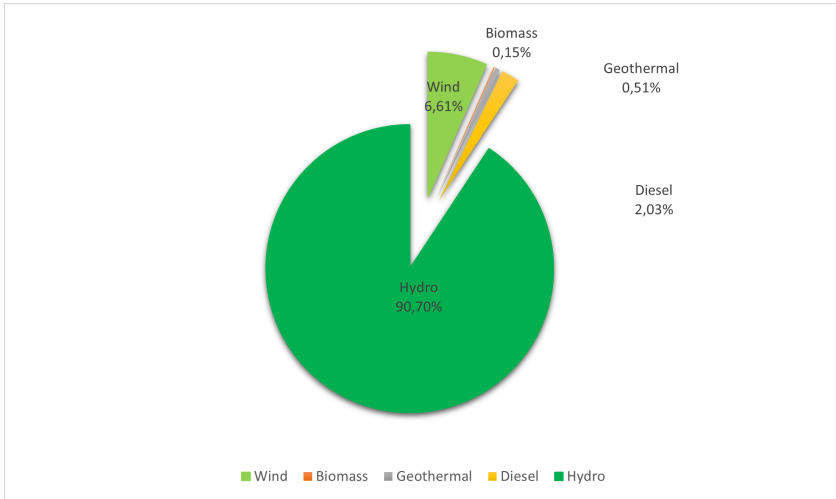


**Figure 2.5:** Ethiopia's current share of installed capacity by sources (%).

transmission lines are the most important for the power flows and interconnecting seven regional power systems. The transmission network is extended to Djibouti on the East and the Republic of Sudan to the North West [31].

A geographic interconnected diagram of the high voltage network of the Ethiopian power grid is shown in Figure 2.6, consisting of 19 sets of 400KV and 34 sets of 230KV transformers, 19 transmission lines with 400KV and 47 with 230KV. These power systems are dynamic, with network topology frequently changing with load demand. The National Load Dispatch Center (NLDC) has the jurisdiction to control the high voltage substations, transmission lines, and power plants. Currently, the total installed generation capacity is over 5,330 MW, and the peak load is now up to 4324.3 MW [32], which is slightly equivalent to electricity consumption by the German Baden-Württemberg state.

Recently, the power infrastructure in Ethiopia has been facing significant challenges due to its scattered nature and the growing demand for electricity in both domestic and industrial sectors. These challenges have made the system highly susceptible to even minor disruptions, resulting in frequent power outages and

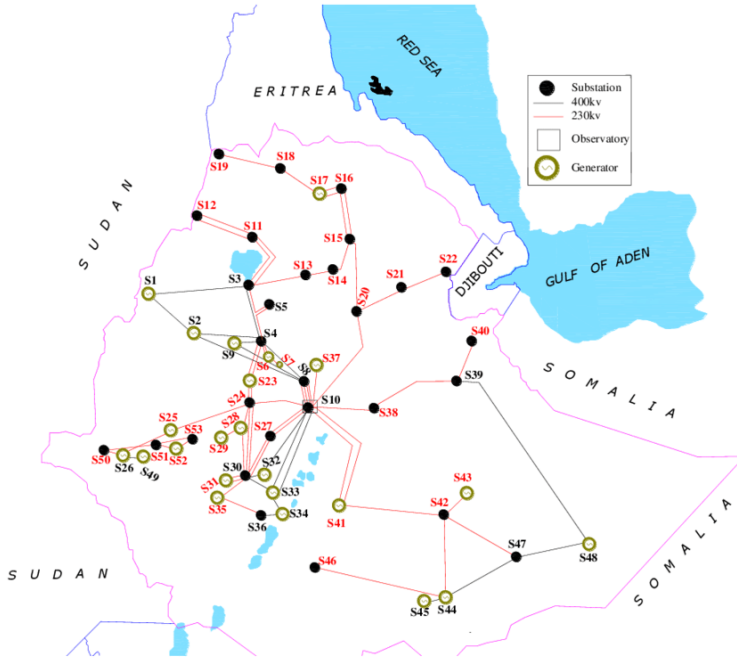


**Figure 2.6:** Geographical interconnection diagram of the dual voltage of Ethiopia power grid [33].

sometimes partial or complete blackouts. These effects have severe societal and economic consequences, threatening the nation’s industrial and socioeconomic development and hindering the achievement of short and long-term development plans. The transmission and distribution networks are troubled by issues such as aging infrastructure, insufficient maintenance, and inadequate investment for the construction of new lines. As a result, the quality of the power supply is compromised, leading to an average of 42 local power outages per month for typical businesses, primarily caused by cable disconnections and circuit breaker problems [4, 5, 34, 35].

## 2.4 Assessment of distribution grid

The distribution system is the largest portion of the network in the electrical power system. It can be defined as the part of a power system that distributes power to various customers in ready-to-use form at their place of consumption. Hence, utilities have to ensure reliable and efficient cost-effective service, while providing service voltages and power quality within the specified range.

The Ethiopian distribution grid is mostly configured in radials, except the main distribution circuit in Addis Ababa, the capital city. A radial system is arranged like a tree, where each end-user has one source of supply and breaks and does not fulfill the N-1 contingency criteria. In a radial system, long distribution feeders experience voltage drop (power factor distortion) requiring capacitors or voltage regulators to be installed.

Furthermore, the distribution grids (medium voltage (MV) and low voltage (LV) networks) lack a real-time monitoring system, due to a lack of sensors and communication systems. Supervisory Control and Data Acquisition (SCADA) is only limited to the transmission network and has limitations in providing real-time access to the distribution system. The facilities management system implemented by EEU has also been limited to load assessment and voltage evaluations at the distribution feeders level and lacks real-time monitoring of distribution transformers and secondary distribution grids. The detection of faults in feeder lines is limited due to the allocation of monitoring points or Remote terminal units (RTUs) locations in the network and is too shallow to detect problems in local or customer premises. As a result, utility providers rely on customer complaints or maintenance inspections to identify power outages or equipment failures [36].

Table 2.1 presents an example of equipment survey assessment results for substations as measured by the facilities management system implemented by EEU. This sample survey showed from the entire Addis Ababa distribution network 53 percent of medium voltage (MV) feeders, 58 percent of distribution transformers, and 82 percent of low voltage (LV) feeders are experiencing overloading [37].

**Table 2.1:** An example of distribution network condition assessment result.

Substation	Feeder	Voltage Issues	Loading issue (% of conductor rating)
Addis Alem	ALM-15-01	yes	-
Addis Alem	ALM-15-02	yes	-
Addis Center	ADC-15-04	yes	179.6
Addis Center	ADC-15-07	yes	173.8
Addis Center	ADC-15-10	x	181.1

To analyze the current state of the distribution network in more detail, the Japan International Cooperation Agency (JICA) study team conducted a one-week field survey study with detailed load measurements [37], shown in Figure 2.7.



**Figure 2.7:** An example of transformer loading measurement result (Transformer rated capacity: 200kVA).

The findings, summarized in Table 2.2, reveal that many transformers are consistently overloaded, with a maximum utilization rate of 151% and utilization rates nearing overload levels. Transformers with a relatively low utilization ratio of around 40% are those that have recently undergone capacity increases through the grid rehabilitation program.

**Table 2.2:** Summary of detailed load assessment result.

Utilization rate	Measurement result
Maximum	151 %
Minimum	42 %
Average	85 %
Over 100 %	6 units
Over 80 %	8 units

To mitigate the risks associated with distribution transformer overload, it is crucial to implement an intelligent monitoring system with a cost-effective solution that fits the economy. Proactive measures must be taken to prevent transformer failures due to overload, as their consequences can be severe and catastrophic for businesses and the overall power supply.

One work in this dissertation proposed a monitored substation and distributed transformer condition status by utilizing distributed sensor data and weather information [191]. This framework can enable the implementation of predictive maintenance and repair plans before any issues occur, thus helping to prevent eventual breakdowns and financial losses.

## 2.5 Ten-year strategic development plan of the government of Ethiopia

In 2021, the Government of Ethiopia (GoE) revealed its 10-Year Development Plan [38] that spans from 2020 to 2030, replacing the prior Growth and Transformation plans (I and II)<sup>3</sup>. The previous plans aimed at restructuring the economy and society to elevate Ethiopia to a middle-income status by 2025. The new 10-Year

<sup>3</sup> GTP I from 2011-2015 and GTP II from 2016-2020 were adopted by GoE II. They are a comprehensive strategy to improve the economic condition of Ethiopia and include energy and renewable energy targets guiding the country's development.

Plan aspires for Ethiopia to emerge as ‘Africa’s Beacon of Prosperity,’ placing significant emphasis on bolstering the economic and infrastructure sectors. Within its energy development objectives, the plan targets a substantial increase in the electricity customer base from 5.8 million<sup>4</sup> to 24.3 million, an increase in power service accessibility from 33% to 96%, and a reduction in electricity loss. The overall aim of the energy development strategy is to offer equitable, affordable, and dependable electricity access while expanding high-quality energy infrastructure.

Through these national development programs, it is planned to increase electricity service coverage from 44% to 100%, increase power generating capacity from 4,180 MW to 17,208 MW, build distribution lines from 16,018 km to 21,728 km, and ultimately increase annual per capita electricity consumption from 86 kWh to 1,269 kWh. This means that Ethiopia needs to significantly increase its power production, transmission, and distribution capacity to drive its expanding economy and provide access to electricity to its rural people.

---

<sup>4</sup> As indicated in the GoE’s Ten Year Strategy Document. EEU reports 4.3 million registered metered connections. The difference might be due to a mix of meter sharing, off-grid clients, and unregistered EEU customers.

## 3 Power Systems Stability

This chapter aims to explore the distinctions between the traditional electrical power system and the modern renewable environmentally-friendly grid system. It focuses on the challenges associated with the integration of more renewable energy sources (RES) into the existing system. The chapter begins by providing a theoretical definition of the electrical network, analyzing stability in power systems and frequency dynamics when contingencies occur. It then delves into an explanation of power blackout mechanisms, followed by a comprehensive review of congestion management measures, specifically outage management.

### 3.1 Traditional Power Systems

Electric power is generated at generating stations and distributed to consumers through an interconnected network of transmission and distribution lines known as grids. Conventional power systems, also called centralized power systems, rely on large power plants that generate electricity and transmit it through this network. The conventional power system design is based on the concept of "economies of scale," where a few large-scale generators transmit power through bulk transmission systems to substations. The voltage is reduced at the substations to a safer level for residential, commercial, and industrial areas (illustrated in Figure 3.1). These power plants primarily use fossil fuels, such as coal, natural gas, and oil, and are situated in centralized locations.

The advantage of conventional power systems is that they can generate significant amounts of electricity and can be easily scaled up to meet growing demand.

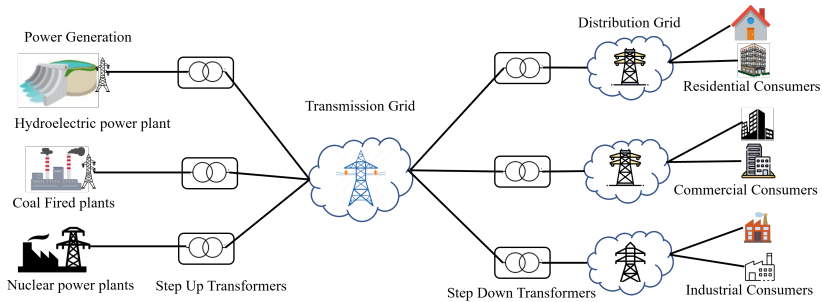


**Figure 3.1:** A high-level structure of modern power grid.

However, their drawbacks include their reliance on finite fossil fuel resources, which contribute to pollution and climate change. Moreover, these systems are susceptible to natural disasters and power outages that can disrupt the entire grid.

Global events profoundly impact fossil fuel and nuclear power plants, which are costly and detrimental to the environment. As a solution, an energy transition is occurring worldwide, shifting away from fossil fuel-based thermal power plants towards renewable energy sources [39]. Solar, wind, hydro, and geothermal energy are considered sustainable options as they do not produce emissions. Power system networks are undergoing substantial infrastructural changes to optimize the utilization of renewable energy. These changes involve installing new transmission lines, integrating flexible loads, and promoting self-sufficiency through microgrid implementation [40]. The rise in renewable energy injections from distant sources to high-load centers has led to more congestion in the transmission grid. Given the high cost of building new transmission lines, it's crucial to explore alternative solutions [41].

A significant challenge for utilities is managing transmission constraints and bottlenecks [42]. The increase in congestion and loop flows within transmission systems compromises system reliability, raises energy costs, and limits the efficient use of existing infrastructure [43, 44]. Active power flow control becomes crucial for grid optimization. The control of real power flow is essential for system operation and supporting electricity markets, as customers purchase real

power (megawatts and MW-Hrs). Congested networks not only affect system reliability but also restrict cost-effective power supply from low-cost generators to interested customers. Additionally, uncontrolled loop flows can cause overloads on existing lines, even if neighboring lines have capacity. To address these issues, cost-effective series VAR solutions are needed to modify power line impedance and voltage angles for power flow control. While traditional series reactive compensation is often limited to long transmission lines due to cost and complexity, dynamic thermal line rating (DLR) implementation emerges as a potential solution (see Chapters 7 and 8), especially for short-distance transmission lines near high-load centers [192].

## 3.2 Principles of active power flow control

Active power flow control strategies are designed to efficiently manage and enhance the flow of real power within a transmission network. By dynamically adjusting the behavior of devices and components, these strategies work to alleviate congestion issues and improve the overall reliability of the power system. Active power flow control involves the active management and regulation of real power flow within an electrical power system, ensuring its effectiveness and dependability [45]. To provide a visual representation of this concept, consider the simplified equivalent circuit for a two-bus transmission system, which is depicted in Figure 3.2.

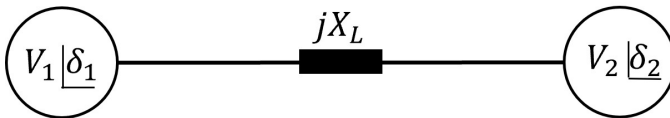


**Figure 3.2:** Active and reactive power transfer between a two-bus transmission system.

The active power flow ( $P$ ) and reactive power flow ( $Q$ ) through a transmission line that links two voltage buses are primarily influenced by the magnitudes of

the voltages ( $V_1$  and  $V_2$ ) at the buses and the phase angle difference  $\delta = \delta_1 - \delta_2$  between these voltages.

$$P = \frac{V_1 V_2 \sin \delta}{X_L} \quad (3.1)$$

$$Q = \frac{V_1^2 - V_1 V_2 \cos \delta}{X_L} \quad (3.2)$$

where  $X_L$  is the impedance of the line, assumed to be purely inductive.

For controlling the real power flow, adjustments need to be made to either the angle  $\delta$  or the line impedance  $X_L$ . Changing the angle  $\delta$  or line impedance  $X_L$  can be achieved through the deployment of a phase-shifting transformer or a series compensator that modifies the effective reactive impedance ( $X_L$ ) of the line. This adjustment enables the manipulation of real power flow between the two buses. The change in impedance is realized by inserting a passive capacitive or inductive element into the line. Another option is to employ a static inverter, which facilitates the implementation of a controllable active element that doesn't introduce losses, such as a negative or positive inductor, or a synchronous fundamental voltage that is orthogonal to the line current [46, 47].

Active power flow control and congestion monitoring are essential aspects of managing modern power systems efficiently and ensuring the reliable delivery of electricity. They involve strategies and technologies aimed at preventing or mitigating congestion issues and maintaining the optimal operation of the power grid.

Congestion in a power system occurs when the available transmission capacity is insufficient to accommodate the desired power flows between different regions or nodes. It can lead to increased costs, reduced system stability, and potential reliability issues [6]. Congestion monitoring involves the continuous assessment and analysis of the power grid to identify areas where transmission lines are heavily loaded or where power flows are causing bottlenecks. More detailed methods are explained in Section 3.6.

In combination, congestion monitoring and active power flow control enable power system operators to proactively address congestion issues, optimize power flows, enhance grid stability, and ensure efficient energy delivery. These strategies are becoming increasingly critical with the integration of renewable energy sources and the growing complexity of modern power systems. In a renewable-dominated power system, the interaction between renewable energy resources and the existing grid differs significantly from conventional plants due to their unique physical characteristics and power electronics-based interface. This situation increases significant concerns for grid operators regarding power stability, and thermal limit issues [48].

### **3.3 Stability in Power System**

Stability in power systems refers to the ability of the power system to maintain a balanced state under different operating conditions. The stability of the power system is affected by various factors such as load demand, generation capacity, transmission line losses, voltage, and frequency control, among others [49].

The stability of a power system is crucial due to its nonlinearity, and the changing environmental conditions. Disconnecting or isolating a critical component of the system can have significant consequences on the system's overall structure. When a fault occurs, it can propagate to other devices in the system, resulting in disturbances in power flow, network voltage, and machine rotor speeds. This impact becomes more severe if the fault affects a critical component. Power system stability can be classified as follows depending upon the severity of disturbance [50],

- Steady-state stability is the ability of the power system to maintain a stable operating condition under normal load demand and generation capacity.
- Transient stability is the ability of the power system to recover from a disturbance such as a fault, generator outage, or a sudden change in load demand.

- Dynamic stability is the ability of the power system to maintain a stable operating condition under small disturbances, such as changes in load or generation. Dynamic stability is the main concern of this dissertation.

A failure of a critical component alters power flow in the power grid, which is leading to changes in network voltage and machine rotor speeds. The voltage variations in turn trigger the voltage regulation systems of generators and transmission lines, while the rotor speed variations activate the prime mover, which leads to frequency variations. The loads in the power system, depending on their characteristics, are affected by voltage and frequency variations, and the protection devices for these loads may also be triggered. The cascading effect of these protection devices can weaken the system, increasing the risk of the power system entering a volatile state that could ultimately result in a total system collapse [51].

Addressing the grid voltage stability problem requires a comprehensive approach. It involves increasing power generation capacity to meet the growing demand and upgrading and modernizing the transmission and distribution infrastructure. Frequency change perturbations and congestion monitoring are related to real-time monitoring, so addressing these via some sensors' actions and artificial intelligence modeling is crucial. Thus, the main focus of this dissertation is more on frequency stability monitoring and congestion management based on existing infrastructure in the Ethiopian power grid system.

## 3.4 Frequency stability

Frequency stability is the system's ability to maintain the grid frequency within an acceptable range according to operational guidelines. This is crucial for ensuring the operational security of the power system. Deviations in frequency outside the specified range can trigger protective measures, such as under-frequency load-shedding devices, which are designed to prevent cascading failures and potential blackouts [52]. Significant frequency deviations typically occur due to the loss of a large generator or load, or a fault in a transmission line connecting a major load

area. These events disrupt the balance between power generation and demand in the system.

A simplified equation that governs the frequency dynamics of an electrical grid is given by [53]:

$$\frac{df_{grid}}{dt} = \frac{P_{gen} - P_L}{M} = \frac{\Delta P}{M} \quad (3.3)$$

Where  $f_{grid}$  represents the synchronous frequency,  $\frac{df_{grid}}{dt}$  represents the rate of change of frequency (RoCOF), and  $M$  denotes the effective inertia constant of the system.  $M$  is a measure of the combined normalized inertia constant of all rotation-based generators. Equation (3.3) illustrates the inverse relationship between RoCOF and  $M$ .

The frequency dynamics of the power grid reflect the balance of supply and demand of the power grid. An excess of generation increases the frequency, and a shortage of generation reduces the frequency value. To keep the power grid stable, the frequency must be controlled and maintained at a nominal frequency [51]. However, it is not easy to maintain a set frequency across an entire power-grid system; systems vary in size and structure, energy sources such as wind or photo-voltaic generators [54, 55] can be unpredictable, and dispatch of electrical energy and market activity [56, 57] also have an influence on overall dynamics. Unlike synchronous generators in conventional plants, which contribute inertia to the system, wind or photo-voltaic generators lack inherent inertia capabilities [52]. As a result of reduced synchronous inertia, frequency events exhibit larger frequency deviations and higher RoCOF in modern renewable energy-dominated generations. With the projected increase in the replacement of conventional units with wind or photo-voltaic generators, the severity of these frequency events is expected to worsen and further complicate load-supply balancing and frequency control [58].

## 3.5 Cascading blackout event

A power outage refers to the temporary or prolonged loss of electricity in a specific area, ranging from a single building to an entire city. Thus, a complete loss of electricity in the entire country or part of the country is known as a blackout, while minor disruption in a specific area is referred to as a power outage. Both blackouts and outages have significant impacts on various sectors, including industries, households, and commercial establishments, leading to the inability to perform daily activities and shortages of products. A failure of one component may lead to other components and a cascade of this event is called cascading outage, finally total blackout will take place [59]. Blackouts or cascading outages are costly events that threaten the integrity of electric energy systems.

Cascading failure triggered by a severe fault leads to out-of-step tripping, line outages, and the loss of synchronism. Actually, a blackout happens when a severe fault in the power system causes one or more groups of coherent generators to be out-of-step. These events will continue until the blackout has spread to a large part of the network. In some cases, the progression of blackouts after the occurrence of initiating events could follow two steps, steady-state progression, and transient progression [60]. Figure 3.3 clearly describes these phases, which are precondition, initiating events, cascading events, final state, and restoration. Among these five phases, cascade events can be further divided into three phases in the process of some blackouts: steady-state progression, triggering events, and high-speed cascade. After the initiating event takes place, the steady-state progression phase will take a longer time before entering the high-speed cascade stage. So, it is possible to take remedial action during the steady-state progression phase to prevent a cascading blackout event with proper real-time monitoring applications [61].

To prevent catastrophic outcomes, power systems are designed to withstand single or double failure events, known as N-1 or N-2 criteria. However, human errors or hidden failures can extend outage propagation, causing further cascading. Such outages cause the redistribution of power flows, causing other components to

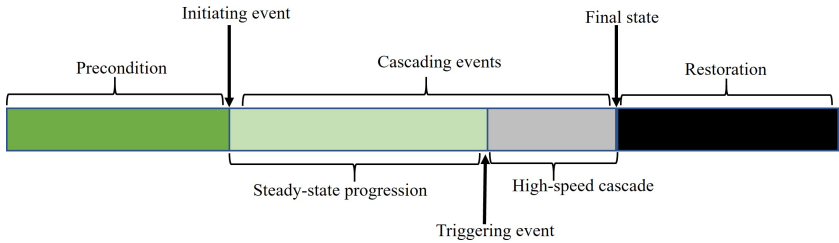


**Figure 3.3:** Power grid cascading outage development phases.

become overloaded. As seen in Figure 3.4 voltage collapse, frequency collapse, cascading overload, system separation, and loss of synchronism are the five types of faults that can lead to blackouts [61, 62].

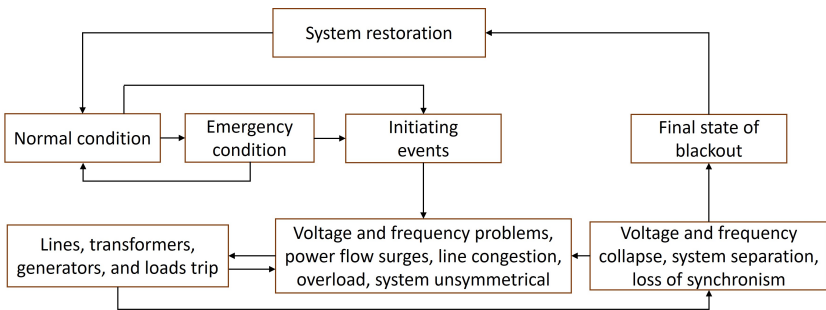


**Figure 3.4:** Mechanism of blackouts [61]

Voltage collapse occurs when there is insufficient reactive power reserve, leading to a decline in voltage, tripping of equipment, and eventual blackout. Frequency collapse happens when there is an imbalance between production and consumption, causing a collapse in frequency. Congestion or cascading overload occurs when lines become heavily congested, leading to redistributed power flow, overloading of other lines, and potential blackouts. System separation occurs when critical lines or transformers are lost, resulting in isolated subsystems and potential voltage or frequency collapse. Loss of synchronism or islanding occurs when two

interconnected power systems experience an imbalance, leading to power oscillations and possible system splitting. Preventing blackouts involves measures such as using FACTS devices, reactive resources, and under-frequency load shedding.

One of the key solutions to mitigating blackouts involves predicting system response and identifying appropriate remedial actions using machine learning methods. Machine learning techniques, specifically frequency prediction, show potential in anticipating frequency deviations in the power grid. Utilizing fast simulation and AI predictions can enable real-time simulations that look ahead, allowing the grid to self-adjust and perform what-if analyses to avoid disturbances. This self-adjusting of the grid would aid in advance repairing measures and/or adaptation to new conditions following an outage. Grid control centers with AI algorithms would then run failure scenarios to determine the optimal corrective response, which operators would approve and implement. If the line still failed, sensors within the network would detect voltage/frequency fluctuations and communicate this information to nearby substation processors. These processors would reroute power through alternative sections of the grid. As a result, customers in the wider area might experience only a brief flicker of lights or may not even be aware of any problem at all.

## **3.6 State-of-art transmission expansion strategies**

The aging power system infrastructure and the growing integration of fluctuating energy sources call for substantial investments in power system infrastructure. This review discusses various expansion measures, focusing on transmission technologies used to strengthen and expand the transmission network. The primary objective of these enhancements is to boost transmission capacity and improve power system security (i.e., avoid blackouts). The review outlines the key features of each technology and compares their effectiveness in addressing power system security issues.

### 3.6.1 AC transmission lines reinforcements

Alternative current (AC) transmission is a mature and reliable technology widely used in transmission expansion planning. It offers simple connectivity between nodes and allows easy power injection and withdrawal along transmission paths. Constructing additional AC transmission links has several benefits, including congestion relief, alleviating instability, and enhancing stability aspects. AC transmission is preferable for shorter distances, while compensation and Flexible AC Transmission Systems (FACTS) devices are suitable for distances up to 300-400 km.

There are three main types of AC transmission technology: Overhead Lines, cables, and Gas-Insulated Lines (GIL). Overhead lines are cost-effective and perform well in power systems. Cables and GIL have limitations in transmission length due to reactive compensation requirements. Cables have lower transmission capacities due to overheating, while GIL is less widely accepted due to the use of  $SF_6$  gas<sup>1</sup>. However, for short distances (e.g. up to 30-40 km for cables and 60-80 km for GIL) and when public acceptance for new overhead lines is an issue (e.g., in Europe), cables or GIL may be preferred options [63].

To enhance power transmission infrastructure, one can consider line reinforcements, which involve either replacing existing conductors with HTLS conductors or upgrading to higher voltage levels. Upgrading voltage levels, especially from 132 KV or 220 KV to 400 KV (for Ethiopian systems), is deemed the most effective measure for enhancing power system security. On the other hand, HTLS conductors can alleviate congestion by increasing network capacity, but they have limitations. Despite enhancing line capacity, other equipment like transformers, breakers, or disconnectors may require upgrades to handle higher loading.

---

<sup>1</sup>  $SF_6$  is a gas used as an insulating medium known to be a potent greenhouse gas and has been of concern due to its potential contribution to climate change.

### **3.6.2 Flexible AC Transmission Systems devices**

Flexible AC Transmission Systems (FACTS) devices are designed to enhance the stability and efficiency of AC grids by injecting or withdrawing reactive power at weak network points. FACTS includes various equipment like mechanical reactors, capacitors, Phase-Shifting Transformers, and power electronics-based devices. Power electronics-equipped FACTS can actively manage voltage and active power flow in the grid. FACTS technology can enhance the transfer capacity in power systems that are constrained by stability issues. This enhancement can result in a 20-30% increase in transfer capability, allowing more electricity to be delivered to consumers in a shorter time and with lower investment costs [64].

FACTS can be categorized into two main types: shunt compensation and series compensation. Shunt compensation includes devices like shunt reactors/capacitors, Static Var Compensators (SVCs), and STATCOMs, which primarily provide voltage support. SVCs and STATCOMs with power electronics can actively control voltage, enhance voltage stability, dampen inter-area oscillations, and reduce reactive loading during transient instability. STATCOMs, utilizing voltage-source technology, outperform standard SVCs, particularly in low network voltage scenarios.

On the other hand, series compensation involves Fixed Series Compensation (FSC), Thyristor Controlled Series Compensation (TCSC), and Phase-Shifting Transformers (PST). These devices increase line flows and contribute to voltage and transient stability. TCSC and PST can actively control power flow, preventing parallel line overloads and assisting in power oscillation damping more effectively than SVC or STATCOM.

### **3.6.3 High voltage direct current transmission**

High Voltage Direct Current (HVDC) technology is a more economical solution for long-distance overhead line transmission exceeding 400 km. It offers advantages such as active power flow control to prevent overloading on parallel

AC lines and the ability to help dampen inter-area oscillations when compared to AC systems. Currently, there is a 2,000 MW HVDC power transmission link between the national electricity systems of Ethiopia and Kenya, through a 1,000 km HVDC overhead line. The HVDC operates as a bipolar configuration ( $\pm 500$  KV), although a monopolar operation is allowed.

There are two main types of HVDC technology: Line commutated converter (LCC) and voltage source converter (VSC). LCC-HVDC has been in use for over 50 years and requires a robust AC network and extensive filters. VSC-HVDC, on the other hand, is more versatile, operating well in weaker networks, requiring fewer compensatory components, and offering independent control of active and reactive power. While LCC technology has lower losses and higher transmission capacity, VSC technology is advantageous for forming HVDC grids that accommodate bidirectional flows. The lack of a commercial-scale DC circuit breaker is a current limitation, but recent developments suggest its availability in the near future, enabling the practical realization of DC grids [65].

### **3.6.4 Dynamic line rating application**

Dynamic line rating (DLR) offers an innovative way for electric utilities to optimize the safe capacity of transmission lines, enabling them to carry more power without the need for costly upgrades. This is achieved by continuously monitoring factors like weather conditions and conductor temperatures to calculate the line's real-time capacity. Data on conductor conditions and the surrounding environment are collected and used to calculate the DLR for the line using wireless sensor networks along an overhead transmission line. DLR allows utilities to save on transmission upgrades, reduce congestion, and ultimately save money. DLR is more effective for shorter transmission (e.g. 80 km).

By implementing DLR, utilities can enhance grid efficiency and reliability without the need for new construction. This technology can be deployed quickly, providing immediate benefits and helping meet the rising demand for electricity due to electrification, giving alternative investment options and reducing congestion on

the transmission network [63, 66] by optimization of grid topology. These allow increased solar and wind integration, reduce curtailment for these variable renewable energy sources, and make power generation dispatch more cost-effective [67]. This concept is one of the main objectives of this dissertation and is presented in Chapter 8.

Prioritizing hotspots is essential when deploying DLR for transmission line monitoring due to potential financial constraints. Instead of implementing DLR on all lines, it is more prudent to select transmission segments based on their typical load levels, with priority given to heavily loaded lines [68]. This selection process should consider optimizing power generation costs, load shedding, and the integration of renewable energy systems. By carefully considering these factors, the implementation of DLR can achieve a balance between economic feasibility and efficient resource utilization [69].

### 3.6.5 Cost comparison and evaluation

In general, it's challenging to estimate the cost of deploying different technologies because it varies significantly depending on specific factors like location, environment, and politics. However, some efforts have been made to provide a relative cost comparison, as demonstrated in Figure 3.5 for primary transmission media in Germany [70].

Figure 3.5 outlines various transmission options and their corresponding technologies. These options include:

- **Basic:** This option utilizes a 380 KV AC overhead line.
- **FLM:** It involves the use of Dynamic Line Rating technology.
- **TAL:** This option entails modifying existing lines by incorporating high-temperature conductors.

- Hybrid: It combines an 800 km 4400 MW HVDC transmission from Schleswig-Holstein (north) to Baden-Württemberg (southwest) with an additional 3100 km of AC overhead lines.
- GIL: This choice involves the use of Underground Gas Insulated Lines.
- HVDC: It's important to note that the values for HVDC correspond to underground cables, while for AC, they refer to overhead lines. Hence, a direct cost comparison between them is not entirely feasible.

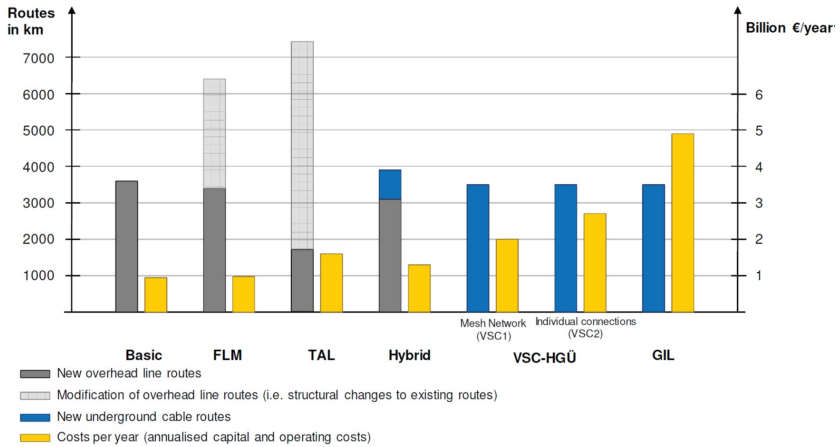


**Figure 3.5:** Dena grid study II expansion and annual costs associated with various transmission options in Germany. Source: dena [70].

The dena grid study ([70]) found that for short transmission distances and low capacity (100 km / 1000 MW), 380 KV AC overhead lines were the best choice. However, for long transmission distances and high capacity (400 km / 4000 MW), HVDC lines performed better. For situations in between, a combination of both technologies was optimal. It's important to note that these conclusions can't be applied universally because each project has unique characteristics.

Additionally, comparing costs for AC line reinforcements or FACTS devices is challenging due to project-specific factors. Nonetheless, it's expected that new

AC, GIL, or HVDC lines will generally be more expensive than reinforcements like DLR or HTLS, as well as FACTS devices like TCSCs or SVCs.

Due to the advantages that the dynamic line rate demonstrates for overhead transmission as an alternative investment option, we will mostly focus on the DLR technology as an expansion and grid optimization measure.

## **4 Case Study – Power outage economic cost**

Energy consumption and economic growth are closely interconnected, and access to reliable electricity is crucial for economic development [71]. However, many developing countries face frequent and prolonged power outages, which hinder firms' ability to plan and carry out production activities. According to data from the National Load Dispatch Center, Ethiopia experiences a concerning frequency of blackouts, averaging 12 blackouts per year or at least one blackout per month [72]. Policymakers need to understand the costs incurred by firms due to unreliable electricity supply, as this information can guide investment decisions in the energy sector [5].

Despite recent advancements in Ethiopia's energy sector, the country still faces frequent power outages due to various challenges such as growing load demands and increasing new connections [36]. Power outages have significant impacts on various sectors, including industries, households, and commercial establishments, leading to the inability to perform daily activities and shortages of products. While assessing the economic damages caused by a power outage can be relatively straightforward as they can be quantified in monetary terms, evaluating damages to the quality of life, institutional disruption, environmental harm, and safety impacts requires a conversion factor that determines how much damage in one category is equivalent to damage in another category. These assessments involve multidimensional considerations and might require the involvement of various stakeholders and experts.

The focus of this chapter is only limited to examining the cost of power outage and its impact on individual households, and industrial firms based on Enterprise Survey data. Furthermore, while both the industry sector and residential consumers contribute equally (38%) to the country's electricity consumption, it is projected that firms' consumption will surpass that of households. Therefore, understanding and analyzing firms becomes crucial in this context.

## **4.1 Power outage economic cost for households in Ethiopia**

Ethiopia has relatively low access to electricity, with a household access rate of 47% [28] and the majority still relies on biomass for cooking, and biofuels account for the largest share of the country's primary energy supply [32]. The National Electrification Program (NEP)<sup>1</sup> aims to expand electrification efforts and increase grid connections to reach 96% by 2030, along with a focus on off-grid solutions [73].

Power outages in Ethiopia have a significant impact on households, leading to financial losses, disruption of daily activities, and damage to appliances. The duration and frequency of outages vary across the country, with an average outage lasting around 8 hours according to World Bank Enterprise Survey data [12]. Despite significant investments in the power sector, the problem of electricity outages persists due to the country's rapid economic and population growth, which strains the existing power infrastructure with an inefficient transmission and distribution network.

To analyze the impact of power outages on households, a nationally representative urban household survey [34] conducted in 2019 was used in this dissertation for power outage economic analysis. Around 54 percent of the sample resides in Addis

---

<sup>1</sup> NEP is an action plan launched in 2017 for achieving universal electricity access nationwide by 2025.

Ababa, the capital city. The survey revealed that households in Ethiopia had an average monthly electricity bill of 275.39 ETB<sup>2</sup> (US\$18.9), accounting for about 3.7% of monthly household expenditure. The average price per kWh of electricity was approximately 2.12 ETB (3 US cents). The frequency and duration of outages varied significantly among households, with some experiencing frequent and long outages. On average, households reported 10 outages per month with a total duration of 48.24 hours.

Despite the prevalence of outages, only 3% of households reported using backup power sources during outages, indicating limited access to alternative solutions. The study also found that households spent additional defensive expenditures to cope with outages, with monthly expenses ranging from 60 to 77 ETB (US\$2.9–\$3.7) depending on the monthly hours of outages. These defensive expenditures could account for up to 14% of the average monthly electricity bill. The sample summary statistics are shown in Table 4.1.

**Table 4.1:** Households power outage descriptive statistics.

Variables	Mean	Median	Std.dev	Min	Max
HH size	5.05	5	2.13	1	13
HH monthly expenditures	7295.9	5606.17	11809.91	214.5	253440.7
Monthly electricity bill (in ETB)	298.38	199.10	399.86	3	6872
kWh	275.39	200.82	342.48	2.03	5985.98
Frequency of outages in per month	10.50	7	9.40	1	70
Total hours of outages per month	48.24	45	36.46	0.8	168
Backup source expenditure	39.37	0	130.42	0	1533

<sup>2</sup> ETB is the Ethiopian currency.

To mitigate these costs, it is important for the government and energy utilities to invest in improving the efficiency of transmission and distribution networks and to invest more in distributed renewable energy sources to ensure a steady power supply for households.

Providing electricity to households in rural areas involves three primary technological options: extending the grid, implementing mini-grids, or employing off-grid (stand-alone) systems. Figure 4.1 illustrates indicative levels of costs of electricity for on-grid, mini-grid, and off-grid technologies in sub-Saharan Africa<sup>3</sup>.<sup>4</sup> The cost-effectiveness of options 2 and 3 often surpasses that of grid extension due to the high expenses associated with extending the electricity grid, especially in regions with low population density [74].

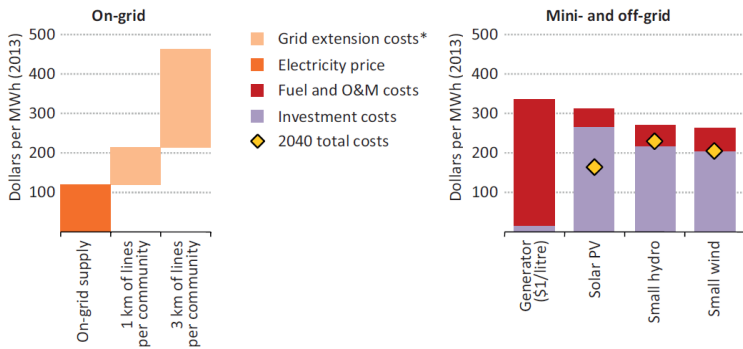


**Figure 4.1:** Indicative levelised costs of electricity for on-grid, mini-grid, and off-grid technologies in sub-Saharan Africa, 2012.

<sup>3</sup> The costs of grid extension are computed based on extending the medium-voltage grid by a certain distance (e.g., 1km) to each community on a levelised cost basis.

<sup>4</sup> Notes: Costs are indicative and could vary significantly depending on local conditions and a range of factors such as population density, electricity tariffs, and the delivered cost of diesel. The quality of service for the different technologies also varies: additional investment in batteries or backup power may be needed to compensate for the variability of renewables or intermittent grid supply. O&M = operation and maintenance.

## 4.2 Power outage economic cost on manufacturing firms

A reliable electricity supply is vital for the functioning of any business, but many developing countries face severe challenges in this regard. In Ethiopia, for instance, the lack of dependable electricity is the main challenge faced by businesses [4]. To ensure a consistent power supply, improving infrastructure and enhancing customer service during technical failures is crucial. However, financing these solutions in developing countries, where outages are frequent and demand is increasing, poses a significant challenge due to high investment costs. One potential solution is gradually increasing tariffs to fund incremental investments. The electricity supply in Sub-Saharan Africa is characterized by frequent and lengthy outages, partly due to publicly owned energy utilities keeping tariffs low to satisfy urban constituents. The low tariff rates make the costly investments needed for supply improvement economically unviable [75].

The study by [5] reveals that power outages impose significant costs on manufacturing firms, particularly micro, small, and medium-sized enterprises, in Ethiopia. On average, these firms incur monthly outage costs of seven times higher than their average electricity bill. The cost of outages also amounts to 3% of the firms' monthly sales, representing approximately 61% of the average monthly cost of using backup generators. The compensating variation for a zero-outage situation corresponds to about three times the current electricity cost. However, there is considerable heterogeneity in costs across sectors, firm sizes, and electricity consumption levels.

For the sake of simplicity in this dissertation, World Bank Enterprise Survey data was used to analyze the economic cost of power outages to firms in Ethiopia. The World Bank Enterprise Survey data collected from 848 firms in Ethiopia highlights the impact of electric outages on manufacturing businesses in the country. Table 4.2 provides further details on this analysis. According to the 2015 World Bank Enterprise Survey [12], about 39.5% of Sub-Saharan African firms identified electricity shortages as a major constraint to their operations, about 33.3% in

Ethiopia, which shows an increase from 23.1% in 2011. In 2015, 80% of the firms in Ethiopia experienced power outages, while the figures for Sub-Saharan Africa and the world were 76.9% and 50.6% respectively.

The average number of power outages in a typical month for Sub-Saharan Africa was 8.4, while for Ethiopia was 8.2 in 2015. Consequently, these firms experienced an average loss of 47 hours of economic activity per month due to power outages. Specifically, Ethiopian firms faced an average loss of 47.56 hours per month. As a result, Ethiopian firms suffered a sales loss of 6.9% annually, while the average Sub-Saharan African firm experienced an 8% loss.

Firms in developing countries have implemented various strategies to mitigate the negative impacts of power outages, including enhancing production flexibility and improving storage capabilities [5]. One common approach is to invest in backup electricity sources like diesel generators. However, these generators are expensive, particularly in Sub-Saharan Africa where they can be three to ten times more costly than grid electricity [76]. Furthermore, even with a generator, the self-generated power may be insufficient to operate production at maximum capacity [77]. Consequently, investing in a diesel generator may not always be the most cost-effective choice, as the funds could potentially be better utilized to increase production capacity [78].

Between 2011 and 2015, the ownership of generators by companies in Ethiopia increased from 40.6% to 49.1%. Additionally, there was a notable rise in the average proportion of electricity sourced from generators by Ethiopian firms, growing from 21.6% in 2011 to 48.9% in 2015.

To enhance the reliability of electricity supply in a country, it is essential to implement long-term and sustainable solutions. This involves investing in generation and distribution capacity while adjusting and adopting flexible electricity price-setting mechanisms, such as peak-load pricing. In truth, underpricing is a significant factor contributing to the shortage of electricity generation capacity in Africa [75].

**Table 4.2:** Firms power outage descriptive statistics

Firm experience	Year 2011			Year 2015		
	Ethiopia	Sub-Saharan Africa	World	Ethiopia	Sub-Saharan Africa	World
% of firms experiencing power outages	89	76.9	50.6	80	76.9	50.6
Number of power outages in a typical month	5.6	8.4	5.3	8.2	8.4	5.3
Average duration of a typical power outage (hours)	8.8	5.6	4.1	5.8	5.6	4.1
Average losses due to power outages (% of annual sales)	4.3	8	4	6.9	8	4
% of firms owning or sharing a generator	40.6	52.6	32.1	49.1	52.6	32.1
Average proportion of electricity from a generator (%)	21.6	29.7	17.4	48.9	29.7	17.4
% of firms identifying electricity as a major constraint	23.1	39.5	30.8	33.3	39.5	30.8

### 4.3 Electricity supply and ease of doing business

Electricity is the second most significant obstacle next to access to finance, with 10.1% of firms indicating it as a major challenge (see Figure 4.2). This could imply that businesses struggle with issues related to power supply, such as power outages and lack of access to electricity. The sustainable and reliable development of the electricity sector is therefore an important element in the socio-economic development and growth targets in Ethiopia. Policymakers and stakeholders need to address these issues to create a more conducive environment for business growth and development.

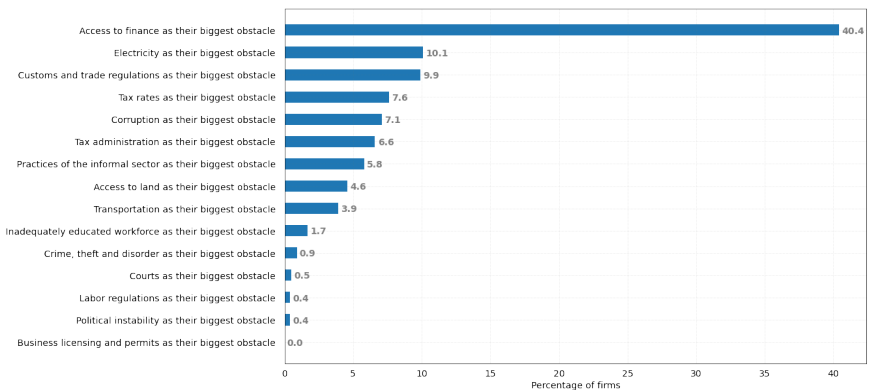


**Figure 4.2:** Ranking of the top business environment obstacle for firms in Ethiopia: Source: World Bank, 2015.

Addressing these challenges typically demands a comprehensive strategy encompassing policy reforms, investment in infrastructure, improvements in regulatory frameworks, and initiatives aimed at diversifying and updating the energy source mix. Ensuring a sustainable and dependable electricity supply is vital for economic progress and can significantly benefit businesses and the overall development of a country.

# 5 Artificial Intelligence in Power Grid Monitoring

Artificial intelligence (AI) is the concept of machines having human-like intelligence and learning autonomously from data to perform specific tasks, whereas Machine Learning (ML) is a subfield of AI, where computers can learn from data without explicit programming. It is a rapidly growing field that has found applications in a wide range of industries, including healthcare, finance, energy, and marketing, among others.

The subfield of ML which is capable of learning from large amounts of data is called Neural networks and can be used for tasks such as image recognition, speech recognition, and natural language processing. More recently, deep learning has emerged as a significant development in machine learning. Deep learning utilizes neural networks with multiple layers and has achieved breakthroughs in speech and image recognition, as well as natural language processing.

The general relationship between artificial intelligence, machine learning and deep learning is illustrated in Figure 5.1. These fields have practical applications in various sectors, including the energy industry, where they are used for renewable energy generation prediction and demand forecasts.

This dissertation addresses research questions concerning time series forecasting using data-driven approaches from the machine learning domain. Due to the vastness and continuous development of both fields, we will concentrate on essential concepts and techniques relevant to our proposed solutions in the subsequent chapters.

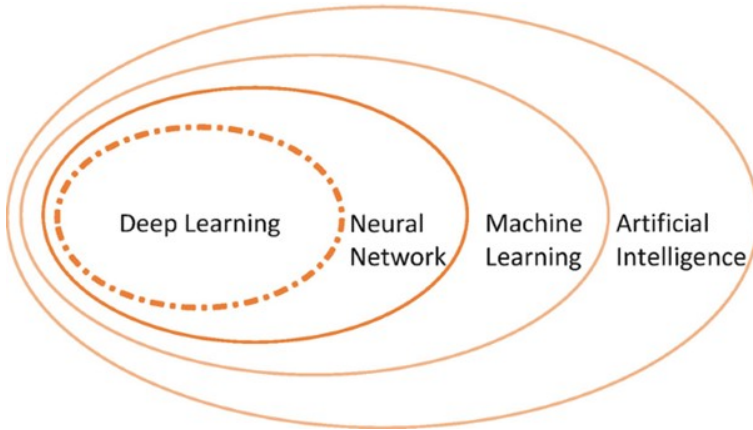


**Figure 5.1:** Venn diagram of AI and its derivations: machine learning and deep learning [79].

## 5.1 Theoretical concept of Machine Learning

According to a definition by [80] machine learning problems aim to improve the performance measure  $P$  for a given task  $T$  by utilizing training experience  $E$ . The first important step in developing a machine learning model is the problem creation step to deal with specific situations at hand. The problem creation stage involves precisely defining the task  $T$  and the performance measure  $P$ . This step guides the experimental design for collecting appropriate data  $E$  to be used for training the learning machine. After the collection of required data for machine training and preprocessing of the data take place to make it suitable for the selected learning model.

After the preprocessing phase is complete, the learning phase begins by defining a model for the task  $T$ . The model definition involves dividing the training experience  $E$  into two parts: one for learning the model's parameters and the other for evaluating the model's performance using the chosen performance measure  $P$ . This phase may include a feedback loop where the model is adapted or modified if the performance on the task  $T$  is not satisfactory.

### 5.1.1 Learning Methods

In problem creation of ML, it is crucial to create a model/hypothesis about a particular scenario in which we can create the presence of an unknown relationship or dependency that needs to be estimated/learned using ML experiments.

The approach to learning in the machine model can be broadly categorized into three: supervised learning, unsupervised learning, and reinforcement learning, depending on the available data, experience, and the task at hand.

Supervised learning involves providing the machine with a dataset consisting of features (represented as  $x$ ) and corresponding labels (represented as  $y$ ) [81]. The machine is trained to predict  $y$  from  $x$  by estimating the probability distribution  $p(y/x)$ . These variables can take different forms, such as time series, images, text, or object classes.

In contrast, unsupervised learning algorithms receive a dataset of features  $x$  and aim to learn the underlying structure of the dataset by reconstructing its probability distribution,  $p(x)$ . Another important advancement is unsupervised learning, where models learn from data without explicit feedback.

Reinforcement learning algorithms interact with the environment, establishing a feedback loop between the learning system and its experiences. They are trained using a reward or penalty function to optimize the output.

This dissertation specifically focuses on supervised learning methods, and the subsequent sections will delve into them further to provide a detailed exploration.

### 5.1.2 Over- and under-fitting

In machine learning contexts, model development follows a set of standard procedures. To execute tasks in the supervised learning method, the utilization of data features on which machine learn is crucial. The features used to train the machine learning model are called the training dataset. This dataset includes input data

and their corresponding target values, allowing the model to learn the patterns and relationships within the data.

To ensure success in machine learning, accurately defining the problem is essential, but equally important is determining the appropriate data size. The quality and informativeness of the data significantly impact the effectiveness of subsequent steps in the machine learning pipeline. In supervised learning, where input/output modeling is performed, it becomes crucial to have training data that is representative of the phenomenon under study and adequately covers the input space. This ensures that the model can learn and generalize effectively from the available data.

During training, the model adjusts its parameters and weights based on the input data to optimize its performance and make accurate predictions. Then, the model is evaluated against the validation dataset, which is a separate subset of data that is used to assess the model's performance and generalization ability. This dataset is not used during the model training phase but is employed during the evaluation stage. The validation dataset allows us to monitor the model's performance on unseen data and check for overfitting or underfitting. By evaluating the model's predictions on the validation dataset, we can make adjustments or select the best model based on its performance metrics, such as accuracy or mean squared error.

In machine learning, overfitting and underfitting are terms used to describe the performance of a learning algorithm. Overfitting occurs when a model is overly complex and trained too well on the training data. This means that the model becomes too specific to the training data and may not generalize well to new, unseen data. Overfitting can be caused by a complex model with insufficient training data or excessive training iterations. To detect overfitting, the model's performance is evaluated on a separate test set. If the performance on the test set is significantly worse than on the training set, it indicates overfitting.

Conversely, underfitting happens when a model is too simple and fails to capture the underlying patterns in the data. The model is not specific enough to the training data and may perform poorly on both the training and test data. Underfitting can occur when the model lacks the complexity to represent the data adequately or

when it is trained for too few iterations. To identify underfitting, the model's performance is evaluated on the training set. If the performance is poor, it suggests underfitting.

To mitigate overfitting and underfitting, it is crucial to select a model that is appropriately complex relative to the available training data. It is also important to stop training the model when overfitting starts to occur. Techniques such as cross-validation, regularization, and early stopping can be employed to prevent overfitting and underfitting. These methods help strike a balance between model complexity and generalization capability, ensuring optimal performance on unseen data.

If the performance achieves satisfactory results, the model is deployed into production, and its performance is monitored. If model performance degrades, a re-training is scheduled, using up-to-date training data.

### **5.1.3 Hyperparameter Optimization**

Hyperparameters are parameters that are not learned directly from the data during the training of a machine learning model. They are set by the user or the model developer and define the characteristics of the learning algorithm. They influence how the model is trained and how it generalizes to new data. Examples of hyperparameters include the learning rate, the number of layers in a neural network, the number of trees in a random forest, and the regularization strength.

Hyperparameter optimization methods are techniques used to find the optimal set of hyperparameters for a given machine learning model. The goal is to find the combination of hyperparameters that yields the best performance or results in terms of accuracy, precision, recall, or any other evaluation metric of interest.

There are several approaches to hyperparameter optimization, including:

- **Grid search:** In this method, a predefined set of hyperparameter values is specified, and the model is trained and evaluated for each combination of hyperparameters. The best combination is selected based on the performance metric.
- **Random Search:** Similar to grid search, random search involves specifying a range or distribution for each hyperparameter. However, instead of exhaustively searching all combinations, random combinations of hyperparameters are selected and evaluated.
- **Bayesian Optimization:** Bayesian optimization builds a probabilistic model of the objective function (the performance metric) and uses it to select the most promising set of hyperparameters for evaluation. It iteratively updates the model based on the evaluation results and focuses on the most promising regions of the hyperparameter space.

## 5.2 Time series forecasting

A time series is a sequence of ordered historical observations or measurements of a particular phenomenon, with each observation  $y$  as  $y_t$  indexed by  $t$  being the temporal index.

The problem of time series forecasting involves predicting future values of a given quantity based on a set of historical observations. To generate accurate forecasts, assumptions are made about the informative nature and underlying dynamics of the time series. The fundamental assumption is that the observed data up to the last available sample (up to time  $t$ ) contains relevant information that can be utilized to predict future values. If the future is independent of past observations, accurate forecasts cannot be generated based on historical data alone.

The autoregressive model is commonly used to represent the unknown data-generating process:

$$[y_{t+h}, \dots, y_{t+1}] = F(y_{t-d}, \dots, y_{t-d-m+1}) + e_t \quad (5.1)$$

where the unknown process  $F$  generates future values of the time series  $\{y_{t+h}, \dots, y_{t+1}\}$ , based on the values of the previous  $m$  time steps, with an optional delay term  $d$ .

From Equation (5.1), the main parameters of this model are the form of the unknown function  $F$  (*linear or nonlinear*), the model order (or lag)  $m$  and the noise term  $e_t$ . The noise term  $e_t$  represents stochastic and independently distributed processes with null mean and fixed variance  $\sigma^2$ .

## 5.2.1 Univariate time series forecasting

### 5.2.1.1 One-Step univariate forecasting

The simplest time series forecasting is one-step forecasting, i.e., predicting the next step in the future in a single step. The main objective is to predict the next step in the future. This problem can be defined as estimating a Single-Input, Single-Output (SISO) autoregressive mapping:  $f : \mathbb{R}^m \rightarrow \mathbb{R}$ .

$$y_{t+1} = f(y_{t-d}, \dots, y_{t-d-m+1}) + e_t \quad (5.2)$$

where  $e_t$  is the noise term or missing information (stochastic i.e., process with null mean and fixed variance),  $d$  is the delay, and  $m > 0$  is called the model order (or embedding lag).

The formulation described is applicable for estimating both linear (Auto-Regressive, AR) and nonlinear (Non-linear Auto-Regressive, NAR) mappings, making it suitable for the implementation of supervised machine learning algorithms [82].

In a linear autoregressive formulation (AR), the function  $f$  is a linear combination of the previous  $m$  values of the time series. This means that the value of the time series at a given time step is predicted based on a weighted sum of its previous  $m$  values, as expressed in Equation (5.3).

$$f(y_{t-d}, \dots, y_{t-d-m+1}) = \sum_{i=t-d-m+1}^{t-d} a_i y_i \quad (5.3)$$

On the other hand, in a non-linear autoregressive (NAR) formulation, the function  $f$  is non-linear and non-parametric. This allows for greater flexibility in modeling, enabling the use of machine learning techniques for one-step-ahead time series forecasting after a specific preprocessing phase [82]. The preprocessing phase transforms the original univariate time series forecasting problem into the task of learning the unknown input-output mapping  $f$  through supervised learning. This means that historical data is used to train a model that can predict the value of the time series at the next time step based on its previous values. Once the model of the mapping  $f$  is learned, it can be utilized to generate one-step-ahead forecasts, providing predictions for future values of the time series.

### 5.2.1.2 Multi-step-ahead univariate forecasting

Unlike the one-step-ahead learning approach, when dealing with multiple-step-ahead forecasting, the target variable to predict is no longer a single value but a vector of  $h$  elements, where  $h$  represents the forecast horizon [82–84]. In this approach, the goal is to forecast multiple future values of the time series rather than just the immediate next value. There are two strategies [82–84] for multiple-step-ahead forecasting tasks: single output and multiple output. The first strategy includes the iterated and direct approaches, and the second approach employs Multi-Input Multi-Output (MIMO) approach.

- Iterated approach: In the iterated approach, also known as the recursive approach, a one-step-ahead model is used to generate forecasts, and these forecasts are then iteratively fed back into the model to predict subsequent values until the desired forecast horizon is reached [85]. Defined as  $f_{rec} : \mathbb{R}^m \rightarrow \mathbb{R}$ .

$$y_{t+1} = f_{rec}(y_t, \dots, y_{t-m+1}) + e_t \quad (5.4)$$

The model is recursively applied  $h$  times to generate multiple-step forecasts. However, errors can accumulate in each step, leading to less accurate predictions as the forecast horizon increases [86].

- Direct approach: The Direct approach [83, 85] learns independently  $h$  models simultaneously  $f_h : \mathbb{R}^m \rightarrow \mathbb{R}, h = 1, \dots, H$

$$y_{t+h} = f_h(y_t, \dots, y_{t-m+1}) + e_t \quad (5.5)$$

The Direct approach generates a multi-step-ahead forecast by concatenating the predictions from all  $H$  models. One advantage of this approach is that it does not rely on estimated values as inputs, reducing the risk of accumulating errors from previous predictions. However, it does not consider conditional dependencies between the predictions [87–89]. As a result, these methods often require more complex models to capture the dependency between distant time points compared to iterative strategies [90]. For example, in a traditional neural network [91, 92], this can be achieved by using multiple neurons in the output layer to predict different horizons.

- MIMO approach: The MIMO approach, also referred to as the Joint approach, offers an alternative to the Direct strategy’s assumption of conditional independence between future values [88, 89, 93]:

$$[y_{t+h}, \dots, y_{t+1}] = F(y_t, \dots, y_{t-n+1}) + w \quad (5.6)$$

where  $t \in n, \dots, N - h$ ,  $F : \mathbb{R}^d \rightarrow \mathbb{R}^h$  is a vector-valued function [94], and  $w \in \mathbb{H}$  is a noise vector with a covariance that is not necessarily diagonal [95].

The MIMO approach involves training a single multiple-output model to capture the relationships between different inputs and outputs. This approach allows for a more comprehensive understanding of the data and enables better predictions by considering the interdependencies among the variables. These strategies are useful when forecasting multiple related variables that have interdependencies and need to be considered together.

A recurrent neural network (RNN) is famous for sequence modeling due to its ability to capture nonlinear relationships, discussed in Section 5.4.2. In this **disertation**, for our evaluation of multi-step time series prediction, we have selected deep learning models. Univariate time series data predictive were modeled with the Long Short-Term Memory (LSTM) model, LSTM Encoder-Decoder, and the Bi-directional LSTM (BLSTM) model for the MIMO approach. In addition, the One-Dimensional Convolutional Neural Network (CNN) was evaluated. Our evaluation study seeks to determine the accuracy of each model as the prediction horizon increases.

## 5.2.2 Multivariate time series forecasting

In contrast to univariate time series that consist of a single variable, multivariate time series incorporate multiple variables that may interact and influence each other over time. A multivariate time series with  $n$  observed variables and  $N$  observations is typically represented in the matrix representation, with each column representing a specific variable, and the rows representing different time steps. This arrangement creates a matrix of size  $N \times n$ .

Like univariate case (Section 5.2.1) direct, iterated, and MIMO approaches can be performed multiple-step-ahead forecasting for multivariate datasets [84].

Two forms of modeling exist for multivariate forecasting, local modeling, and global modeling. In local modeling, each time series in a multivariate forecasting task is treated independently, resulting in a separate model being estimated for each series [96]. This approach decomposes the task into individual Single Input Single Output (SISO) or Multiple Input Single Output (MISO) tasks. For SISO tasks, each forecasting task is treated as an independent problem, disregarding any cross-dependencies with other series.

In the case of MISO (Multiple Input, Single Output) tasks, it is possible to utilize multiple series as input covariates to predict a single time series. This means that instead of using just one series to forecast the output, several other series

can be incorporated as additional inputs to improve the accuracy and predictive capabilities of the model. By considering multiple related series as covariates, the forecasting model can leverage the information and patterns present in these input series to make more accurate predictions for the target time series.

In the context of global modeling, the multivariate forecasting problem is approached as a single Multiple Input Multiple Output (MIMO) problem. This is achieved by utilizing a Non-linear Vector Auto-Regressive (NVAR) formulation.

## 5.3 Data preprocessing and engineering

It is possible to improve the accuracy and/or reduce the computational complexity of a model by modifying the inputs of the problem. To enhance data quality, a significant phase following data collection is preprocessing. During this step, raw data is analyzed and modified to optimize the model's learning performance for subsequent fitting. Processing the data can improve the quality of the predictions, increase training speed, and transform data into more meaningful representations to facilitate model training. Here, we will only focus on the relevant techniques pertaining to time series forecasting, our domain of interest.

### 5.3.1 Missing value handling

A common assumption in supervised learning is that all samples in a dataset are sampled from the same data-generating process and are independent of each other. However, this assumption does not hold in the case of time series forecasting, as it overlooks the existence of temporal dependence among the values to be estimated (represented by the unknown mapping  $f$ ). Consequently, it is not advisable to use general-purpose missing value imputation techniques in this context, and instead, specific techniques tailored for temporal data should be preferred.

Various techniques for handling missing values in time series data are available in the literature [97], along with their corresponding implementations. These

techniques encompass a range of approaches, starting from basic replacement methods such as Last Observation Carried Forward (LOCF) or Next Observation Carried Backwards (NOCB), which involve using the last available value to fill in missing data points.

More advanced techniques include model-based approaches that rely on forecasts generated by autoregressive models, Kalman filtering, or exponential smoothing. These methods utilize the inherent temporal structure of the data to make predictions and impute missing values. Additionally, statistical techniques such as interpolation or rolling statistics can be employed to estimate missing values based on the surrounding data points.

### **5.3.2 Feature selection**

Traditional supervised learning algorithms are typically designed for problems with a small input space and relevant input variables. However, they can perform poorly when applied to tasks with limited data and numerous input variables. To address this, feature selection is commonly used to eliminate irrelevant features. Feature selection approaches can be categorized into three main types: filter methods, wrapper methods, and embedded methods. Filter methods assess feature relevance solely from the data, while wrapper methods evaluate subsets of variables based on their usefulness to a specific learning technique. Embedded methods incorporate variable selection as part of the learning procedure and are tailored to specific learning machines.

### **5.3.3 Data scaling**

In the presence of input variables having different orders of magnitude, a rescaling process is necessary to ensure a meaningful learning process. The purpose of this rescaling process is to adjust the scale of the variables, aligning their magnitudes with each other while attempting to preserve the original distribution of the variable under consideration.

One commonly used rescaling technique is the min-max scaling Equation (5.7), where the minimum and maximum values of the variable are determined, and then each value is transformed to a new range between a specified minimum and maximum. This method ensures that the variable's values are adjusted proportionally within the new range while preserving the original distribution.

$$x_{scaled} = \frac{x - x_{min}}{x_{max} - x_{min}} \quad (5.7)$$

or

$$x_{scaled} = \frac{x - x_{mean}}{x_{max} - x_{min}} \quad (5.8)$$

Another option for rescaling is the interquartile scaling Equation(5.9). In this approach, the interquartile range (the range between the 25<sup>th</sup> and 75<sup>th</sup> percentiles) of the variable is determined. Each value is then transformed based on its position within the interquartile range, effectively preserving the variable's distribution while adjusting its magnitude to be compatible with the other variables.

$$x_{scaled} = \frac{x - Q_1(x)}{Q_3(x) - Q_1(x)} \quad (5.9)$$

where  $\min(x)$ ,  $\max(x)$ ,  $Q_1(x)$  and  $Q_3(x)$  represent the minimum, maximum, 1<sup>st</sup> and 3<sup>rd</sup> quartile of the  $x$  variable, respectively.

Alternatively, if it can be assumed that the variable follows a normal distribution, the z-score rescaling method (5.10) can be employed. This rescaling technique ensures that the variable's mean is equal to zero and its variance is equal to one, thus standardizing the variable.

$$x_{scaled} = \frac{x - \mu_x}{\sigma_x} \quad (5.10)$$

where  $\mu_x$  and  $\sigma_x$  represent the mean and the standard deviation of the  $x$  variable, respectively.

### 5.3.4 Feature engineering

Feature engineering (or feature pre-processing) in time series forecasting involves creating relevant and informative input features that can improve the accuracy and performance of a forecasting model. Time series data is characterized by its temporal nature, where the order and dependencies of data points over time play a crucial role in forecasting future values [98].

In cases where the available data has limited informative content, feature engineering is conducted to generate new features from the existing data. This process involves creating additional features by combining the original  $N$  variables using both linear and non-linear methods. By constructing these new features, the aim is to enhance the information present in the data and improve the performance of machine learning algorithms. This action aims to capture these temporal patterns and provide meaningful inputs to the forecasting model.

Rolling averages, rolling counts, and rolling standard deviations are commonly used in sliding window-based feature engineering in time series data. If a time window of size  $w$  is considered, the resulting new feature is a time series of length  $N - w$ .

### 5.3.5 Learning phase reconstruction

The native format of time series data is typically not suitable for addressing the forecasting problem using supervised learning techniques. To overcome this challenge, an embedding or reconstructing phase procedure is necessary to reorganize the existing observational data. It is commonly used in time series forecasting to capture the underlying patterns and relationships within the data.

Thus, following the feature engineering process, we apply the embedding procedure to the original time series data. Through this process, the original one-dimensional time series is transformed into a higher-dimensional format suitable

for the learning process [99]. To perform embedding reconstruction, methods such as delay embedding or phase space reconstruction can be used.

Phase space reconstruction (PSR) is a specific method used in nonlinear time series analysis to reconstruct the underlying dynamics of a system from observed time series data. It assumes that the system's dynamics can be represented by a trajectory in a higher-dimensional space called the phase space. The process of phase space reconstruction requires selecting an appropriate embedding dimension  $m$  and time delay  $\tau$ . The embedding dimension is determined by the number of variables or features used to represent the system, while the time delay represents the lag between successive observations. These parameters are chosen to capture the dynamics and preserve the topological structure of the original system.

In PSR, if we have a one-dimensional time series data represented as  $x = x_1, x_2, \dots, x_N$ , the embedding dimension is denoted as  $m$ , and the delay time is represented as  $\tau$ . Using these parameters, the set of time series reconstructed through phase space can be mathematically expressed as in Equation 5.11.

$$\begin{bmatrix} \mathbf{X}_1 \\ \mathbf{X}_2 \\ \vdots \\ \mathbf{X}_M \end{bmatrix} = \begin{bmatrix} x_1 & x_{1+\tau} & \cdots & x_{1+(m-1)\tau} \\ x_2 & x_{2+\tau} & \cdots & x_{2+(m-1)\tau} \\ \vdots & \vdots & \cdots & \vdots \\ x_M & x_{M+\tau} & \cdots & x_N \end{bmatrix} \quad (5.11)$$

where  $M = N - (m - 1)\tau$ .

The phase space reconstruction procedure involves two steps, the first is choosing an embedding delay  $\tau$ , and the second concerns choosing an appropriate number of embedding dimensions to embed the time series. One way to estimate  $m$  is by False Nearest Neighbor (FNN) analysis [100].

## 5.4 Machine learning algorithm

This section provides a theoretical overview of the key machine learning algorithms utilized in the study. The primary focus is on artificial neural networks, which serve as the foundation for understanding other neural network models. Specifically, recurrent neural networks (RNNs) and convolutional neural networks (CNNs) were the main forecasting models employed for frequency fluctuation prediction. Additionally, the study utilized a quantile regression forest for conducting risk-averse analysis in dynamic line rating.

### 5.4.1 Artificial Neural Networks

The concept of Artificial Neural Network (ANN) is inspired by the structure of biological neural networks found in animals' central nervous systems. These biological networks consist of interconnected cells (neurons) that process information. The strength of connections between neurons can change over time in response to external stimuli, allowing the network to learn from experiences.

In deep learning, ANN is a mathematical model designed to replicate the structure and functions of biological neural networks. At its core, an artificial neural network consists of artificial neurons, which are simple mathematical models governed by three fundamental operations: multiplication, summation, and activation. When inputs are fed into an artificial neuron, they are multiplied by individual weights, which represent their relative importance. The weighted inputs, along with a bias term, are then summed within the neuron. Finally, the sum is passed through an activation function, also known as a transfer function, at the neuron's output. This entire process is illustrated in Figure 5.2. Neurons in the network are interconnected by weighted links, allowing signals to propagate from one neuron to another. The output signal of a neuron is transmitted through its outgoing connection, which splits into multiple branches, carrying the same signal. These branches terminate at the incoming connections of other neurons within the network.

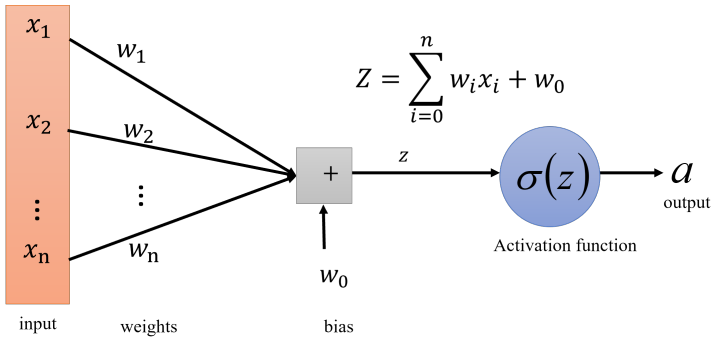


**Figure 5.2:** The basic structure of an artificial neuron (perceptron structure): Each input element is weighted by a corresponding weight. The combined sum is used to make a decision. The neuron computes the weighted sum of the input signals and compares the results with a threshold value of the activation function.

In our task, we will focus on a specific type of ANN called the Feedforward Neural Networks (FNNs), also known as Multilayer Perceptrons (MLP) [101–103] as illustrated in Figure 5.3. The MLP is organized into layers, with each layer fully connected to the next layer. FNNs consist of three types of layers: input, hidden, and output layers. Each layer is composed of neurons or nodes, with connections between nodes in adjacent layers through weighted interconnections or links [104].

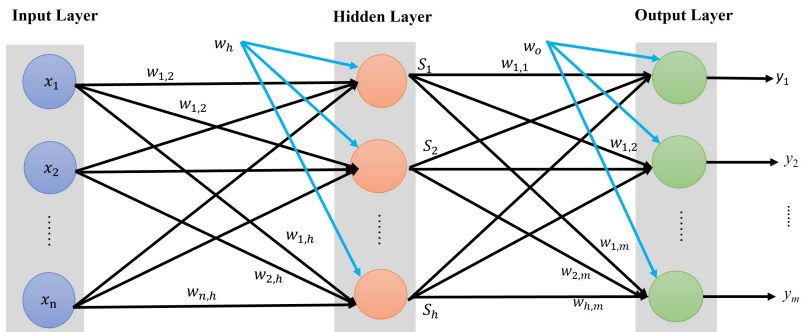


**Figure 5.3:** Shows a single hidden layer of MLP network, with  $x = (x_1, x_2, \dots, x_n)T$  represents  $n$  input vector,  $S = (S_1, S_2, \dots, S_h)T$  represents  $h$  hidden layer, while  $y = (y_1, y_2, \dots, y_m)T$  represents  $m$  output vector in the output layer.  $w_h$  and  $w_o$  represent hidden neurons biases, and output neurons biases, respectively.

In an artificial neuron, information is received through weighted inputs, multiplying each input by a corresponding weight. The inputs are then summed along with a bias term, and the sum is processed using an activation or transfer function. The processed information is then passed through the neuron's output(s). The simplicity of the artificial neuron model can be observed in its mathematical representation as:

$$y(k) = F\left(\sum_{i=0}^m w_i(k) \cdot x_i(k) + w_0\right) \quad (5.12)$$

Where,  $x_i(k)$  is the input value in discrete time  $k$  where  $i$  goes from 0 to  $m$ ,  $w_i(k)$  is the weight value in discrete time  $k$  where  $i$  goes from 0 to  $m$ ,  $w_0$  is bias,  $F$  is an activation function,  $y_i(k)$  is output value in discrete time  $k$ .

The optimal weights,  $w_1, w_2, \dots, w_n$  for the connections between neurons, are found in the training process using an optimization algorithm. Especially in deep learning, the stochastic gradient descent (SGD) algorithm is applied for this. SGD is a version of the well-known optimization algorithm gradient descent (GD), in which the whole training set is divided into small sets, called mini-batches, to reduce the calculation time while still getting a good optimum estimation.

Gradient descent runs iteratively to find the optimal values of the parameters corresponding to the minimum value of the given cost function  $J(w_0, w_1)$ . Mathematically, the derivative technique is essential to minimize the cost function because it helps get the minimum point. The derivative refers to the slope of the function at a given point. We need to know the slope so that we know the direction (sign) to move the coefficient values to get a lower cost on the next iteration.

The simplest cost function for neural networks is given as:

$$J(w_0, w_1) = \frac{1}{2m} \sum_{i=0}^m (h_w(x_i) - y_i)^2 \quad (5.13)$$

Where  $h(w)$  refers to the output of activation functions mapping from input features to output target variable for a specific  $i$  value, indicating the predicted line using the equation 5.14 for one-dimensional input data case.  $m$  number of training samples,  $y_i$  denotes the value of the actual data point we've already obtained. The  $i$  value represents the count of data points for which we have computed the differences.

$$h_w(x) = w_0 + w_1x \quad (5.14)$$

Gradient descent is just the differentiation of the cost function. It is given as:

$$\frac{\partial J(w_0, w_1)}{\partial w_j} = \frac{\partial}{\partial w_j} \frac{1}{2m} \sum_{i=0}^m (h_w(x_i) - y_i)^2 \quad (5.15)$$

For  $j=0$  and  $j=1$ ,

$$\frac{\partial J(w_0, w_1)}{\partial w_0} = \frac{1}{m} \sum_{i=0}^m (h_w(x_i) - y_i) \quad (5.16)$$

$$\frac{\partial J(w_0, w_1)}{\partial w_1} = \frac{1}{m} \sum_{i=0}^m (h_w(x_i) - y_i)x_i \quad (5.17)$$

and gradient descent 5.18, repeat until convergence for every  $j$ .

$$w_j := w_j - \alpha \frac{\partial J(w_0, w_1)}{\partial w_j} \quad (5.18)$$

In the above equation,  $\alpha$  is known as the learning rate, determining the pace of descent along the slope. A small  $\alpha$  means slow convergence, while a large  $\alpha$  may not converge. If  $\alpha$  is excessively high, it might skip the minimum error point, leading to inaccurate results. Conversely, if it's too low, model optimization takes longer, wasting computational resources. Too low value of learning rate leads to

the solution getting stuck in local minima instead of the global minima of the cost function. Hence, selecting an optimal  $\alpha$  value is crucial. Figure 5.4 illustrated the effect of learning rates over epoch [105].

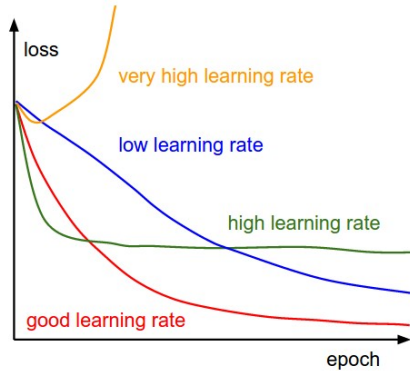


**Figure 5.4:** Shows the effects of different learning rates. At low learning rates, progress is steady and linear. With high learning rates, the improvements become more rapid, even exponential. Higher rates accelerate loss reduction but risk getting trapped in poorer states of loss (green line). This happens due to excessive "energy" in the optimization process, causing parameters to bounce around, and preventing them from finding a stable position in the optimization landscape.

The derivative of a function ( $J(w_0, w_1)$ ) on each parameter (weight) tells us the sensitivity of the function with respect to that variable or how changing the variable impacts the function value. Gradient descent, therefore, enables the learning process to make corrective updates to the learned estimates that move the model toward an optimal combination of parameters ( $w_0, w_1$ ). The cost is calculated for a machine learning algorithm over the entire training dataset for each iteration of the gradient descent algorithm. In Gradient Descent, one iteration of the algorithm is called one batch, which denotes the total number of samples from a dataset that is used for calculating the gradient for each iteration. The GD algorithm optimizes by following the direction of the gradient of a cost function. It converges when this gradient tends to zero. The cost function in machine learning is usually the sum of the training examples of a per-example loss function.

A numerical calculation of the gradient to execute the SGD algorithm can be computationally expensive. Therefore, its estimation for the cost function,  $J(w)$ , with respect to its parameters, is typically done using the backpropagation algorithm. The procedure consists of applying the chain rule recursively to execute the derivative of the loss function with respect to the output vector,  $y$ , as a multiplication of the derivatives of the outputs of each neuron for its respective inputs.

The choice of the transfer function, or activation function, is a crucial aspect of the artificial neuron model. Activation functions define the behavior of the neuron and can be any nonlinear function. Figure 5.5 illustrated the most commonly used activation functions in neural networks, including Sigmoid, Tanh, and rectified linear unit (ReLU). These functions introduce non-linearity to the network's computations, enabling it to learn complex patterns and relationships. The final output of the network is determined by the weights leading up to the output layer. To compute a prediction, the output is passed through an activation function.

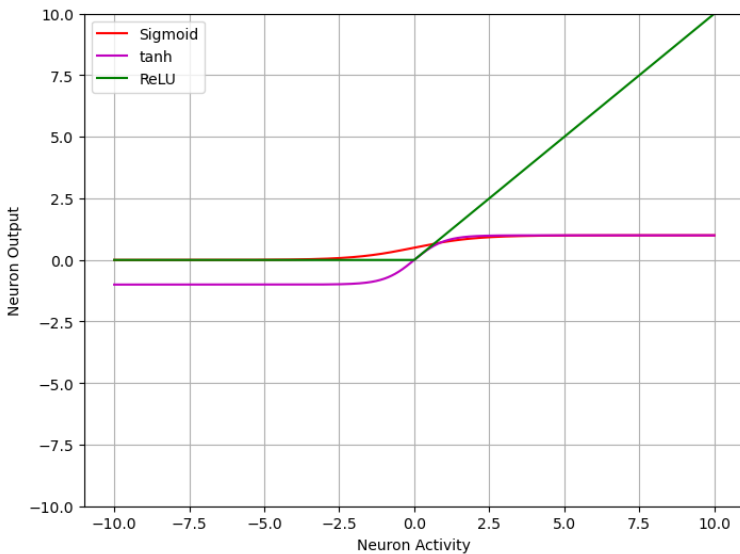


**Figure 5.5:** Mostly used activation functions, Sigmoid, *tanh*, and ReLU.

Sigmoid (red line):

$$f(x) = \frac{1}{1 + e^{(-x)}} \quad (5.19)$$

Tangens Hyperbolicus, *tanh* (blue line):

$$f(x) = \tanh(x) = \frac{2}{1 + e^{-2x}} - 1 \quad (5.20)$$

Rectified Linear Unit, ReLU (green line):

$$f(x) = \max(0; x) \quad (5.21)$$

Deep feed-forward neural networks were introduced to address the limitations of single-layer neural networks, which struggle to learn complex dependencies, particularly spatio-temporal dependencies. The architecture of a deep feed-forward neural network is similar to that of a single-layer network but with the key difference lying in the number of hidden layers which determines the depth of the network. The following section presents variants of deep neural networks.

## 5.4.2 Recurrent Neural Networks

Recurrent neural networks (RNNs) [91] introduce recurrent connections in the hidden layers of a feed-forward network, enabling them to model dynamic temporal dependencies in the input data. RNNs process sequential or time-series data and feed the output from the previous step as input to the current stage [92]. They have a "memory" that allows them to impact current input and output based on past elements in the sequence. Figure 5.6 demonstrates the fundamental architecture of an RNN. It depicts the components involved in the RNN model, namely the input ( $X_t$ ), hidden state ( $S_t$ ), and output ( $O_t$ ) at each time step ( $t$ ). The parameters  $U$ ,  $V$ , and  $W$  are parameters for the hidden matrices and their values can differ at each time step. The hidden state is computed using the formula  $S_t = f(U_{(x_t)} + W_{S_{(t-1)}})$ , where  $f$  represents a non-linear activation function.

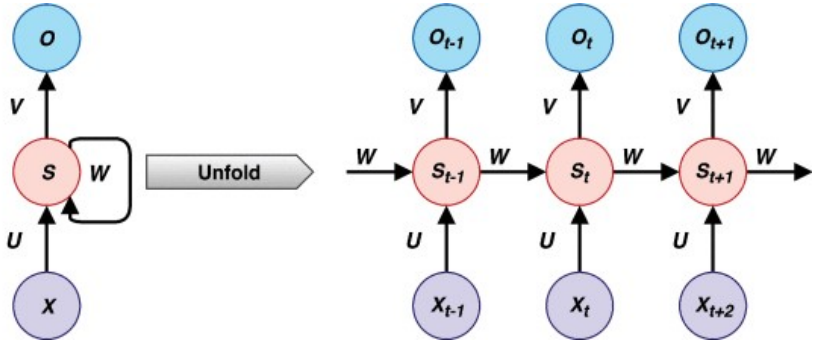


Figure 5.6: Basic architecture of Recurrent Neural Network.

RNNs' outputs are dependent on the previous inputs in the sequence [91], unlike typical deep neural networks, which presume that inputs and outputs are independent of one another. However, standard RNNs face the challenge of vanishing gradients, making it difficult to learn from long sequences of data. To address this issue, several popular variants of RNNs have been developed. Among these, LSTM and GRU are the most popular.

#### 5.4.2.1 Long short-term memory

Long Short-Term Memory (LSTM) [106] has emerged as the most stable and powerful model for capturing long-range temporal dependencies in various practical applications, outperforming standard RNNs and their variants [107]. The repeating LSTM cell's architecture, depicted in Figure 5.7, is responsible for its superior performance. LSTM addresses the problem of vanishing gradients by incorporating special units called gates that enable the network to store data for long periods. The flow of information into and out of the memory cell is managed by three gates: the Forget Gate, Input Gate, and Output Gate.

- Forget Gate: determines which information from the previous state is retained or discarded.

- **Input Gate:** determines what new information should be added to the network's long-term memory (cell state), given the previous hidden state and new input data.
- **Output Gate:** controls the outputs or the new hidden state.

Long Short-Term Memory (LSTM) networks enhance simple RNNs by incorporating a time-varying internal state ( $c_t$ ). They employ a three-step mechanism to update the internal state, combining the previous output ( $h_{t-1}$ ) with new input values ( $y_t$ ) through input and forgetting gates. The updated state ( $c_t$ ) is combined with the output activation vector ( $o_t$ ) to generate the new neuron output ( $h_t$ ). Figure 5.7 illustrates the LSTM architecture.

LSTM has a bidirectional variant that connects two hidden layers running in opposite directions, allowing the network to incorporate information from both the past and the future. Bidirectional LSTMs (BD-LSTM) enhance model performance by predicting both positive and negative time directions simultaneously [108]. Another variant of LSTM is the encoder-decoder LSTM network (ED-LSTM) which is a sequence-to-sequence model for mapping inputs to output vectors [107]. LSTM networks are often used in multivariate and multistep forecasting in hybrid architectures with linear models.

#### 5.4.2.2 Gated Recurrent Units

Gated Recurrent Units (GRUs) are another variant that uses gating methods to control information flow within the neural network [109]. GRUs have fewer parameters compared to LSTMs, with a reset gate ( $R_t$ ) and an update gate ( $Z_t$ ) instead of the output gate. This structure allows GRUs to capture dependencies from large sequences of data adaptively without discarding earlier information.

Like LSTM, Gated Recurrent Unit (GRU) is a method used to avoid the vanishing or exploding gradient problem by using gates to control the flow of information to the next time step. Figure 5.8 illustrates the GRU architecture. Unlike LSTM,

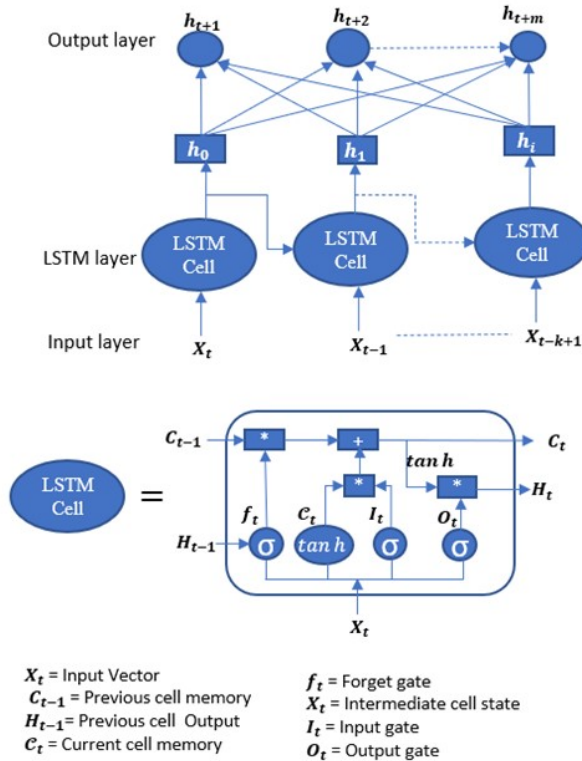


**Figure 5.7:** Long-Short-Term Memory (LSTM) networks. The LSTM cell denotes memory cells that use gates and cell memory for remembering long-term dependencies.

GRU does not pass on a cell state to the next step but instead transfers information using the hidden state, making it faster and more memory-efficient.

Both LSTM and GRU have demonstrated their effectiveness in various applications, although GRUs may perform better on smaller and less frequent datasets [110, 111].



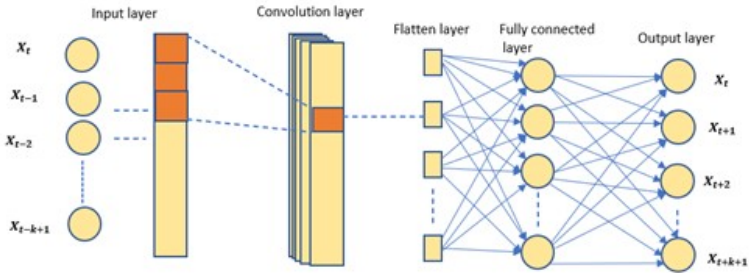


**Figure 5.9:** One-dimensional convolutional neural network for multi-step ahead time series prediction.

It is worth noting that a multi-output network with  $h$  output neurons, one for each of the  $h$ -step ahead predictions to perform, can be employed to model a MIMO forecasting approach. A multi-output network could also be used to perform one-step-ahead multivariate prediction.

#### 5.4.4 Quantile Regression Forests

Quantile Regression Forests (QRFs) [115] is a supervised machine learning model, probabilistic regression algorithm, which is derived from random forest [81]. In graph theory, a tree is defined as a continuous graph with no closed loops, which is built with a set of nodes and edges. Nodes always divide into two other nodes and their edges have a defined direction.

QRF can predict non-parametric distribution data and deliver an accurate way of estimating different quantiles for high-dimensional predictor variables. Consequently, QRF is an ensemble learning model based on the aggregation of several decision trees to establish the model output, as shown in Figure 5.10 using a QRF algorithm procedure flowchart. A decision tree refers to a decision support tool that relies on tree-like structures that consist of links and nodes to achieve potential model outputs (see Figure 5.11). The starting point of each decision tree is a parent node that serves as a decision point; the parent node keeps creating branches until a decision is reached. Each tree is trained to predict the observable target variable  $Y$ , for a horizon  $h$ , at time  $t + h$  using the predictor variables  $X$

at time  $t$ . Then all outcomes held in the leaves for each tree are used to build the probabilistic forecast.

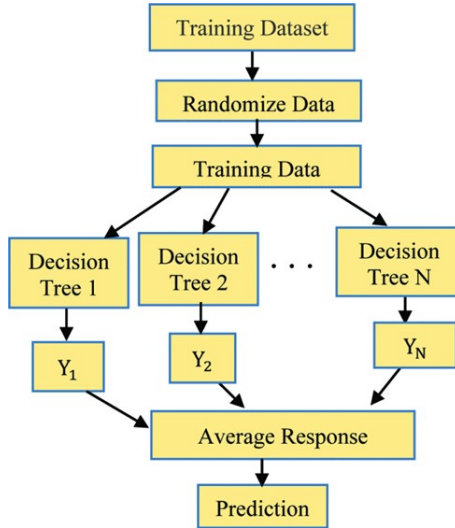


**Figure 5.10:** Quantile regression forest algorithm procedure flowchart.  $Y_1, Y_2, \dots, Y_N$  presents the average response and decision tree output.  $N$  denotes the sample sets in which randomized and produced  $N$  decision tree.

An ensemble of outputs from several binary trees trained with randomly selected input data element is called a random forest [81]. A random forest prediction result can be calculated as a weighted average of all outputs of binary trees. A prediction  $\hat{Y}$  can be calculated as a weighted average of all outputs  $y_i$  with Equation (5.22), where the weights  $w_i$  are defined by Equation(5.23).

$$\hat{Y} = \sum_{i=1}^N w_i y_i \quad (5.22)$$

$$W_i = \frac{1}{N_b} \sum_{k=1}^{N_b} \frac{1 \{X_i \in R_{l_{k,p}}\}}{\neq \{q : X_q \in R_{l_{k,p}}\}} \quad (5.23)$$

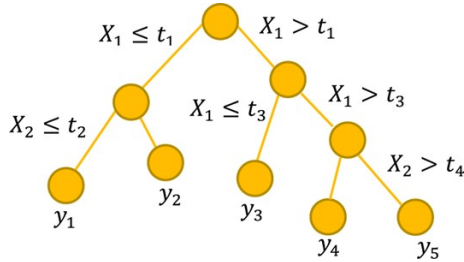


**Figure 5.11:** A multidimensional binary decision tree [116].  $X_i$  denotes predictor variables. The tree has four internal nodes and five leaves (terminal nodes).  $X_i \leq t_k$  and  $X_i > t_k$  correspond to the left and right branches of each internal split, respectively.  $y_i$  denotes the mean of the observations at leaf  $i$ .

Random forest prevents overfitting most of the time, by creating random subsets of the features and building decision trees using these subsets. Finally, it combines all subtrees to generate a single prediction result.

In this dissertation, QRF was utilized to develop a model that can predict the ampacity of OHTL with a two-year dataset. The reason behind choosing QRF over other machine learning techniques is associated with its behavior which allows for the make use of variables outside the point forecast, making it useful in understanding outcomes of probabilistic forecasting that are non-normally distributed and nonlinear associated with weather forecasting uncertainties.

### 5.4.5 Explainable machine learning

Deep neural networks have found significant use in critical areas like healthcare, self-driving vehicles, and the military, directly impacting human lives. However, complex ML models are often non-explainable black-boxes, i.e. they do not provide insights about how inputs are mapped to outputs [117, 118]. This is particularly problematic for critical infrastructures such as power systems, where the black-box character poses a security risk [119, 120]. To address this, the field of explainable machine learning (XAI) has emerged, aiming to create tools and methods that provide understandable explanations for AI decisions [121].

In the context of electric power systems, maintaining stable operation requires adhering to strict frequency limits. Fluctuations and external influences can lead to significant deviations and increased control efforts. Although machine learning can model these complex relationships, the lack of transparency in many models restricts their usability and insights.

In power grids, unpredictable factors like fluctuating renewable energy sources and societal events can disrupt frequency stability. To maintain stability, operators monitor the system closely and allocate resources. Machine learning (ML) techniques, which are adept at handling vast data sets, including frequency recordings and various features, offer a way to analyze and predict grid frequency with data-driven models [116]. However, complex ML models often lack explainability, making them problematic for critical systems like power grids.

The importance of model explainability in the realm of machine learning becomes evident through the usual post-training inquiries. These include queries about how various features impact predictions, which features hold the most influence, and whether the seemingly impressive model performance metrics warrant trust. Understanding these aspects becomes pivotal for multiple reasons, such as debugging, guiding feature engineering/enhancement, directing future data-gathering efforts, aiding human decision-making, and establishing confidence in the model's outcomes.

This dissertation proposed solution introduces an explainable multivariate (Section 5.2.2) ML model that predicts frequency including other external features as post-modelling explanations for black-box models [122]. Deep learning models are employed for their strong performance and the ability to calculate SHAP values, which offer insights into predictions. SHAP stands for “SHapley Additive exPlanations” and draws from cooperative game theory’s Shapley values. These values gauge each player’s contribution within a coalition toward the final outcome while ensuring their combined contributions match that outcome. In the model explanation, SHAP values precisely quantify input feature impacts on individual predictions.

The advantages of SHAP values over alternative techniques include:

- **Global Interpretability:** Beyond displaying feature importance, SHAP values indicate whether a feature positively or negatively influences predictions.
- **Local Interpretability:** SHAP values enable the calculation of contributions for each prediction, offering insight into how features influence individual outcomes. This differs from techniques providing aggregated results for the entire dataset.
- **Model Versatility:** Unlike certain methods limited to specific model types, SHAP values accommodate various models, such as linear regression, XG-Boost, neural networks, and more.

In this work, the model takes input from meaningful features related to load, generation, and frequency time series. XAI approaches, including inherently transparent models and post-modeling explanations for black-box models [122], are used, with SHAP values offering a unified and consistent way to measure feature effects [123, 124]. The models are fed with significant input features derived from time series data related to load, generation, and frequency measurements. These models also allow for the quick and efficient computation of SHAP values [125], which help explain prediction outcomes.

## 5.5 Evaluation Metrics

The machine learning models can be compared to each other in a benchmark if tested under the same conditions. For this, a set of evaluation metrics has to be defined. They primarily consist of the difference between the forecast produced by the model and the ground truth, or label.

### 5.5.1 Mean absolute percentage error

In this dissertation, the Mean Absolute Percentage Error (*MAPE*) was used for probabilistic DLR performance evaluation. It is defined with Equation (5.24),

where  $\hat{y}$  is the predicted value,  $y$  is the true value, and  $N$  is the number of samples. This metric is expressed in percentage when multiplied by 100. It favors risk-averse systems. The *MAPE* gives importance to errors occurring at low current-carrying capacities, which have a higher probability of being reached in everyday operations.

$$MAPE = \frac{1}{N} \sum_{i=1}^N (y - \hat{y}) \quad (5.24)$$

### 5.5.2 Mean absolute error

Mean Absolute Error (MAE) was used to train the networks. Given that,  $\hat{y}$  represents the predicted value of  $i^{th}$  the sample and  $y_i$  is the true value, then the mean absolute error calculated over  $N$  is defined as

$$MAE = \frac{1}{N} \sum_{i=1}^N |y - \hat{y}| \quad (5.25)$$

### 5.5.3 Root mean squared error

Root Mean Squared Error (RMSE) was employed to evaluate the performance of various algorithms.

$$RMSE = \sqrt{\frac{1}{N} \sum_{i=1}^N (y - \hat{y})^2} \quad (5.26)$$

## 6 Machine Learning for Grid Frequency Deviation Predictions

Grid frequency is one of the observable variables that inform grid operators of the status of stability of the power grid. Based on frequency dynamics in the grid, the system frequency response action may activate certain frequency response services to maintain the frequency within acceptable limits or inform manual intervention in critical situations.

The Ethiopian National Load Dispatch Center (NLDC) operating procedure outlines the necessary actions for system operators to ensure network security in the case of contingencies. It also outlines the actions required to maintain system variables such as voltage, frequency, and current at nominal values during day-to-day operation. However, there are instances where the system operates beyond the initial planning assumptions. Deviations from the assumptions have consequences if not possible to identify in advance before it happen [126].

In Ethiopia, grid frequency encounters sudden changes due to factors such as load variations, generator outages, transmission line trips, and transformer failures [72]. Following the contingencies, in the time frame of seconds, governors in generators and certain loads automatically adjust to counteract frequency deviations. If the problem sustains for minutes, AGC action takes place to bring frequency to nominal operation. However, for large frequency deviations, additional frequency response services are deployed to restore the frequency deviation to setting limit [126].

## 6.1 Frequency variation pattern of Ethiopian grid

Frequency deviation reflects an imbalance in power generation and demand. Fluctuations in the demand directly affect the power balance, where demand forecasting errors and holiday events can lead to significant unexpected frequency deviations. The variability of renewable energy sources causes additional frequency fluctuations due to their intermittency or generation forecasting errors. Ethiopia's frequency deviation range is far wider with respect to German/European, and the frequency limit is illustrated in Table 6.1. For example, the operating frequency variation is set at  $\Delta f = \pm 0.50$  Hz from a nominal frequency of 50 Hz. Moreover, if the frequency deviates more than  $\Delta f = \pm 0.50$  Hz due to contingencies, the existing control systems, i.e., primary and secondary control, are activated to compensate for the imbalance in the power grid and to return the frequency to the nominal one.

**Table 6.1:** Frequency limits in the EEP transmission system.

Operating condition	Frequency limits
Under normal operation	49.50 Hz to 50.50 Hz
Under system disturbance	49.00 Hz to 51.00 Hz
Maximum band under fault system	48.75 Hz to 51.25 Hz
Under extreme system operation or fault condition	$f < 47.50$ Hz or $f > 51.50$ Hz for 20 sec.

Mostly the demand evolves continuously as shown in Figure 6.1 (blue color), however, Ethiopia's generation pattern is load-following, in which the generation follows the general trending of load pattern within the day. This is usually performed by involving the starting and stopping of quick-start hydro facilities. The spinning reserve strategy helps correct the load balance. Figure 6.1 shows a typical daily curve with a step-like generation of the Ethiopian grid.

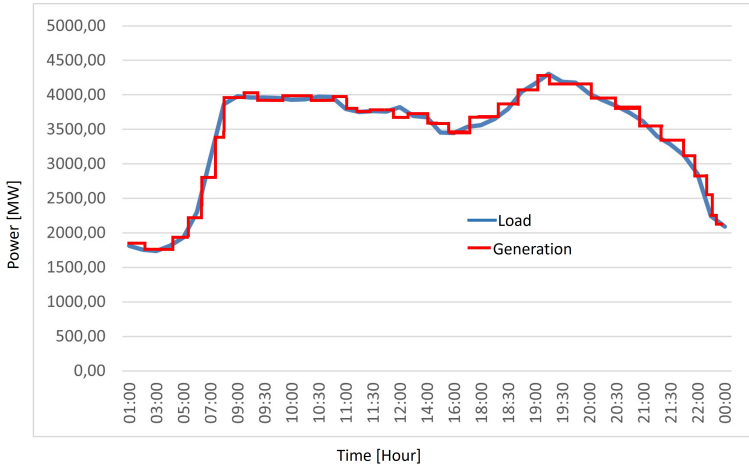


**Figure 6.1:** Load trajectory of the electricity supply in Ethiopia on January 28, 2020.

Furthermore, power generation exhibits discontinuous behavior due to renewable fluctuations, and the resulting changes in the power plant dispatch or spinning reservoir activation. As a result, the imbalance between the step-like behavior (Figure 6.1 (red color)) of the generation and the continuous behavior of the load leads to stochastic frequency jumps at the beginning of the generation response and spinning reserve response [56]. Figure 6.2 shows power grid frequency fluctuates over time in the Ethiopian grid system that exhibits non-deterministic frequency fluctuation behavior.

The nature of load and generation patterns in the grid suggests a strong real-time monitoring system is necessary for reliable supply. The frequency dynamic is time-sensitive and highly related to the balance between load and generation change. Ethiopia's grid has no well-established grid optimization system to handle sudden changes in the grid system. In this study, the focus is on improving the reliability of the Ethiopian grid network by utilizing a machine learning model for frequency fluctuation prediction.

Accurate frequency predictions enable precise active power balancing, and effective resource scheduling, so reducing the risk of outages. The critical task of

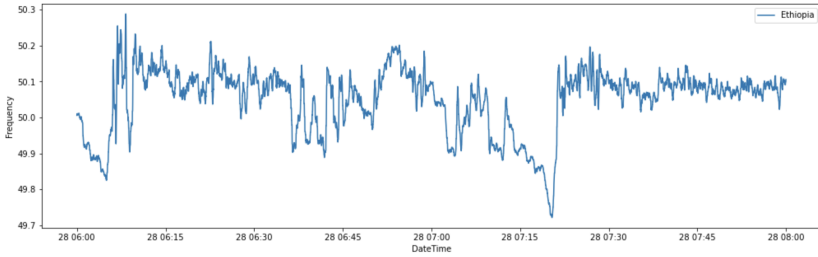


**Figure 6.2:** Illustration of power-grid frequency fluctuates overtime on December 18, 2020. The frequency characteristics are influenced by other external factors that are rather exhibiting a stochastic nature.

managing fast fluctuations in load or generation in a power system is achieved through centralized control centers sending control signals to generating units and responsive loads capable of fast adjustments. These strategies ensure balance during regular power system conditions. Practical tools to forecast power system frequency in the next few minutes can significantly aid grid operators in making timely and well-informed decisions. Frequency forecasting aids in understanding load trends and is vital for power system planning, and economic dispatch.

One typical grid disturbance occurred in Ethiopia on October 7, 2022, when a transmission line to Djibouti tripped at 3 pm as shown in Figure 6.3. The line trip caused generation at the center and the frequency rose to 50.84 above the normal operation. Due to this, Gilgel Gibe III (GGIII) hydropower generators were activated to reduce generation.

## 6.2 Feature engineering and data reconstruction

The necessary data for this dissertation was collected from Ethiopian Electric Power, Ethiopian Electric Utility, the Ethiopian National Meteorology Agency, and the Ethiopian National Load Dispatch Center (NLDC) office.

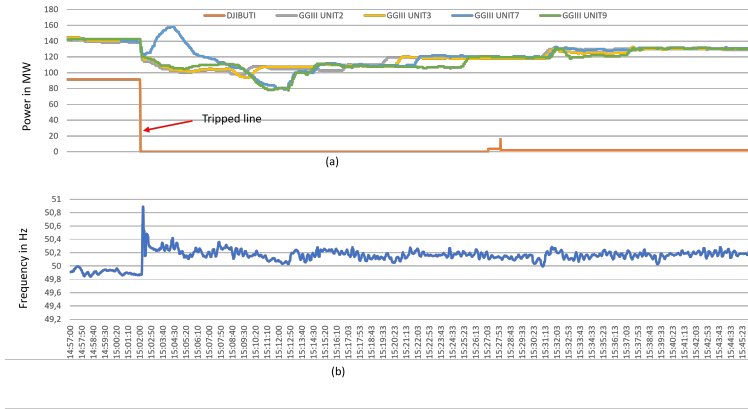


**Figure 6.3:** Grid outage disturbance due to transmission line to Djibouti trip. (a) Djibouti transmission line outage and Gilgel Gibe III (GGIII) units response, (b) Grid frequency response.

## 6.2.1 Data preparation

The time series data were normalized before training the deep learning networks. This involved creating the distribution of features between  $[-1, 1]$  as discussed in section 5.3.3. The maximum and minimum values of the data were recorded to be used later for the denormalization process of converting the predicted frequency value back to its original scale.

Two forms of data were considered data used in this dissertation, first historical frequency data which has a sampling rate resolution of one second, and second generation mix and load data that have a 15-minute resolution.

## 6.2.2 Feature engineering

Since the data for power grid frequency is in the form of a time series, time series forecasting techniques discussed in Chapter 5 were utilized. The machine learning algorithm learns from past and current observed values to make predictions for future frequency fluctuations. The algorithm undergoes a training process where

it learns the mapping function ( $Y = f(X)$ ) between input and output datasets, continuously adjusting its parameters to achieve accurate predictions. The workflow of the machine learning algorithm development in this work is illustrated in Figure 6.4.

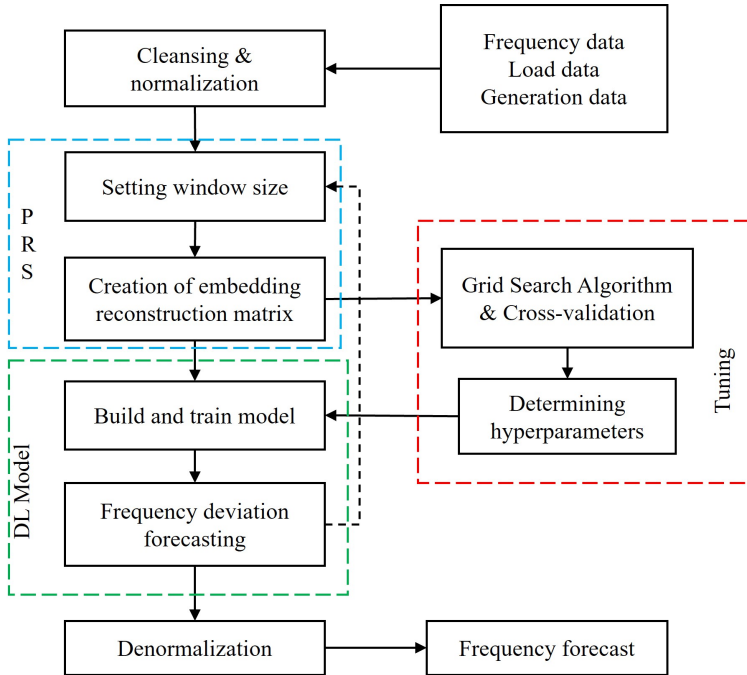


**Figure 6.4:** Flowchart of deep learning forecasting model development process.

After the scaling process, the dataset is categorized into specific time intervals. The optimal embedding dimension  $w = 30$  and prediction horizon  $h = 10$  were determined to incorporate richer temporal features by manual tuning. Then the deep learning model is constructed by using the embedding matrix formation (see Section 5.3) as the training and target set and employing grid research and cross-validation to optimize the hyperparameters of the network. Data was divided into 80% training and 20% testing for validation purposes then undergoing testing with

unseen datasets. The details of hyperparameter tuning were explained in Section 5.1.3. The trained deep learning model was adopted to predict the frequency value of future time steps.

Finally, the frequency deviation prediction value returned by the deep learning model was denormalized by applying the maximum and minimum values, and then the actual frequency forecasting value was obtained.

### 6.2.3 Data Reconstruction and learning phases

The fundamental assumption in supervised learning is the existence of an unknown stochastic dependency, which describes the relationship between the input variables  $x$  and the output (target) variable  $y$ . It can be represented as:

$$y = f(x) + e \quad (6.1)$$

where  $e$  represents the noise term, assumed to have a zero mean and constant variance. The noise term accounts for all unmeasured factors contributing to the variability of  $y$ . Additionally, we assume that each sample in the observed data  $D_N$  is independent and identically distributed, generated from the stochastic process described by  $f$ .

The step in developing the learning phase involves the creation of a structured dataset of the observable dataset into a higher-dimensional format suitable for a multi-step-ahead learning process. Figure 6.5 shows the form of the reconstructed dataset in a tabular form. The training set was defined as  $k$  samples. The test set  $N - (\omega - 1 + h)$  samples. For each network, a sequence  $X$  is randomly selected and prepared for training. The preparation involves defining an embedding window of size  $\omega = 30$  and several steps ahead  $h = 10$ , satisfying the conditions:  $h < \omega < k < N$ .

The generated dataset was represented as a structured matrix  $M \times D$ , where  $N$  is original dataset length,  $D = \omega + h$  and  $M = N - (\omega - 1 + h)$ , composed of  $M$  pairs  $\langle x_i, y_i \rangle$  (also named samples) of observations  $x_i$  and the corresponding

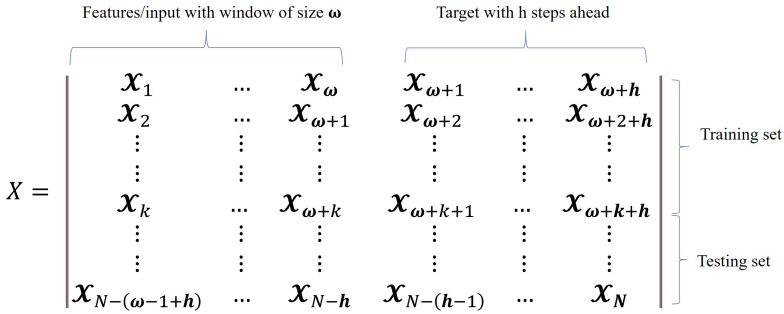


**Figure 6.5:** Example of generic dataset  $M \times D$  of  $M$  samples, resulting of feature engineering of the original  $N$  variables, split into a training set  $M_{train}$  of  $k$  training samples and a testing set  $M_{test}$  of  $M - k$  testing samples, where  $h < \omega < k < N$ .

targets  $y_i$ . Moreover, as part of the learning model, the dataset will be divided into two parts: a training set used for training the model parameters and a testing set used for validating its accuracy, to assess the performance and generalization ability of the trained model.

### 6.3 Determination of deep network structure

Deep learning models often require setting various hyperparameters. The effectiveness of adjusting these hyperparameters significantly impacts the accuracy of prediction models. Poorly chosen hyperparameters can result in a notable rise in prediction errors. The configuration of hidden layers in a deep neural network significantly impacts prediction outcomes. Finding the right balance is crucial to avoid under-fitting or over-fitting. Adjusting the number of hidden layers is more influential than the number of neurons within each layer, so neurons are kept constant to identify the optimum hidden layer. The number of hidden layer architecture were chosen based on empirical observations. To enhance prediction accuracy in the models, a cross-validation approach is employed to optimize these parameters. This is depicted as a red dotted line in Figure 6.4.

For the input layer of the models, since the original load data is input to deep learning models after passing through the embedding matrix, the number of the input layer neurons of models does not need to be tuned and can be directly set to embedding dimensions  $\omega$ . For the model output layer, when the model input is a row of elements in the embedding matrix, it is equivalent to input the position vector of the moving point in the embedding matrix at a certain moment. Then it needs to output the predicted value of the moving point position vector at the next moment. The optimum embedding window size and prediction horizon are set after optimum hyperparameters are determined.

To optimize the hyperparameters of the model, we perform a grid search over selected parameter values and evaluate the performance via 2-fold cross-validation on our training set. Then, we retrain the optimal model with optimal hyperparameters on the whole training set and calculate the ML prediction of the frequency deviations for every minute  $t_i$  in the unseen test set. We evaluate the performance on the test set using the RMSE.

We use rectifier linear units (*Relu*) in all the respective models. All models shared the same architecture and training approach, consisting of 2 hidden layers and a dense layer with a size equivalent to the number of steps ahead required for prediction.

We conduct experiments for hyperparameter optimization with the following parameter definition:

*batchsize* : [32, 64, 72, 128, 256],

*learningrate* : [0.01, 0.005, 0.001, 0.0005],

*neurons* : [64, 128, 256, 512],

*epochs* : [10, 20, 50, 80]

Finally, batch size = 64, epochs=50, learning rates = 0.005, and hidden neurons = 256 were chosen as hyperparameters.

The training and validation loss values are significant indicators that offer insights into the learning performance changes across epochs. They aid in identifying issues leading to underfitting or overfitting. The networks undergo 20 epochs of training using the Adam optimizer with learning rates  $\ell = 0.005$ . The primary objective is to minimize the Mean Squared Error (MSE) loss between the predicted values and the targets. The outcomes of the proposed models are graphically depicted in Figure 6.6, with the orange curve representing validation and the blue curve illustrating training. Notably, model results exhibit a high training accuracy of 98% and minimized training loss of 0.0028. This suggests favorable predictive outcomes, particularly for power grid system diagnosis.

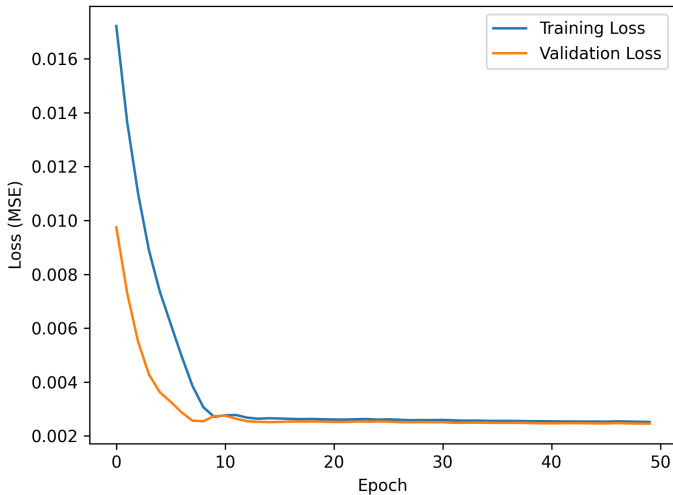


**Figure 6.6:** Training and validation loss values over several training epochs.

## 6.4 Model evaluation for frequency forecasting

The study evaluates various deep learning models including LSTM, Bi-directional LSTM, Encoder-decoder LSTM, GRU, and CNN. While their error range and prediction accuracy are comparable, the Encoder-decoder LSTM (ED-LSTM) performs best in prediction accuracy, while CNN excels in computational speed, showing its practicality in real-world applications. For this purpose, we measure the computation time of the proposed forecasting methodology in generating a forecast for the minutes ahead. The time required to calculate each sample is just 8 milliseconds (ms) with Intel(R) Xeon(R) CPU E5-2699A v4 @ 2.40 GHz with 8 GB RAM, which proves that the proposed given models can be used for real-time frequency dynamics diagnosis using Python scripts.

The MSE was utilized for training the networks, while RMSE was employed as the performance evaluation metric among different algorithms. Performance metrics are based on multi-step frequency predictions compared to empirical benchmarks like the naïve persistence model (NPM), where the forecast for the next period is simply the same as the current period's value. The lower RMSE values indicate better performance. We used the RMSE (see section 5.5) as the main performance measure for the different prediction horizons in test data. Table 6.2 illustrates the result for the simulated frequency prediction in terms of the RMSE, where the lower values indicate better performance.

**Table 6.2:** Forecasting performance evaluation in terms of RMSE.

Model used	RMSE (%)				
	1min ahead	3min ahead	5min ahead	7min ahead	10min ahead
LSTM	0.0953	0.1101	0.1113	0.1253	0.1478
GRU	0.0915	0.1234	0.1245	0.1277	0.1527
BD-LSTM	0.0904	0.1092	0.119	0.1252	0.1476
ED-LSTM	0.0881	0.1054	0.1071	0.1186	0.1391
CNN	0.0749	0.1087	0.1227	0.1298	0.1493
Benchmark	0.0592	0.1022	0.1257	0.1395	0.1656

For verification, the RNN models and CNN model are tested alongside the benchmark to predict the frequency of December 28, 2020, using historical data from December 27 as a training dataset from Ethiopian Electric Power. As illustrated in Figure 6.7 there is a decline in prediction accuracy as the prediction horizon increases, yet deep learning techniques still outperform the benchmark, with ED-LSTM being the most effective.

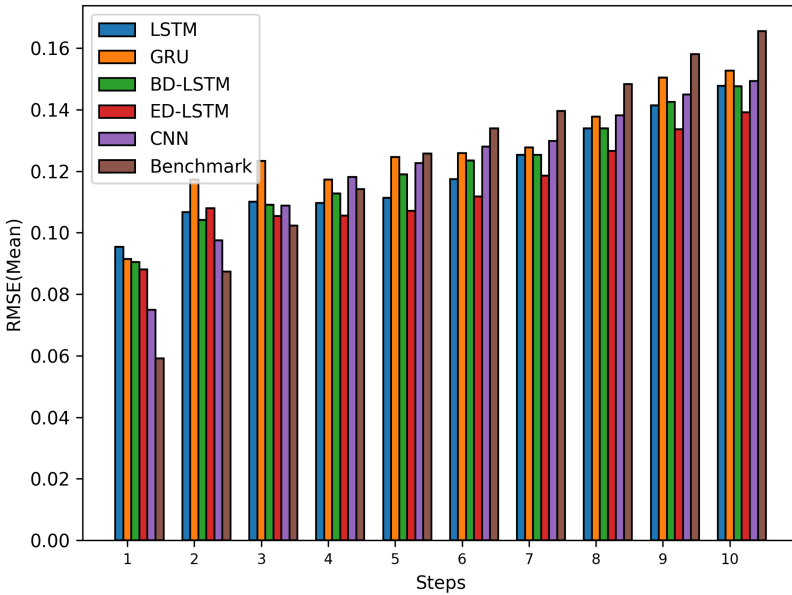


**Figure 6.7:** 10-step ahead prediction performance evaluation in terms of RMSE as error bars.

The graph illustrated in Figure 6.8 presents the predicted frequency values compared to actual measurements for 2- steps ahead for the December 28, 2020, measurement. Figure 6.9 illustrates 10-steps ahead of a 30-minute frequency forecast that follows the general trend of the actual frequency measurements, furthermore, it shows frequency prediction deterioration as the prediction horizon increases.

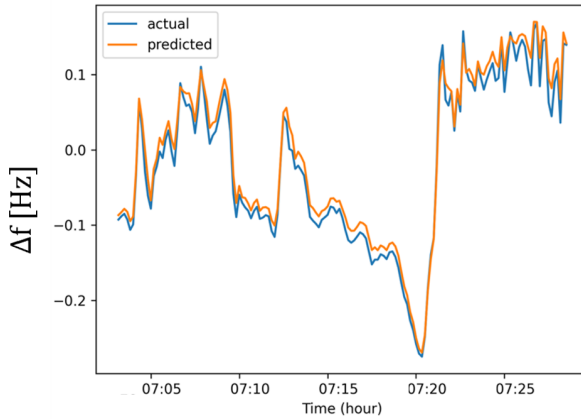


**Figure 6.8:** Example of 30-minute frequency forecast for 2-steps ahead for interval 7:00 a.m.-7:30 a.m. on December 28, 2020. Where  $\Delta f = f - f_0$ ,  $f = 50$

## 6.5 Model prediction explanations

Understanding the dynamics of the power grid, including its frequency, is crucial for the safe operation of existing and future power grids. In section 6.4 historical frequency data has been the basis for forecasting frequency time series. Yet, there's a query: How might we incorporate extra details, such as generation mix or power demand changes? Figure 6.10 depicts the influence of generation changes and line trips on frequency.

To improve the accuracy of the power grid frequency fluctuation forecast, a new post-disturbance power grid frequency forecast model in multidimensional scenarios was proposed in this dissertation. A predictive model, specifically the CNN model, was employed to make predictions, and the aim is to explain these predictions using a technique called SHAP values [124]. These values were calculated on a test dataset to provide insights into the CNN model's predictions. They quantify how different features related to generation and load impact the model's predictions across various time points. This model used a dataset with a 15-minute resolution, which was selected due to the availability of external

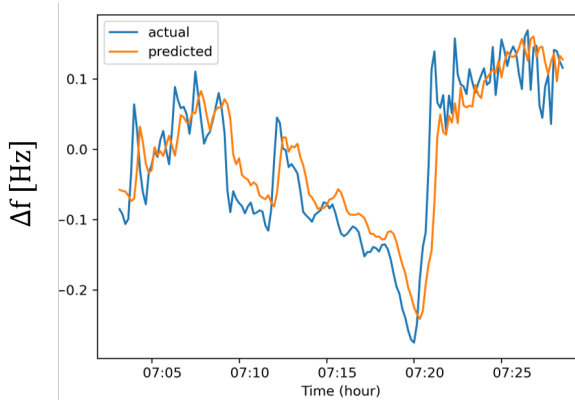


**Figure 6.9:** Examples of 30-minute frequency forecast with 10-steps ahead predictions for interval 7:00 a.m.-7:30 a.m. on December 28, 2020. Where  $\Delta f = f - f_0$ ,  $f = 50$

data, such as load and generation information from the Ethiopian Electric Power company, at this granularity and frequency data was also downsampled to 15 minutes. By leveraging the SHAP method and employing multivariate predictions, the intention is to enhance the understanding of the CNN model's predictions and unveil the factors contributing to deviations in power grid frequency.

The input matrix for the forecasting methodology is denoted as  $X$ , defined as a matrix composed of three components: power system frequency ( $f$ ), power system load ( $P$ ), and power system generations ( $G$ ) with 20 elements. This matrix is processed sequentially by the neural network in the proposed methodology.

Global explanations of the model's predictions highlight significant features using different representations, such as the normal summary plot and the bar summary plot. The normal summary plot, illustrated in Figure 6.12, showcases the top twenty influential features of the CNN model and their effects on the predictions. This plot compares the importance percentages categorized by feature types in a frequency prediction model. It showcases the significance of each feature in predicting frequencies. It sorts the features by decreasing order. The graph reveals that the Gibe III feature exerts the most substantial influence on predictions,

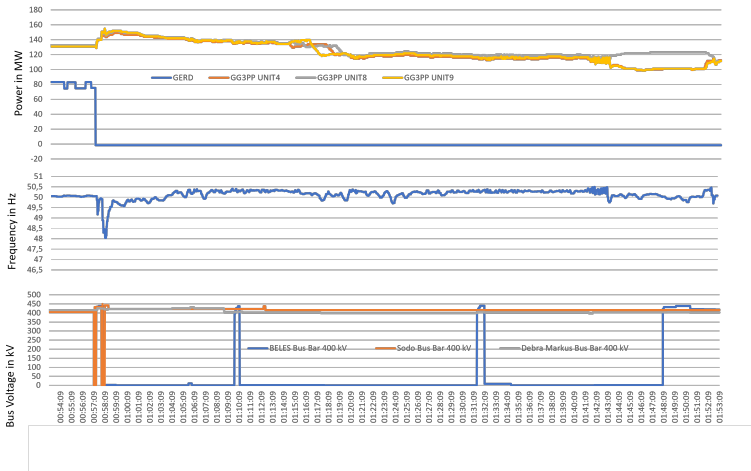


**Figure 6.10:** Illustrates some additional information for grid frequency perturbations. Measurement was taken from a disturbance that occurred in Ethiopia’s grid on May 11, 2022. GERD generator loss triggered overload or power shortage, so frequency declined in response and led to a transmission line trip that extended to Beles bus bar.

followed by total load and aggregate scheduled generation, both of which also have a noteworthy impact. Conversely, the Tis Abay II feature contributes the least to frequency prediction. The features Adama Wind II and Genale Dawa exhibit a nearly identical effect on frequency prediction. Importantly, this plot solely focuses on elucidating the importance of features and does not encompass other aspects.

The feature importance plot is solely informative about feature significance, lacking additional details. Contrarily, the summary plot integrates both feature importance and their effects. Every point on this plot denotes a Shapley value corresponding to a feature and instance, positioned along the y-axis by the feature and along the x-axis by its Shapley value. Additionally, color coding reflects feature values, varying from low to high. To address overlapping points, they’re dispersed along the y-axis to visualize the distribution of Shapley values per feature. These features are arranged in order of their importance. Figure 6.12 illustrates an alternative representation of the summary bar plot, known as a feature-importance

plot. Essentially, the normal summary plot illustrates predictions by revealing the importance of features and how they affect prediction outcomes.

For example, high values of the Adama Wind II variable have a high negative contribution to the prediction, while low values have a high positive contribution. High values of GIBE III, scheduled generation, and total active load have a high positive contribution to the frequency deviation prediction, whereas low values have a negative contribution. Gibe III hydro plant, total scheduled generation forecast, and active load have the most impact, causing predictions to increase with lower values. Conversely, the Tis Abay II feature has minimal impact on prediction frequency. Changes in Adama wind II generation lead to lower predictions for higher values and vice versa. The influence of smaller power generation plants like Tis Abay II and Ashegoda Wind on predictions is relatively limited, whether its values are high or low. Higher Melka Wakena values result in higher predictions, while increased Genale Dawa values lead to lower predictions.

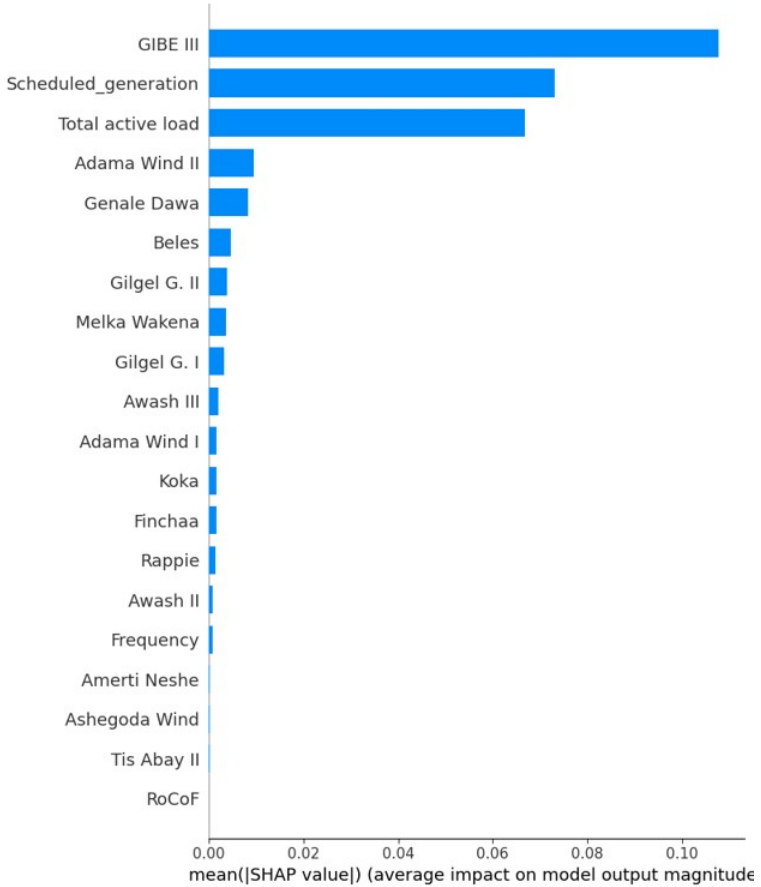


**Figure 6.11:** Model summary bar plot for identification of predictors of frequency deviation predictions. The SHAP feature importance as the mean absolute Shapley values. The amount of Gibe III was the important feature, changing the predicted absolute frequency deviation probability on average by 11% (0.011 on the x-axis)

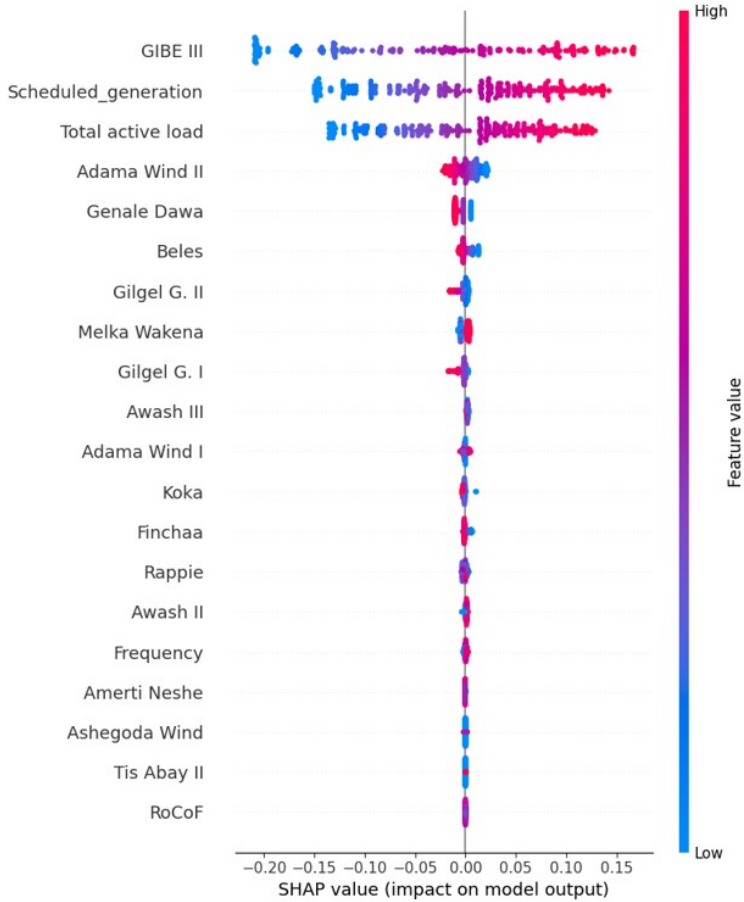


**Figure 6.12:** Effect of different generations and total active load on the frequency deviation predictions. The summary plots illustrate how SHAP effects impact frequency deviations, which have been normalized by their highest absolute value for better clarity and visualization.

# 7 Dynamic Line Rating for Overhead Transmission Line Monitoring

The current-carrying capacity of a transmission line conductor is set by utilities during design time as a static value based on worst-case weather conditions, the so-called, Static Line Rating (SLR). For Ethiopian utility, conservative weather conditions for calculating the thermal capacity of the conductor are shown in Table 7.1.

**Table 7.1:** Surrounding weather conditions.

Items	Figures
Thermal emissivity	0.9
Solar radiation energy	$0.09 W/cm^2$
Wind velocity	0.6 m/s
Ambient Temperature	$25^{\circ}C$
Allowable Temperature	$75^{\circ}C$

Instead of relying on conservative assumptions that only apply a few days a year, Dynamic line rating (DLR) can be applied to continuously monitor the thermal rating of overhead power lines which is tremendously varying throughout the day due to its dependence on weather conditions [127]. This involves installing temperature sensors on the conductor or using nearby weather stations to gather data. By utilizing this data information, utilities can calculate the dynamic change

in the current-carrying capacity of the line. However, the significant temporal variations in the thermal rating pose challenges for operators to fully utilize the benefits of DLR in real-time [128]. Figure 7.1 illustrates the variation in current-carrying capacity over time for a specific overhead line in the case study mentioned in the dissertation. The graph illustrates a significant fourfold increase in the line’s transmission capacity, occurring approximately at 7 AM.

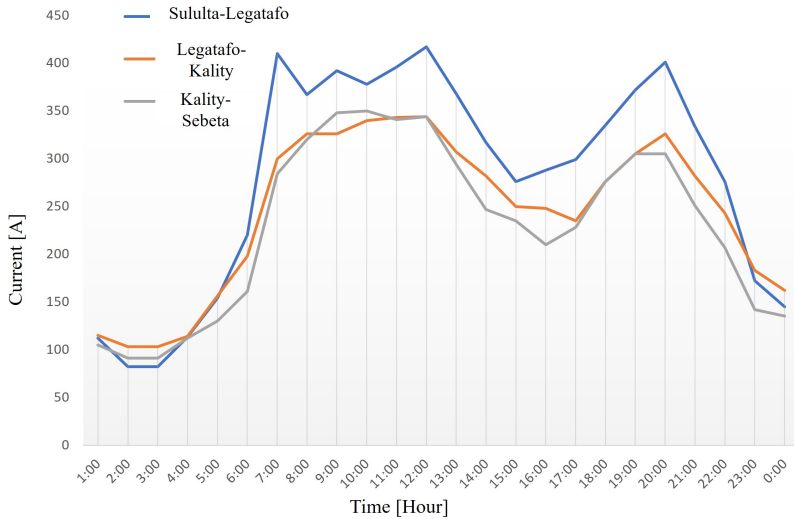


**Figure 7.1:** Sample of current variation throughout the day for three different transmission lines.

DLR offers a more accurate assessment by addressing both the issue of underutilizing transmission capacity and the potential hazards linked to surpassing rated capacity. DLR inherently improves the efficiency of transmission line operations and boosts the network’s ability to manage issues after contingencies. As a result, utility companies can make the most of their current infrastructure and prevent expensive upgrades. Furthermore, the likelihood of overloading the line, leading to power outages or service interruptions, is significantly reduced. In the short-term

plan strategy, there is a possibility to delay or push back investments intended for enhancing transmission line infrastructure.

## 7.1 Thermal rating of overhead lines

DLR involves monitoring the capacity of power lines by analyzing the heat balance of the conductor at each time step and considering weather and system conditions. The thermal heat balance OHTL equation is used to calculate the temperature of a transmission line based on the heat generated by current flow and the heat dissipated through various mechanisms [129]. Two prominent models developed by IEEE and CIGRE are used for calculating the line's heat balance, particularly for overhead lines. The heat balance analysis takes into account factors such as ambient temperature, solar radiation, wind speed, and other relevant parameters to determine the safe operating capacity of the line.

Due to the principles of thermodynamics, the temperature variation of an overhead line is influenced by the exchange of heat between the line and its surrounding environment. This heat balance can be described using Equation (7.1), which considers the heat gained from the Joule effect, magnetic heating, and solar radiation, as well as the heat lost through radiative, convective cooling, and evaporative cooling. The balance between these heat gains and losses determines the change in temperature of the conductor over time. The conductor's temperature change is further influenced by its mass per unit length ( $m, kgm^{-1}$ ) and its heat capacity ( $c, Jkg^{-1}K^{-1}$ ).

Heat balance of the overhead transmission line, according to the CIGRE loading guidelines [130] is defined as:

$$mc \frac{dT_c}{dt} = P_J + P_S + P_M + P_i - P_c - P_r - P_{ev} \quad (7.1)$$

where  $P_J$  is a Joule heating,  $[W/m]$ ,  $P_s$  is a solar heating,  $[W/m]$ ,  $P_c$  is a convective cooling,  $[W/m]$  and  $P_r$  is a radiative cooling,  $[W/m]$ ,  $P_M$  is magnetic

heating,  $[W/m]$ ;  $P_i$  is a corona heating,  $[W/m]$  and  $P_{ev}$  is an evaporative cooling,  $[W/m]$ .

Solving Equation (7.1) involves analyzing the conductor's temperature in an unsteady state or transient analysis. This approach captures the dynamic behavior of temperature changes over time. Alternatively, a steady-state solution ( $\frac{dT_c}{dt} \rightarrow 0$ ) can be employed to determine the maximum temperature the conductor can reach, assuming the surrounding conditions remain constant for an extended period.

### 7.1.1 Joule heating

Joule heating represents the heat generated by the current flow in the conductor. As current flows through the line, it encounters resistance, resulting in the generation of heat. The heat generated is proportional to the square of the current and the resistance of the line and can be represented as:

$$P_J = I^2 R_{dc} \quad (7.2)$$

where  $I$  is the root-mean-square (RMS) value of AC current flowing through a conductor ( $A$ ),  $R_{dc}$  is the DC resistance per unit length ( $\Omega m^{-1}$ ) solved as,

$$R_{dc} = R_{20}(1 + \alpha(T_c - 20)) \quad (7.3)$$

where  $R_{20}$  is the conductor AC resistance at 20 °C ( $\Omega, m^{-1}$ ),  $\alpha$  is the temperature coefficient of resistance ( $K^{-1}$ ),  $T_c$  is the average temperature of aluminum strand layers ( $^{\circ}C$ ). The catalog value of conductor DC resistance represents maximum aluminum resistance after stranding at a certain temperature, most often 20°C.

### 7.1.2 Convective cooling

Convective cooling represents the heat dissipated through convection. Convection refers to the transfer of heat through the movement of air around the transmission

line. It is the most important cooling factor for overhead transmission lines. The amount of heat dissipated through convection depends on factors like the temperature difference between the line and the surrounding medium, the velocity of the fluid or air, and the surface area of the line.

$$P_c = \pi\lambda(T_c - T_a)N_u \quad (7.4)$$

Where  $T_a$  is the ambient temperature in ( $^{\circ}C$ )

The formula describes the relationship between the thermal conductivity of air ( $\lambda$ ,  $Wm^{-1}K^{-1}$ ), the temperature difference between the conductor and ambient, and the dimensionless Nusselt number ( $N_u$ ).

The thermal conductivity of air ( $\lambda$ ) represents how efficiently heat is transferred between the surface of the transmission line and the surrounding air. It is influenced by factors such as air velocity, temperature gradient, and the physical properties of both the air and the transmission line surface.

$$\lambda = 2.368 \times 10^{-2} + 7.23 \times 10^{-5} \times T_f - 2.763 \times 10^{-8} \times T_f^2 \quad (7.5)$$

where  $T_f = \frac{1}{2}(T_c - T_a)$  for  $T_f < 300^{\circ}C$

The value of the Nusselt number is influenced by the wind conditions, specifically whether the heat transfer occurs through natural convection or forced convection.

### 7.1.3 Radiative cooling

This term represents the heat dissipated through radiation. Radiation refers to the heat transfer through electromagnetic waves emitted by the transmission line. The amount of heat dissipated through radiation depends on factors such as the temperature of the line and its surface characteristics, including emissivity.

The radiative cooling equation is typically given as:

$$P_r = \pi D \sigma_B \epsilon_S [(T_c + 273)^4 - (T_a + 273)^4] \quad (7.6)$$

Where  $D$  is the conductor diameter ( $m$ ),  $\sigma_B$  is Stefan-Boltzmann constant,  $\epsilon_S$  is the conductor surface emissivity.

### 7.1.4 Solar heating

Solar heating describes the phenomenon of solar radiation heating transmission lines in power grids. When sunlight interacts with the conductors and structures of the transmission lines, some of the solar energy is absorbed, resulting in temperature rises along the line. This phenomenon can be mathematically represented by the transmission line solar heating equation:

$$P_s = \alpha_s DS \quad (7.7)$$

where  $D$  is conductor diameter( $m$ ),  $\alpha_s$  is the absorptivity factor (with values between 0.2 and 0.9), and  $S$  is the solar irradiance ( $Wm^{-2}$ ).

Solar irradiance represents the amount of solar radiation incident on the transmission line surface. It depends on factors such as time of day, season, cloud cover, and geographic location.

### 7.1.5 Current-carrying capacity

The current carrying capacity of an overhead line, also known as ampacity, can be calculated from the heat balance equation considering that the steady state condition applies, i.e., the conductor has reached its maximum permissible temperature ( $T_c = T_{c,max}$ ). Inserting the Joule heating Equation (7.2) into Equation (7.1) and considering  $\frac{dT_c}{dt} \rightarrow 0$  (steady state),

$$0 = I_{RMS}^2 R_{dc} + P_S + P_M + P_i - P_r - P_c - P_{ev} \quad (7.8)$$

While all other heat balance components in equation (7.1) play a significant role in heat balance, the effect from magnetic, corona heating, and evaporative cooling

have a less substantial impact on the resulting current and conductor surface temperature and Equation (7.1) is expressed as:

$$m_c \frac{dT_c}{dt} = P_J + P_S - P_c - P_r \quad (7.9)$$

Each part of the heat balance equation is a function of several parameters that determine the current-temperature relation for each time instant. The steady state, heat balance as a function of weather and load conditions, is then defined by

$$P_J(I_{RMS}, T_c) + P_S = P_c(T_a, T_c, V_{speed}) + P_r(T_a, T_c) \quad (7.10)$$

where  $T_a$  is an ambient temperature [ $^{\circ}C$ ];  $T_c$  is the conductor temperature [ $^{\circ}C$ ];  $V_{speed}$  is a wind speed [ $m/s$ ].

By substituting Joule heating Equation (7.2) into Equation (7.10) as current magnitude can be expressed

$$I_{RMS} = \sqrt{\frac{P_c + P_r - P_S}{R(T_{avg})}} \quad (7.11)$$

where  $R(T_{avg})$  is the AC resistance per unit length at the temperature  $T_{avg}$  ( $[\Omega/m]$ );  $T_{avg}$  is the average temperature across the conductor's cross-section ( $^{\circ}C$ )

By combining equation (7.10) and (7.11), the effective current can be represented as a function of ambient conditions and pre-defined system parameters as:

$$I_{RMS} = \sqrt{\frac{P_c(T_a, T_s, V_{speed}) + P_r(T_a, T_s) - P_S}{R(T_a, T_c)}} \quad (7.12)$$

The maximum current rating of the overhead transmission line at each time step is a function of the weather parameters such as ambient temperature, wind speed, wind direction, and solar radiation, and of maximum allowable temperature limits for Overhead transmission lines. The maximum allowable temperature of the line

is different for power networks in different countries, and is usually chosen to provide high safety of operation. By using equation (7.12) and a constant value for maximum allowable conductor temperature  $T_c^{max} = \text{constant}$ , the maximum allowable conductor current can be represented by,

$$I_{RMS} = \sqrt{\frac{P_c(T_a, T_c, V_{speed}) + P_r(T_a, T_c^{max}) - P_S}{R(T_a, T_c^{max})}} \quad (7.13)$$

and can be further simplified to,

$$I_{RMS} = \sqrt{\frac{P_c(T_a, V_{speed}) + P_r(T_a) - P_S}{R(T_a)}} \quad (7.14)$$

## 7.1.6 Dynamic state

The steady-state method provides a convenient and straightforward approach to determine the allowable ampacity based on weather conditions. However, this method overlooks the thermal inertia of the power line. The knowledge of the conductor temperature over time gives TSOs the flexibility to solve momentary congestion cases, without reaching the maximum conductor temperature. The time-dependent conductor temperature is obtained from the heat Equation (7.9) given the electrical current and the weather conditions during the period of study. It is a non-linear ordinary differential equation and can be solved either by numerical integration or by linearizing the radiative cooling term [131, 132].

The Cigre-601 method suggests that this equation can be solved numerically to calculate the temperature of the line, with 5-15 minute time steps as suitable [8]. However, it is not suitable to use this method for fault current applications. In these cases, due to the short time frame of a high current fault, it is more suitable to consider adiabatic conditions.

## 7.2 State-of-art conductor dynamic line rating

There are also plenty of technologies [133, 134] used for the exploitation of overhead dynamic line ratings, for instance, sag-based techniques that monitor the sag of the conductors through optical sensors [135], tension-based techniques which use sensors installed on OHTLs to determine the tension of the conductor [136, 137], temperature-based techniques that monitor the operating temperature of the conductor through sensors installed on the OHTLs [138–140] and current rating-based methods that calculate the maximum current rating by monitoring or estimating the weather conditions and feeding them into one of the standard models. The last category, the main focus in this work for its interesting features and direct link between the thermal states of overhead conductors and energy harnessed from intermittent renewable resources.

DLR can be classified as indirect or direct dynamic rating methods. Direct dynamic line rating (DLR) methods involve installing measuring devices directly at the location of the line span or on the line itself, providing higher accuracy and real-time information but requiring a larger investment and more complex installation. Indirect DLR methods, such as numerical weather models (NWM) and weather forecasts (WF), utilize existing historical weather data and existing weather measuring devices located at sites. Although indirect methods may not offer high accuracy and have limitations on maximum ratings, they require lower investment and can be installed easily.

One example of a direct DLR technique is Power Donut, the first commercial system to be directly installed on the conductor, monitoring conductor temperature that translates to conductor sag value [140]. Other sensor systems, like the Emo System and Overhead Transmission Line Monitoring (OTLM) sensor system, measure conductor temperature from a single spot. Indirect temperature measurement systems, such as Ampacimon and Astrose, use low-frequency mechanical vibrations or sensor node angles to derive line sag and conductor temperature.

Optical systems, such as LiDAR<sup>1</sup> developed by Lindsey, also plays a great role in Overhead line monitoring (OLM). It is installed on electrical towers or on the ground, simplifying installation and maintenance. However, careful calibration and model checking is necessary to ensure accurate observations. An example of each measuring sensor device is shown in Figure 7.2.

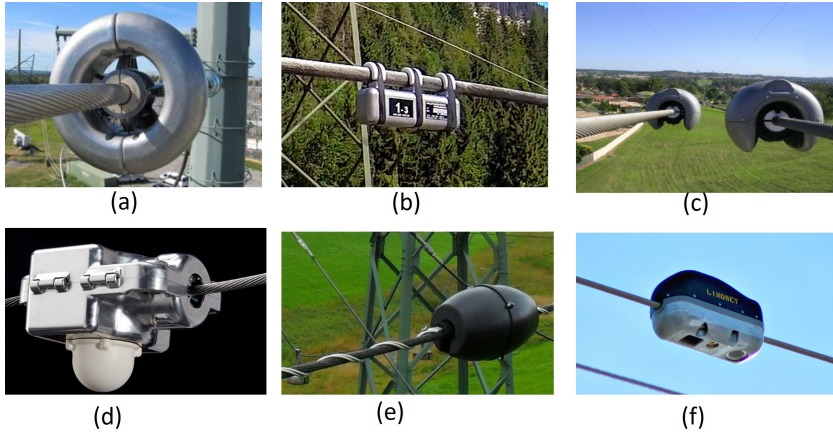


**Figure 7.2:** Overhead line monitoring sensors:(a)Power Donut [141];(b)Emo system [142];(c)OTLM [143];(d)Ampacimon [144]; (e)Astrose [145];(f)Lindsey-TLM sensor [146].

OLM systems have been available for many years but have not been widely applied in electrical system operations due to the challenges of temporal variations in thermal rating [128]. Recent efforts have focused on current-carrying capacity forecasts, allowing TSOs to plan power plant relaxed operation in advance.

<sup>1</sup> LiDAR stands for Light Detection And Ranging. It is a remote sensing method that uses light in the form of a pulsed laser to measure distances to objects or surroundings.

## **8 A Methodology for Assessing Risk of Dynamic Line Rating Utilization**

Managing power flow in transmission networks amidst the increased integration of renewable energy sources and the limitations in constructing new transmission corridors due to financial constraints and social opposition requires innovative strategies.

Recently, Ethiopia has witnessed a significant rise in energy demand driven by various factors, including universal electrification, rapid industrial park development, extensive agricultural irrigation schemes, and plans for power exports to neighboring countries [27]. The Ethiopian government has been heavily investing in renewable power generation to meet the growing energy demand. However, large-scale renewable power generation faces challenges from transmission and distribution network development due to line overloads and network congestion caused by limited network capacity. Expansion of the transmission and distribution grid infrastructure poses economic, social, and political challenges for the country. To address this, the nation should look for innovative approaches that optimally use the current transmission and distribution grid systems. Constructing new transmission lines is complex due to land rights, high cost, and project time requirements factors. To overcome this issue, this dissertation proposed a real-time overhead transmission line monitoring scheme for congestion monitoring at high-load centers. Furthermore, shorter transmission lines covering distances of just a few tens of kilometers are constrained by thermal factors [147]. Real-time

weather conditions significantly affect the heat-handling capabilities of overhead lines [8].

Effectively controlling the thermal capacity of power lines through dynamic line rating (DLR) is a method that involves continuously monitoring the temperature of the lines and the weather conditions surrounding them. This approach ensures the safe operation of power grids. Furthermore, by using DLR, it becomes possible to utilize the increased thermal capacity of overhead lines when weather conditions are favorable, thus optimizing their performance through dynamic management and allowing for maximum accommodation of renewable power in the existing grid before considering new line expansions. This approach also opens up alternative investment options, such as short-term expansion planning.

Despite DLR advantages for monitoring ampacity, including AC-Optimal Power Flow [148] and economic optimization [149], there will always be uncertainty in line rating [150, 151]. Understanding the advantages of DLR under various sources of uncertainty is crucial for optimizing grid operations and enhancing power system reliability. This dissertation recognizes the presence of forecast uncertainty and aims to incorporate the most realistic inputs possible. Studies in this area focus on accurately modeling DLR through probabilistic forecasting methods, taking into account feasible risks, rather than relying solely on point estimates from deterministic forecasts with no indication of the distribution of possible errors [152–154].

## **8.1 Probability-based dynamic line rating models**

Transmission System Operators (TSOs) rely on accurate predictions of the current-carrying capacity to effectively plan power generation and prevent congestion in the electrical grid. The capacity of transmission lines is influenced by local weather conditions, which can vary based on factors such as vegetation, mountains, and rivers in the surrounding topography. To obtain precise predictions, combining

weather measurements taken along the transmission lines with meteorological prediction models is crucial. This combination enables TSOs to acquire reliable estimates of the current-carrying capacity, empowering them to make informed decisions regarding power generation and grid management.

Deterministic models were largely presented in CIGRÉ and IEEE models, and a probability-based model was developed in this study. Probability-based models offer advantages due to their ability to work with distributions that provide more accurate descriptions of environmental and load conditions. These models also allow for the inclusion of a risk factor associated with these probabilities, providing additional information for system operators. The conductor temperature depends on five main factors, including four environmental variables (wind speed, wind direction, ambient temperature, solar radiation) and one load variable (conductor current). To calculate conductor temperature and DLR, accurate predictions for these environmental variables are necessary.

Figure 8.1 depicts the sequential steps followed in this case study. The dataset employed for this case study encompasses weather observations, weather forecasts, conductor properties, and the corresponding current-carrying capacities for design time weather conditions. The data has been formatted to train and test machine learning models. Finally, the dataset is organized as a two-dimensional structure, comprising timestamps and weather parameters such as ambient temperature, wind speed, wind direction, and solar radiation.

The model considered in this work utilizes two distinct sources of information: weather observations collected from nearby weather stations and corresponding weather extrapolation along overhead lines. Since there are no direct weather stations along OHTLs, weather extrapolation was employed for the case study. The machine learning model then extracts useful information from weather observation and forecasts to generate dependable current carrying capacity predictions from the thermal model of the conductor.

The attainment of accurate results depends on the utilization of appropriate pre-processing methods and machine learning algorithms. Quantile Regression Forests (QRF) [115] have been utilized to develop a model that can predict the

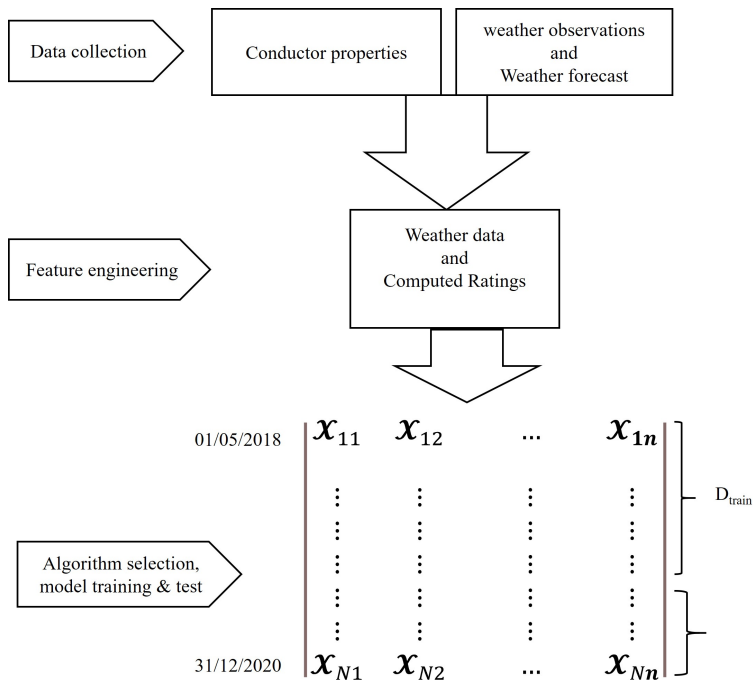


Figure 8.1: Summary of machine learning forecast model.

ampacity of OHTL with a two-year dataset. QRF is chosen over other machine learning techniques due to its ability to incorporate variables outside the point forecast, making it useful in understanding non-normally distributed, and non-linear outcomes associated with weather forecasting uncertainties. The aim is to implement a DLR algorithm for the Ethiopian power grid, specifically to monitor congestion at high-load centers.

## 8.2 Dynamic line rating integration into Ethiopian grid

As explained in chapter 2, the power demand in the capital city and the surrounding area is anticipated to rise significantly, from 835 MW in 2014 to 3,576 MW in 2034, due primarily to population growth and development plans [37]. To address this issue, there has been a significant amount of investment in the power sector, resulting in the establishment of new power plants, and an increase in the power generation capacity of existing stations. However, it has been observed that the construction of transmission and distribution networks, including substations, has not kept pace with the rapid economic growth and demand rise. To support future economic growth, it is essential for the power sector in Ethiopia to prioritize the improvement of transmission and distribution networks. One option could be the construction of new lines to cope with power demand growth in the future. However, this will take intensive investment and time. Another option which is the main focus of this dissertation is to exploit the latent current-carrying capacity of existing overhead transmission lines. It takes into account applying DLR in real-time rather than SLR, line ampacity forecast, and power flow analysis. Probabilistic forecasts for the current rating of transmission lines are generated, paying particular attention to the reliability of the lower part of the probabilistic distribution to reduce the risk of prediction error [155].

Long-distance transmission lines are transporting high power lines to the high-load area in the Ethiopian grid system. Those transmission lines at the load center are associated with the most severe line overload/congestion, or sometimes result in partial or total blackout in the country. These line overloads are predominantly along the highest voltage transmission lines (400 KV & 220 KV) connecting the regional power systems of the country to Addis Ababa, the capital. Almost all the line overloads affect the high-load centers, i.e., Addis Ababa and central regions. The loading violation contingency is up to 204.1% for the most severe line outages [72].

The main high-voltage transmission grid of the Ethiopian grid and this dissertation interest area is shown in Figure 8.2. Implementation of DLR all over transmission lines is not a wise idea, as it is not cost-effective. Therefore, it is good to apply DLR to specific lines (or hotspots) that have economic benefits and a high probability of high current flow or congestion. Consequently, the 220 KV lines that transport electricity to Addis Ababa and the central part of Ethiopia are the most important transmission lines and were considered in this dissertation for the evaluation of DLR. They connect high-power transmission lines from hydropower generators and wind farms to high-load centers, which leads to a high probability increase in the ampacity that leads to most blackouts in the country.

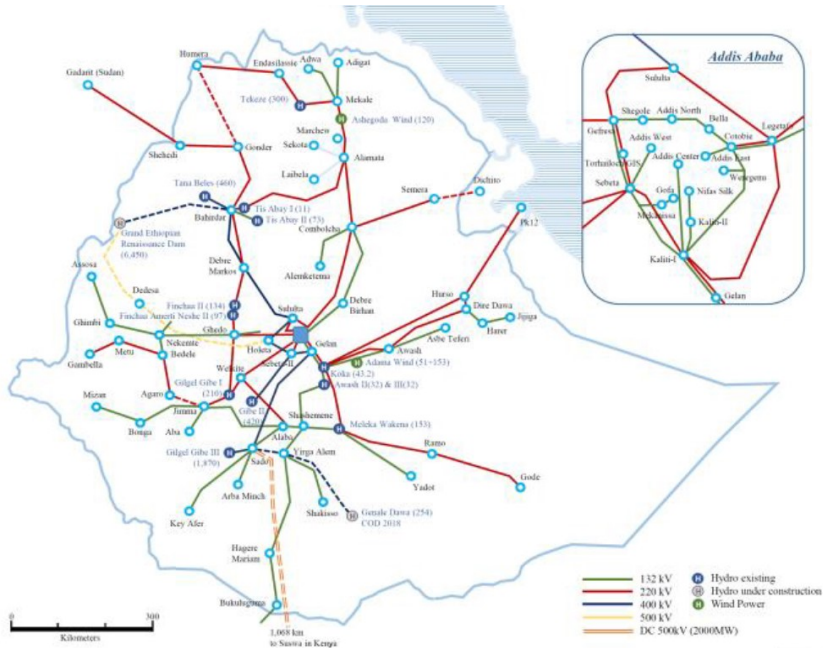
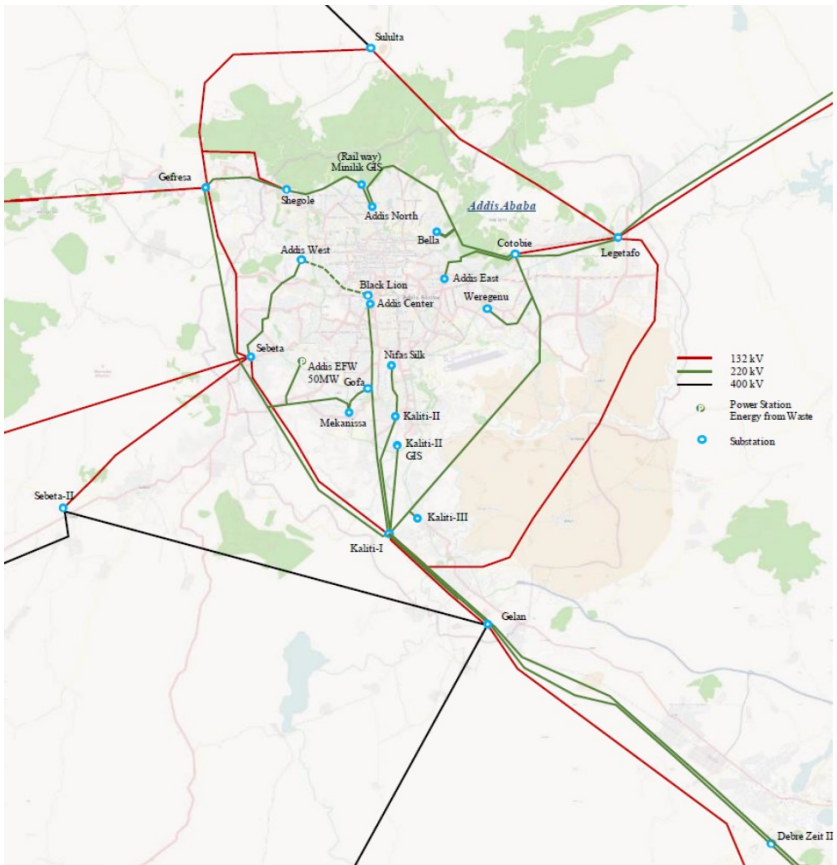


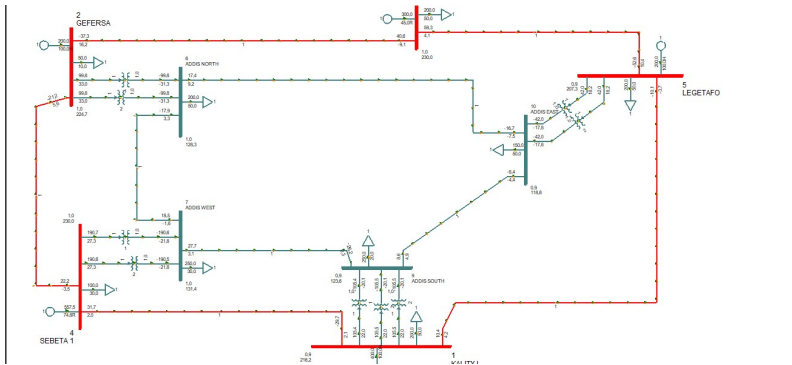
Figure 8.2: High Voltage Grid layout of the Ethiopian grid, including the dissertation focus area.

Figure 8.3 illustrated the main transmission network of the study area. The transmission line is configured in a ring shape to surround the center of the city. However, the Addis Center substation, Addis West substation (ADW), Addis East substation (ADE), etc., which are the important feeding points for power demand are supplied as a radial line from the 132 KV ring network. Therefore, these substations do not satisfy the N-1 criteria.



**Figure 8.3:** Illustrate the main transmission network of the study area. It is part of the network that interconnects central Ethiopia and Addis Ababa to other regional networks.

The case study was done by representing the long transmission lines that extend from generation stations to transmission stations (i.e., from the generators to transmission stations surroundings of Addis Ababa) by infinite bus and generators to characterize short transmission lines that extend around Addis Ababa (more detail explanation was presented in reference [192]). The test network was meshed and has two voltage levels, 230 KV, and 132 KV. The 220 KV transmission lines between Sululta and Lagatefo, Legetafo and Kaliti I, and Sebata and Geferesa are adopted for the case study. The study was first carried out using the simulation software PSS/E for static power system analysis such as power system security; optimum power flow, state estimation, and continuation of power flow, as shown in Figure 8.4. Newton-Raphson method is used for load flow studies due to its good convergence. PSS/E simulation was also run to assess for the overload of respective lines as shown in Figure 8.5.



**Figure 8.4:** PSS/E simulation for the portion of the main transmission grid network of Addis Ababa, the capital city, and the surrounding area.

Capacities of critical spans are forecasted based on the interpolated weather forecasts from the nearby National Meteorology Agency of Ethiopia (NMA) weather stations. Hourly measurements of historical records for wind speed, wind direction, solar radiation, ambient temperature, and other weather parameters relevant to the calculation of DLR, for the year 2018-2020 have been used for this case study.

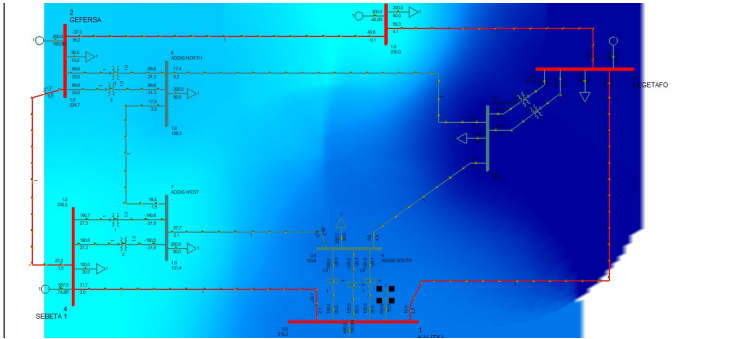


**Figure 8.5:** The transmission grid network with PSS/E simulation, the blue area shows the region with more overload area to other regions.

Transmission lines are widely protected by distance relays due to their simple operation and high coordination characteristics [156]. The operation of distance relays is based on impedance calculation by measurement of voltage and current at the relay location. In principle, the operating principle of a relay is that it should trip only when a fault or unstable swing occurs. However, the short period of overload phenomenon may cause the mal-operation of distance relays. Figure 8.6 illustrates the impedance locus seen by the relay was changed and moved from the load area into the third zone area and may activate the relay many times to trip. Unintended tripping occurs when the impedance trajectory enters the impedance locus of the distance relay (inner circle of zone 3) because of impedance reduction due to overload, despite that no conductor temperature exceeds the set point. The subsequent operation of distance protection in response to the overload power swing will lead to unnecessary outages.

Dynamic ratings can be used to describe the delayed variation in conductor temperature in response to a change in the current loading on the transmission line. The dynamic line ratings are calculated based on real-time measurements rather than conservative weather conditions. The delayed response of the conductor temperature to a change in line current is depicted in Figure 8.7.

Application of the DLR algorithm into a distance protection relay can prevent a trip off the line, even if its nominal load is exceeded since the conductor

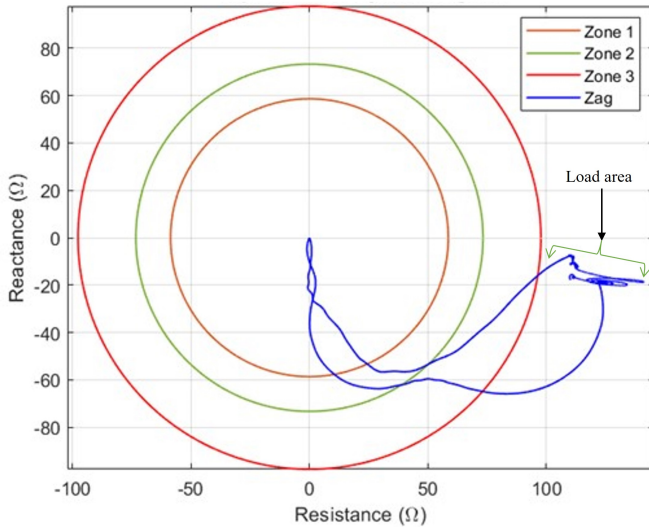


**Figure 8.6:** Trajectory of impedance during unintended tripping (blue color,  $Z_{ag}$ ), the load impedance decreases and enters transmission line relay protection zones from the load area.

remained below permissible levels. This can restrain the relay from operation tripping, allowing the line to operate safely for short time overload conditions under favourable weather conditions.

## 8.3 Ampacity forecasting models

### 8.3.1 Forecasting methodology

The approach introduced in this dissertation offers a way to predict the ampacity of overhead power lines using quantile regression forests (QRF) a nonparametric probabilistic method (see Section 5.4.4). This enables the selection of forecasts with low ampacity overprediction risk for OHTL monitoring. However, it's important to note that no power grid is completely risk-free, and even a conservative

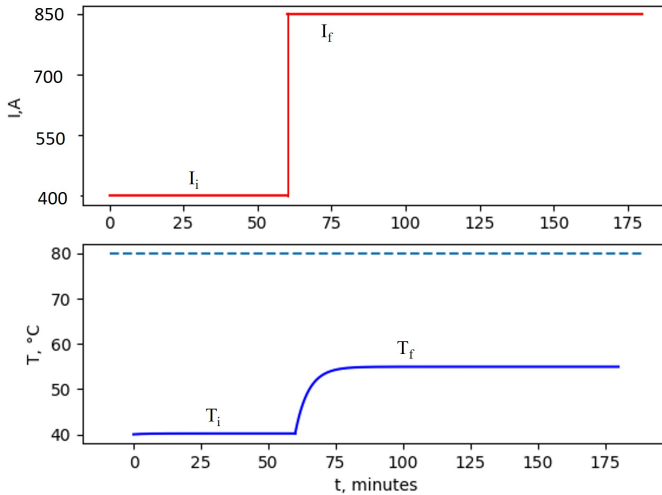


**Figure 8.7:** A step change in the current from initial current  $I_i$  to final current  $I_f$  and exponential curve for conductor temperature from initial temperature  $T_i$  to final temperature  $T_f$ .

SLR safety margin has inherent risks. The proposed method establishes a model connecting local observations and weather-based forecasts. It utilizes historical weather measurements and statistically adjusted local measurements to generate ampacity of the line. The methodology's application in a case study involving Ethiopian utility transmission lines, involved both weather measurement stations and statistical adjustments, as discussed in Section 8.3.2.

The weather variables are used as inputs for the QRF model [192], which was employed to predict ampacity from minute- to hour-ahead in the future. Unlike previous methods, which focused on fixed point forecasts, a probabilistic approach produces a probabilistic prediction. Point forecasts often come with uncertainty, which can be represented as prediction intervals. These intervals define a range of potential values within which the forecasted magnitude is expected to fall in the future with a predefined probability. Traditionally, a parametric approach estimates the parameters of a probability density function (PDF), often assuming a

Gaussian distribution, resulting in symmetric prediction intervals centered around point forecasts. Nevertheless, ampacity prediction depends on wind speed, which follows an asymmetric Weibull distribution and is further complicated by varying wind behavior.

Addressing these challenges with a nonparametric approach, predictions are made without assuming a specific PDF shape. Empirical prediction intervals or quantiles can be computed, accommodating potential asymmetry and lack of alignment with point forecasts. Consequently, expressing probabilistic forecasts as quantiles becomes crucial. These quantiles are defined with a probability parameter  $\tau$ , indicating the likelihood of the forecasted value  $\hat{X}_{t+h}^\tau$  exceeding the observed value  $X_{t+h}$ , as represented in Equation 8.1.

$$P(\hat{X}_{t+h}^\tau > X_{t+h}) = \tau \quad (8.1)$$

In this work, different probability levels of  $\tau$  (1%, 2.5%, 5%, 10%, and 25%) were tested.

### 8.3.2 Weather data forecast models

A machine learning model uses weather data to predict ampacity or conductor temperature. The data needed for the ampacity forecast are the historical weather station measurements and the regional numerical weather prediction (NWP) model forecast. In the forecasting process, the NWP output is adapted to the site where the OHTL is located. Algorithms utilize forecasts from the NWP model, offering predictions up to 24–48 hours ahead. These predictions are used to anticipate upcoming weather conditions around the conductors [152]. However, these forecasts lack precision in considering local wind effects on conductors. To enhance accuracy, adjustments are needed, achieved through physical or statistical methods. The physical approach combines an atmospheric model with a terrain model (downscaling) to correct systematic errors. Forecasts are then interpolated based on distance, and a wind speed correction is applied using

a wind profile power law [128] to account for terrain roughness. The forecasts are validated by comparing the historical weather forecasts and the historical weather measurements. An uncertainty analysis is carried out, giving as a result some uncertainty indicators. The uncertainty indicators are important because they validate the value of a given forecast. Figure 8.8 provides an overview of the system's processes, and a more detailed explanation for ampacity prediction is given in Section 8.4.

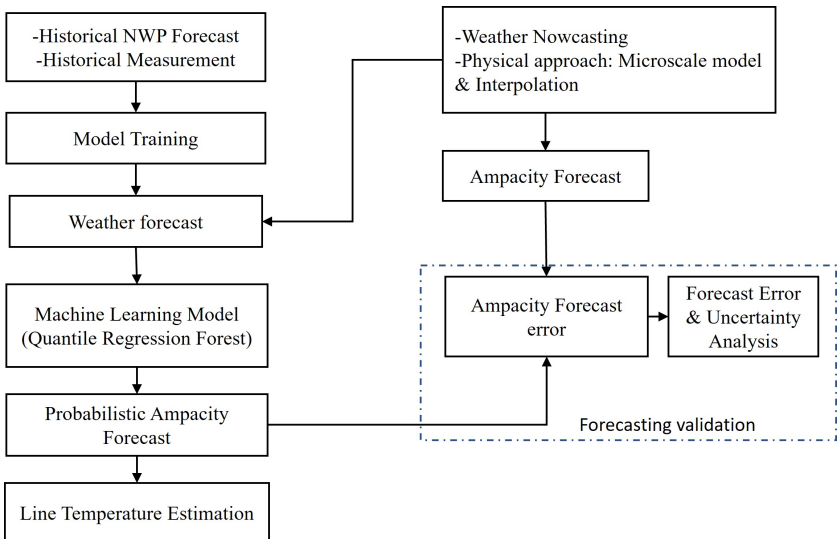


**Figure 8.8:** Summary of ampacity forecasting process. This system falls under the category of an indirect dynamic line rating system, using weather forecasts to determine ratings.

Due to the relatively high cost of weather stations, the resolution of the weather station network is coarse for OHTL monitoring applications. Typically, meteorological departments install weather stations at specific locations such as airports, agricultural areas, and areas with high-density populations. According to WMO regulations [157], weather stations provide measurements for different weather elements at specific altitudes, such as 2 m for air temperature and 10 m for wind measurements. For OHTL monitoring applications, a minimum of one year of

weather measurements is required to build a machine learning-based monitoring model along the span of the transmission line.

The ampacity of OHTL depends strongly on the weather conditions along the entire length of the transmission line. Hence, the probabilistic ampacity forecasting for transmission lines can be computed from the corresponding weather forecasting along the neighborhood of the entire line span. For this, a distributed weather measurement system has to be installed on the transmission line tower and along the entire line-span, which measures local weather conditions and provides statistical weather predictions.

There were no weather sensors installed along the transmission line towers for the considered model in this dissertation. Hence, weather forecasts from nearby weather stations are spatially interpolated into chosen spans using the inverse distance weighting [158–160]. Weather predictions at each selected span are approximated as a weighted average of predictions from the neighborhood of weather stations, as shown in equation (8.2),

$$\hat{y}(k) = \frac{\sum_i^n w(d_{i,k})y(i)}{\sum_{i=0}^n w(d_{i,k})} \quad (8.2)$$

Where  $\hat{y}(k)$  is the predicted value at the unsampled location,  $n$  is the number of measured points used for the interpolation,  $y(i)$  is the known value, the weighting factor  $w(d_{i,k})$  is the inverse square distance between points and is defined as in equation (8.3):

$$w(d_{i,k}) = \frac{1}{d_{i,k}^2} \quad (8.3)$$

The height of the weather station considered for this study is at a different height from that of OHTL towers usually in ranges from 15 to 55 meters, wind speed predictions  $V_{S_{h_o}}$  are thus corrected using the wind profile power law, as illustrated in equation(8.4) [158, 161]:

$$V_{S_h} = V_{S_{h_o}} \left(\frac{h}{h_o}\right)^a \quad (8.4)$$

where,  $h_o$  height of weather station,  $h$  height of the tower, the exponent  $a$  for different ground types can be found in [161].

By integrating extrapolated weather forecasts and localized weather observations, this model aims to provide more precise forecasts of the current-carrying capacity of power lines, contributing to improved grid monitoring planning and stability.

Five weather stations were selected around Addis Ababa and its vicinity, as depicted in Figure 8.9 for modeling weather parameters along the transmission line. The choice aimed to create realistic geographical setups resembling the routes of the line. This study relies on measurement records spanning from 2018 to 2020, documented hourly.

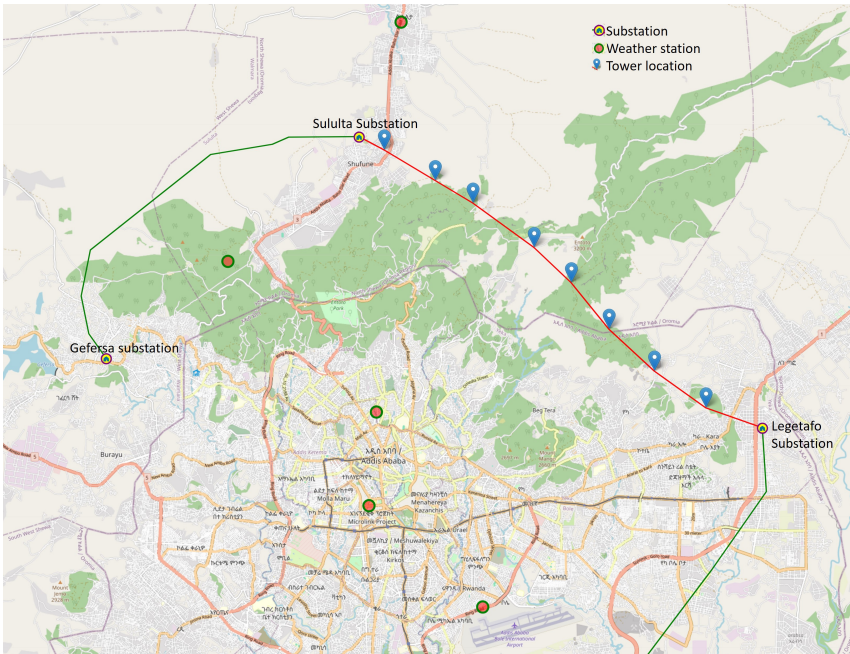


**Figure 8.9:** Case study - selected weather stations from Addis Ababa and its area.

## 8.4 Probabilistic ampacity forecast

To benefit from DLR, operators need necessary information in advance and sufficient time to respond to changes in the current-carrying capacity of power transmission lines. This requires minutes-to-hours-ahead forecasts to effectively respond to changes in line capacity. In this regard, the focus is to accurately model DLR through probabilistic forecasting methods to predict future values of ampacity variables, considering potential risks [152–154]. The methodology combines time series analysis and weather forecasts using machine learning algorithms to generate reliable ampacity forecasts for areas or spans with complex terrain.

Figure 8.10 shows the Mean Average Percentage Error (MAPE) for up to 24-hour forecasting period which is below 20% as set by FlexNet report from the Twenties Project [155, 162] which refers to a maximum MAPE acceptable by most of the TSO in Europe. Moreover, the most important prediction hours are the first 0–2 hours for real-time congestion and overload monitoring. Considering that the actual current-carrying capacity of an overhead line is smaller than predicted, it is necessary to react on time to avoid overloads. The generation adjustment for conventional power plants takes from six to eight hours. In the case of Ethiopia, given that enough water in dams, hydro generation adjustment will take in few minutes.

The static line rating is set by Ethiopian Electric Power (EEP) TSO based on the manufacturer's data sheet and the worst weather scenario under steady-state conditions. For dynamic line rating modeling, the overhead lines rating is monitored in real-time to decide loading limits using weather stations' weather interpolations. Therefore, in SLR constant loading limits are used whereas in DLR time-varying loading limits are set [192]. The ampacity calculations were based on the Ostrich ACSR 176 conductor a typical conductor used by Ethiopian Electric Power (EEP), with the following features listed in Table 8.1.

QRF machine learning model is modeled for up to 24-hour ampacity prediction and loading limits. QRF with different quantiles is used to exploit the capacity of OHTL in real-time. Thus, the proposed method provides better enhancement

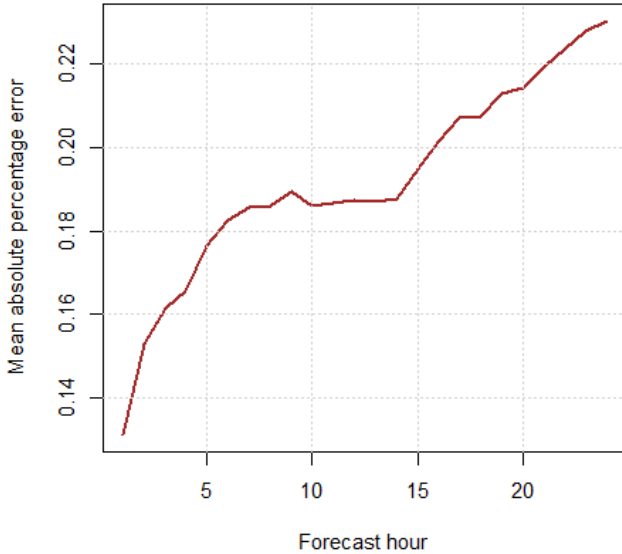


**Figure 8.10:** Mean Absolute Percentage Error (MAPE) for 24-hour forecasting model, trained on a variable  $D_{train}$  ranging from 1 to 24.

and safe operation for the lowest quantiles probabilistic prediction to mitigate decision-makers risk-averse. The QRF input-output structure is shown in Figure 8.11. Past weather observations enter the model. The QRF then forecasts the current-carrying capacity directly, obtaining 24 models, one for each forecast hour, using the direct prediction approach discussed in section 5.2. The actual capacity values are calculated from the actual weather measurements along the overhead line.

In the training and test processes, the past and the future are relative. In both cases, a sliding window is used. It has as its center the present time,  $t_o$ , and from there, the past and future are defined. In reality,  $t_o$  corresponds to real-time. The number of past time steps,  $D_{train}$ , to consider for each input weather parameter was optimized. This value can range from one, i.e., only the current observation; to the entire measurement history.

**Table 8.1:** Specification of the typical Conductor under study.

OHTL conductor	Ostrich (ACSR 176)
Dia [ $mm^2$ ]	17.28
Al [ $mm^2$ ] and dia AL [mm]	152.2 (26/2.73)
St [ $mm^2$ ] and dia St [mm]	24.71 (7/2.12)
Solar absorptivity	0.5
Thermal emissivity	0.9
Max. conductor temperature	$75^\circ C$

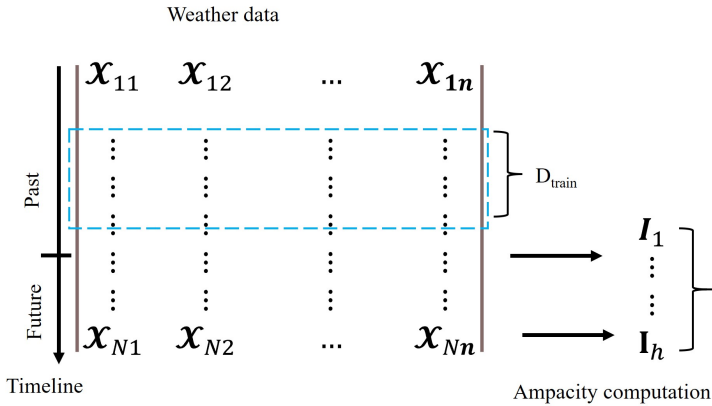


**Figure 8.11:** Structure of QRF forecasting development scheme.

For better simulation and experiment consideration, it is very crucial to consider the spatial distribution of weather data measurement along the OHTL in preference to weather data measured from a single point around the OHTL [127, 163] to forecast the ampacity of the OHTL conductor. However, for this case study, it is difficult to get spatially distributed weather stations.

The modeling of probabilistic DLR forecasting was implemented considering the weather parameters from the Ethiopian National Meteorology Agency. The most important weather parameters for this model contain different weather features such as temperature ( $^\circ C$ ), solar radiation ( $W/m^2$ ), wind speed ( $m/s$ ), and wind

direction ( $^{\circ}$ ). For the sake of training and testing phases, first, the hourly measured weather data must be preprocessed. Then a forecast model was produced for the number of past measurements that have to be given as input to the model ( $D_{train}$ ) to forecast for  $n$  hours.

A technique has been developed for predicting the ampacity of overhead power lines, taking into account various risk levels. This method uses empirical probabilistic forecasts derived from weather predictions to predict ampacity. This forecast is valuable for managing grid operations and scheduling. The method presented in [192] adapts statistical weather forecasts to the scale of power line spans. Its goal is to generate dependable predictions that assist Transmission System Operators (TSOs) and Distribution System Operators (DSOs) in choosing a conservative risk level to avoid excessive heat in overhead conductors. Figure 8.12 for visualization of ampacity values associated with different risk levels examined. The dataset is split into two data subsets: the training data subset, which is used only to train the model, and the test subset, which is used to assess the proposed model. Accordingly, for the training subset, data from the year 2018 was used as explained in section 8.3.2. After training was done, a test set representing the year 2019 was used to predict the probabilistic ampacity and calculate the accuracy of the proposed model.

The primary focus of this work is to predict highly reliable DLR forecasts to enhance the performance of the lowest quantiles for risk-averse TSO decision-makers. This is crucial because conductor ampacity needs to be set with a very low probability of overestimation to ensure that the operating temperature remains below the allowable point ( $75^{\circ}C$ ). TSOs can select values from the distribution's tail with very low probability levels of being overestimated. As shown in Figure 8.12, the lower quantiles (up to 25%) were consistently below deterministic observations and 50% quantiles, reducing the likelihood of overestimation in DLR forecasts. This probabilistic approach allows for better decision-making and reduces losses associated with DLR.

Thus, deploying DLR based on below 50% forecasted quantile leads to increased economic benefits while also improving network safety, with fewer instances when

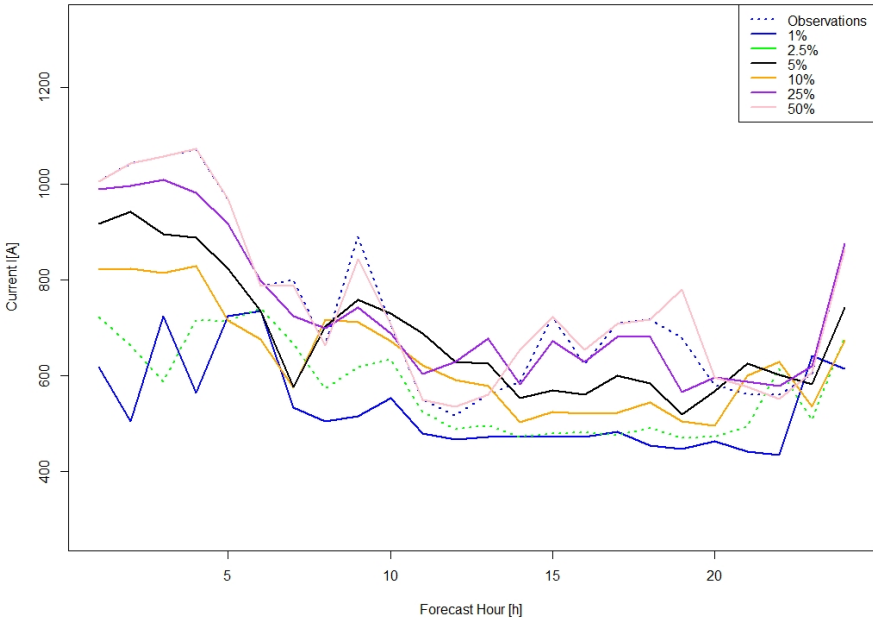


**Figure 8.12:** Quantile of ampacity quantile forecasts, and observational models for a 24-hour forecasting model, trained on a variable  $D_{train}$  ranging from 1 to 24. We notice a very close agreement between the computed 0.5 quantiles and the deterministic rating.

the N-1 criterion is not met. The selection of the optimal quantile dynamically varies at each time step based on the risk profile of the line where DLR is applied. This approach offers a promising solution to enhance the efficiency and reliability of DLR forecasting in power systems.

The proposed frameworks for setting DLR based on probabilistic forecasts recommend using low quantiles for real-time monitoring of the OHTL network. This approach reduces the risk-averse nature of decision-makers and avoids both overestimation and higher losses associated with deterministic DLR forecasting.

# 9 Intelligent sensors network for Power Grid Monitoring

This chapter focuses on introducing and explaining the fundamental ideas required to establish a mesh-based wide area network (LPWAN) that is both economical and energy-efficient. It offers insights into various LPWAN technologies, outlines key routing protocols, and highlights their constraints. This knowledge is crucial for comprehending the proposed methodology.

## 9.1 LPWANs and LoRa technology overview

### 9.1.1 LPWAN networks

A Low Power Wide Area Network (LPWAN) is a communication network designed for long-range coverage while consuming minimal power. LPWANs are well-suited for sending small data packets from remote sensors to a base station, often at speeds under 50 kbit/s for two-way communication [164]. This technology is particularly suitable for relaying sensor data such as temperature, humidity, or oil levels. NB-IoT (Narrowband IoT), LTE-M, SigFox, and LoRaWAN are among the main LPWAN technologies [165]. They offer different advantages and cost considerations. While NB-IoT is easily deployable through cellular carriers, SigFox requires a subscription with a network operator, and LoRaWAN is an open standard with no subscription needed.

LPWANs address the limitations of legacy wireless systems regarding coverage range by enabling data transmission across several kilometers. However, this range

is insufficient for extensive infrastructures like transmission lines in developing countries like Ethiopia. To tackle this challenge, a mesh network based on the LoRa protocol is proposed as a solution to extend transmission distance in this dissertation.

### 9.1.2 LoRa and LoRaWAN technology

Low Range Wide Area Network (LoRaWAN) is an open standard communication protocol that utilizes the LoRa modulation on the physical layer, enabling long-range, low-power wireless communication. LoRa is a physical layer modulation that was developed and patented by Semtech [166]. In contrast, LoRaWAN is a MAC layer standard that coordinates the medium as specified by the LoRa Alliance [167].

The LoRaWAN network topology consists of three main components: network servers, gateways (GWs), and end nodes. End nodes communicate with the network server (or data server) via GWs, and Node-to-GW communication can be either LoRa or FSK modulation with different data rates and channels. Network servers manage the GWs through standard IP technology and data frames are sent through end nodes, received by GWs, and routed through the network server. An overview of the LoRaWAN architecture is presented in Figure 9.1 with a star topology between GW and sensor nodes.

LoRa networks operate in the unlicensed ISM (Industrial, Scientific, and Medical) bandwidths (USA: 915MHz, EU: 433MHz and 868MHz, and Asia: 433 MHz). This allows private networks to be established and requires a lower cost of installation setup compared to other LPWANs. A LoRa message can be of two types: uplink or downlink. The message structure is similar in both cases, however, only the uplink message adds a verification code (CRC) to ensure the integrity of the payload (PHYPayload). To facilitate bidirectional communication, LoRaWAN defines three device classes: class A, B, and C.

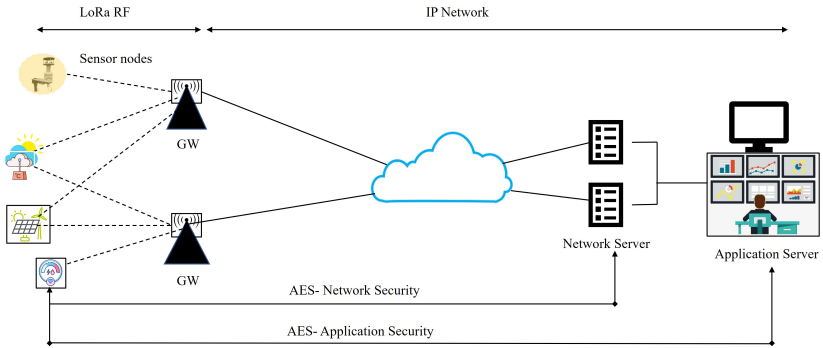


Figure 9.1: Schematic structure of LoRaWAN architecture.

### 9.1.3 LoRaWAN Protocol Architecture

Figure 9.2 illustrates the protocol architecture of LoRaWAN, which comprises a MAC layer and an application layer, utilizing the LoRa physical layer. The packet format is depicted in Figure 9.3, and the maximum payload lengths change according to the data rate, as specified in reference [168].

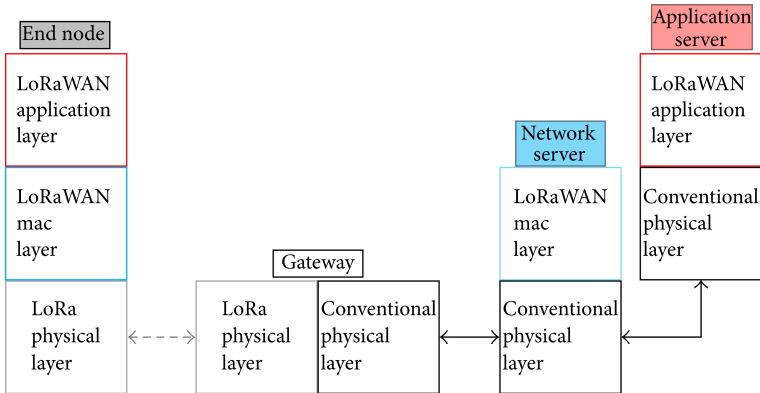
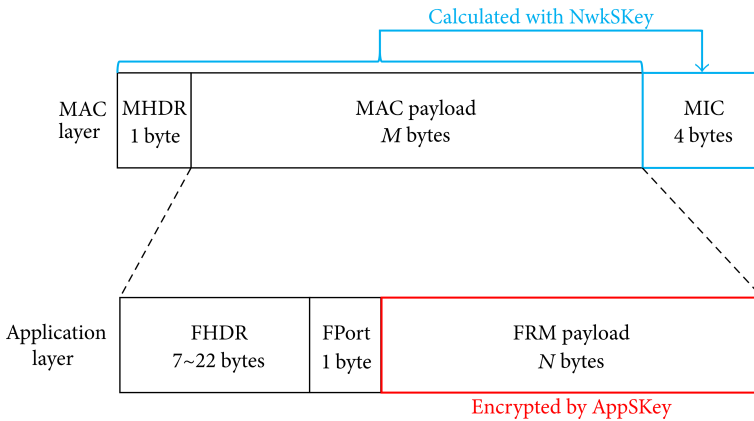


Figure 9.2: LoRaWAN protocol architecture.

- Medium access control (MAC):** The MAC layer processes packets containing a MAC Header (MHDR), MAC Payload, and Message Integrity Code (MIC). In a join process for end node activation, the MAC Payload can be swapped with join request or join accept messages. Both the MAC Header and Payload are used to calculate the MIC using a network session key (NwkSKey) to prevent message forgery and authenticate the end node [169].
- Application layer:** The application layer deals with the MAC Payload, which comprises an FRM Header (FHDR), FPort, and FRM Payload. FPort varies with the application, and the FRM Payload is encrypted using an application session key (AppSKey) through the AES128 algorithm.



**Figure 9.3:** LoRaWAN packet format.

Each LoRaWAN node possesses a unique device identifier called DevEUI, which is 64-bit long and must be globally unique. The node also requires knowledge of its join server, with its identifier called the JoinEUI which is also 64-bit long, and the intended network for joining.

A LoRaWAN network is distinguished by a 24-bit NetID, assigned by the LoRa Alliance [168]. This network comprises various components, including end

nodes, LoRaWAN gateways, a network server, a join server, and an application server. Communication via the LoRa physical layer takes place only between end nodes and gateways, while other communication uses standard internet protocols. End nodes periodically transmit data, which is received by gateways and then forwarded to the network server. Depending on the message type, the network server directs the message to the join server or the application server, serving as a communication endpoint at layer 2. The network server manages the data rate and frequency of each end node to optimize transmission.

LoRaWAN networks are encrypted and support over-the-air activation [169]. During this process, devices are provisioned with two root keys: AppKey and NwkKey, both known by the join server. To join the network, a device sends a join request to the join server, including DevEUI and JoinEUI. While the join request isn't encrypted, a message integrity code (MIC) is calculated using NwkKey and added to the message. Upon receiving the join request, the join server verifies the message's integrity with the shared NwkKey. Upon successful verification, the join server generates a new pair of keys, AppSKey and NwkSKey, for encrypted data transmission. The join server responds with a join accept message containing the unencrypted NwkSKey and an AppSKey encrypted with AppKey, along with NetID and device address. This confirms that both device and join server possess the root keys, establishing successful network entry.

An alternative encryption method is activation by personalization, where pre-configured AppSKey and NwkSKey are used. Devices don't require a join process, having a device address and NetID in advance. To ensure secure communication, devices encrypt every transmitted data packet with the AppSKey.

### 9.1.4 LoRa physical layer

LoRa is a unique physical layer modulation technique derived from chirp spread spectrum (CSS) technology [170]. It operates in wideband sub-GHz frequency bands, setting it apart from other wireless networks. LoRa's CSS modulation allows for increased sensitivity, enabling long-distance connectivity [171] and

making it a promising candidate for ITIV Smart-e-Meter joint project for grid monitoring in Ethiopia.

To maximize efficiency, LoRa offers various options for orthogonal transmissions, including carrier frequency (CF), spreading factor (SF), bandwidth (BW), and coding rate (CR). These parameters enable collision-free communications and allow for data rates ranging from 250 bps to 5.5 kbps using CSS modulation and up to 50 kb/s with FSK modulation [164]. SF, CR, BW, and CF are transmission parameters in LoRa that need to be defined [172] during setup. SF is an integer value ranging from 7 to 12, and it inversely affects the data rate (DR). Increasing SF leads to longer symbol lengths, resulting in a lower DR. Thus, users can trade data rate for an extended range by adjusting the spreading factor of the transceiver. Multiple Spreading Factors are available to control the bit rate, improve range, and reduce energy consumption.

LoRa's modulation technique also called LoRa spread spectrum (LSS) is based on CSS modulation [170]. In CSS, the data is encoded into the phase shift between the modulated chirp and the reference chirp. A chirp is a signal whose frequency increases or decreases over time. With the bandwidth  $B_c$  of the chirp, the chirp duration  $T_c$ , and the minimum frequency  $f_o$  a linear chirp can be defined by

$$k_r = \frac{B_c}{T_c} \quad (9.1)$$

$$y(t) = \cos(2\pi(f_o + k_r t).t) \quad (9.2)$$

where  $k_r$  denotes the frequency change in time, also called the chirp rate. This creates a signal that linearly increases its frequency from  $f_o$  to  $f_o + B_c$  within a time span of  $T_c$ . An exemplary linear chirp is displayed in Figure 9.4 with the momentary frequency plotted on the right side. The linear characteristics of the chirp signal can be seen in the frequency ramp on the right side.

To modulate data onto the signal using CSS, the chirps are circularly shifted inside each symbol period. This means that the chirp does not start with  $f_o$ , but with a higher frequency  $f_o + f_{off}$ . The time  $\tau_{off}$  where the frequency of the chirp reaches  $f_o$  is also shifted with respect to the start of the symbol period. These

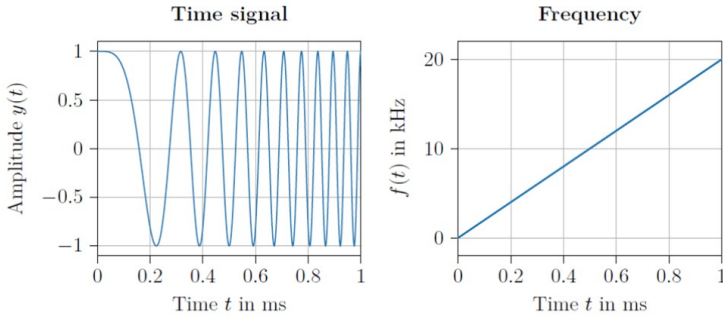


**Figure 9.4:** Chirp with bandwidth  $B_c = 20$  kHz, chirp duration  $T_c = 1$  ms and minimum frequency  $f_o = 0$  Hz.

shifts depend on the data being transmitted and the number of bits per symbol  $N_b$ . They are all related to each other and can be expressed as a fractional offset  $\gamma$  with the following equation:

$$\gamma = \frac{f_o + f_{off}}{B_c} = 1 - \frac{\tau_{off}}{T_s} = \frac{\text{data in decimal}}{2^{N_b}} \quad (9.3)$$

Figure 9.5 shows the chirp with the data modulated on it. The frequency and the time offset can be seen in the frequency curve on the right side.

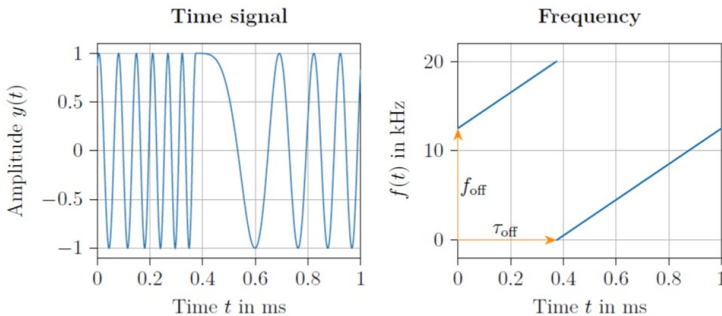


**Figure 9.5:** Data '101' modulated on a chirp with bandwidth  $B_c = 20$  kHz, chirp duration  $T_c = 1$  ms and minimum frequency  $f_o = 0$  Hz.

To decode a modulated chirp at the receiver, the modulation parameters need to be known. The bandwidth and symbol time can be extracted from the signal, but the number of bits per symbol  $N_b$  needs to be known. This is because the offset can be retrieved from the signal, but without  $N_b$  the granularity of the modulation is not known.

The main difference between LoRa spread spectrum and the chirp spread spectrum lies in the introduction of the spreading factor. This SF controls the number of bits ( $N_b = SF$ ) that are encoded in each symbol, as well as the symbol time ( $T_s$ ). The symbol time is also influenced by the chosen bandwidth ( $B_c$ ) and is defined as follows:

$$B_c = \frac{2^{N_b}}{T_s} \quad (9.4)$$

This means that the symbol time doubles with every increment of the spreading factor. The LSS also introduces a variable forward error correction (FEC) that is controlled with the code rate parameter CR. It specifies the number of parity bits that are added for every 4 bits of data, and can have values from 1 to 4 [173]. With this, the effective bit rate  $R_b$  can be calculated as

$$R_b = SF \cdot \frac{4}{4 + CR} \cdot R_s \quad (9.5)$$

It becomes obvious, that the spreading factor has the biggest influence on the performance of the system because it controls the symbol time and number of bits per symbol. Together, this defines the energy per bit  $E_b$  that reaches the receiver. When increasing the spreading factor by one, the symbol time is doubled, but only one extra bit is encoded into each symbol. Because of this,  $E_b$  is higher for larger spreading factors, allowing transmissions over longer distances. But the trade-off for this is a reduced data rate, and thus the transmission time  $t_{air}$  for the same number of bits is increasing for higher spreading factors. Without cyclic redundancy checking (CRC), the air-time of a packet can be calculated as:

$$t_{air} = N_{pre} + 12.25 + [(8N_{pay} + 4SF + 28)/4SF](4 + CR)T_s \quad (9.6)$$

where  $N_{pay}$  is the number of payload bytes the packet is carrying and  $N_{pre}$  is the length of the preamble.

## 9.2 Wireless mesh networks

Many existing wireless transmission systems are limited in coverage range [174, 175]. However, LPWAN technologies enable long-range transmission of small data packets with low energy consumption, making them suitable for battery-powered devices [176, 177]. For infrastructure projects that are distributed over a wide geographical area, even LPWAN with star topology (see Figure 9.6(a)) may not be enough, so it is crucial to extend the transmission distance of the end node via a mesh network to the gateway as illustrated in Figure 9.6(b). Therefore, a mesh network based on the LoRa protocol proposed in this dissertation was devised to close this gap.

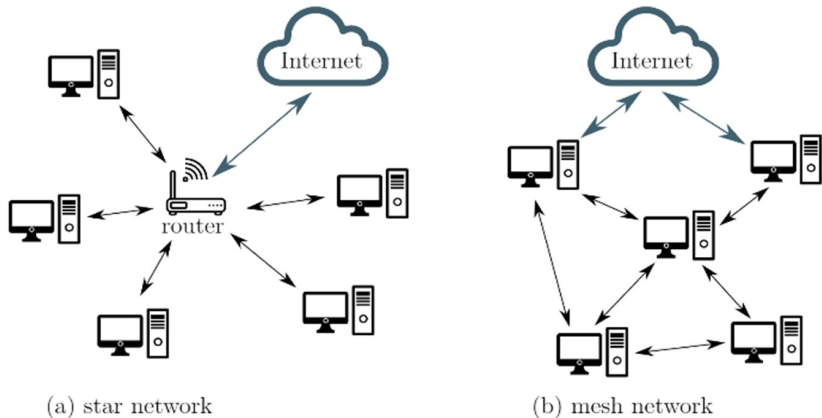


**Figure 9.6:** Sample networks with a star topology (a) and a mesh topology (b).

The proposed network protocol aims to establish an affordable LoRa Wireless Mesh Network (WMN) that can cover extensive areas without relying on numerous gateways. A related study in [178] also explored using LoRa modulation from Semtech to expand the reach of LPWANs. In this WMN, nodes can establish multiple connections, not just with gateways but also with other nodes, ensuring connectivity in remote regions. Most nodes in the mesh network have multiple links, creating multiple communication paths with gateways. While this redundancy can be beneficial, it may cause more collisions as the node count increases. To enhance connection quality and decrease collisions, the network employs a strategic process called routing. Routing is a vital concept in modern communication protocols and is crucial for comprehending network operations.

Routing protocols, defined at the network layer, do not directly influence collisions like the MAC layer but can reduce collisions by eliminating unfavorable links and optimizing overall network traffic.

## 9.3 Routing

The core challenge in establishing a network is routing, which involves finding paths to a destination across multiple hops. Routing algorithms aim to connect nodes that are not direct neighbors. The algorithms select the best path based on predefined metrics or policies when multiple paths are available. Routing tables store path information, and they can be either static (unchanged since network startup) or dynamic (constantly updated to adapt to changes in network topology) [179]. Routing protocols differ based on when path information is exchanged between nodes: proactive routing sends information periodically to neighboring nodes, while reactive routing gathers information from incoming packets.

The following section introduces various routing protocols, which will serve as the basis for selecting a suitable routing protocol in chapter 10.

### 9.3.1 Flooding

Flooding is a basic routing protocol where a packet is broadcast to all neighbors when it needs to be sent to a specific node with address A. All receiving nodes then forward the packet as a broadcast to their neighbors, leading to the packet spreading throughout the entire network until it reaches its destination at node A. This process is displayed in Figure 9.7.

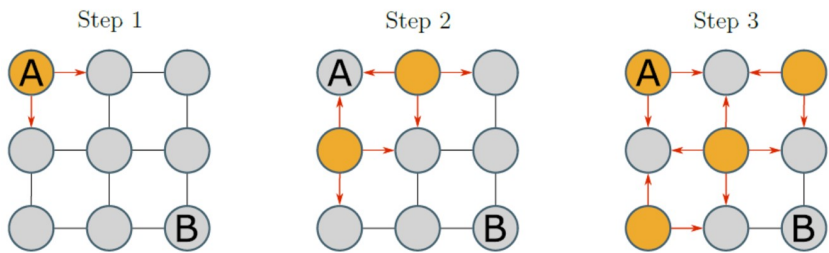


**Figure 9.7:** Schematic displaying the flooding algorithm on a simple three-by-three grid network.

However, this approach has significant disadvantages. The packet can return to the sender, causing the sender to forward it again unknowingly. Similarly, all other nodes also rebroadcast the packet, resulting in an ever-increasing number of packets in the network, eventually leading to network congestion and communication failure. To address these issues, each packet is given a limited time-to-live (TTL). As the packet is forwarded, its TTL decreases, and when it reaches zero, it is no longer forwarded. This prevents indefinite packet circulation.

### 9.3.2 Data-centric

Data-centric routing differs from other routing algorithms by focusing on the data itself rather than the addresses of specific nodes. Instead of requesting data from a particular node, data-centric routing seeks any node that can provide the required data. Before sending any data, it must be requested by the interested node (sink)

issuing an interest in the specific data resource [180]. This interest propagates through the network through flooding or geographic routing, known as diffusion.

When a node receives an interest, it checks if it can provide the requested resource. If it can, it starts transmitting the data to the sink in the form of events. The data packets are sent over the reverse path of the interest, which may not always be the most effective path to the sink. To improve the data packet's path, the sink can issue another interest with a higher monitoring frequency after receiving the first events. This new interest serves as a reinforcement message, and nodes receiving it prioritizes one neighbor for further communications related to this interest. This reinforcement process creates a more efficient communication link between the sender and the sink [181].

Data-centric routing proves to be highly beneficial in diverse networks as it eliminates the need to know all nodes in the network to receive their data. Instead, it enables a flexible and efficient way to access required data resources.

### **9.3.3 Location-based routing**

Location-based routing is an algorithm that prioritizes the position of communicating nodes to improve the efficiency of certain applications. Instead of relying on routing tables, this approach selects the next hop in a network based on the shortest distance to a nearby node [180]. The distance between nodes may affect the quality of their communication link. Nodes can obtain their position information through various methods, such as GPS data, central assignment, or pre-provisioning before deployment.

The limitation of this approach lies in requiring precise knowledge of the position of the current node and the positions of all neighboring nodes. This becomes particularly challenging when dealing with moving nodes, making it an unsuitable routing algorithm for such scenarios. However, in static networks, where node positions remain fixed, this approach can prove to be an effective routing algorithm.

### 9.3.4 Routing Protocol for Low-power and Lossy networks - RPL

The Routing Protocol for Low-power and Lossy networks (RPL) is a standardized protocol by the Internet Engineering Task Force (IETF) primarily designed for use in IoT projects. It is specifically tailored to operate in lossy networks and with power-restricted devices. RPL employs distance vector routing and utilizes directed acyclic graphs (DAGs) to store routing information [182]. It is designed to be compatible with various MAC protocols, especially those where nodes are not continuously active. Moreover, RPL is adaptive to changes in network topology and considers device constraints, such as low battery levels and poor link quality.

In an RPL network, the basic structure is a tree, with an internet-connected router acting as the root of a subnet. From this root, a destination-oriented directed acyclic graph (DODAG) is constructed to determine link costs. Join requests are sent out by the root, and nodes can decide to join the network. If a node is not a leaf, it rebroadcasts the join request with itself as the root, establishing its distance to the root, known as node rank [183]. Each node can only be part of one RPL network, but virtual roots with multiple physical roots in different locations can achieve broader network coverage

Once the DODAG is constructed, the actual routing information is exchanged using the distance vector routing protocol. Communication costs of links are calculated based on a predefined objective function that considers various characteristics such as transmission reliability, encryption, and power sources of nodes. Nodes broadcast the cost table to their direct neighbors in a DAG information object (DIO). Upon receiving a DIO, a node updates its routing table with the communication costs and may adjust its node rank. The iterative process of finding the best routes from each node to the root is driven by the given objective function [184].

However, the iterative nature of the algorithm can sometimes lead to issues like constant changes, resulting in a down-ranking spiral, where nodes keep down-ranking in response to each other, potentially causing inefficiencies in the network's operation.

## 9.4 Combination of LPWAN and WMN

To extend the coverage and capabilities of traditional LPWAN networks, integrating them with wireless mesh networks appears to be an ideal solution. However, due to the low-power nature of LPWANs, this combination poses several challenges. In traditional LPWAN networks, nodes primarily remain in sleep mode and wake up only to transmit data or optionally allow for downlink communication. For multi-hop communications in a mesh network, intermediate nodes must be awake to relay packets. This requires the nodes sending intervals to be synchronized. This can be achieved with scheduled sending intervals, or the nodes need the ability to wake up when receiving a packet (wake-on-receive). However, implementing the appropriate synchronization technology depends on the specific use case. For instance, event-based transmission cannot rely on scheduled synchronization, and power-limited nodes cannot utilize wake-on-receive as their receive-detection cannot be put to sleep. Addressing these challenges requires tailored approaches for each scenario, ensuring efficient and effective communication within the combined LPWAN and wireless mesh network infrastructure.

# 10 Wireless Sensor Network Grid Monitoring for Developing Economies

The electricity demand in Ethiopia is rapidly increasing due to population growth, urbanization, and economic development [2, 3, 18]. Although the current level of power production is sufficient for a grid-connected society, there are still frequent local power interruptions. The current status of the Ethiopian grid and the main reasons for interruption were explained in Chapter 2. To address this, real-time monitoring integrated with machine learning tools becomes essential to control and manage the dispersed and geographically isolated components of the power grid. Machine learning models for ampacity forecasting have been developed to improve prediction accuracy, but obtaining the necessary data for training these algorithms is challenging, especially in developing countries with limited data transmission networks.

To overcome this challenge, a wireless sensor network with LoRa mesh has been proposed as a cost-effective solution for data collection in large infrastructure projects like transmission lines and power distribution networks. The LoRa mesh network extends the coverage of Low Power Wide Area Networks (LPWANs) without the need for numerous gateways. This approach allows for regular sensor data logging and facilitates remote monitoring and control of infrastructures located in remote regions where weather measurements are valuable. The lack of network connectivity in these regions can be addressed by implementing a LoRa mesh network, providing a cost-effective and suitable solution for the country's developing economy.

The work under this focused on the challenges faced in monitoring and controlling infrastructures in Ethiopia, particularly in remote regions, and proposed solutions using wireless sensor networks with LoRa mesh network. The proposed LoRa WMN system communicates at 5-minute intervals, providing continuous monitoring and analysis of various grid parameters. The integration of real-time monitoring and machine learning tools is crucial for ensuring efficient and safe operation of the power grid, especially with the increasing production of renewable energies and fluctuations in the energy grid.

## 10.1 Design requirements and design choices

### 10.1.1 Design requirements

The LoRa mesh system is designed for real-time grid condition monitoring, utilizing a low-cost IoT gateway and sensor module to collect grid data information. This data is transmitted through the LoRa mesh network, and finally via the gateway to the server.

As explained previously in chapter 9, the main goal of this network is to monitor large infrastructure projects such as transmission lines, distribution infrastructures, and transformers, which are often situated over long distances in remote areas or urban environments with limited network connectivity and electricity supply.

Figure 10.1 shows an exemplary transmission line with the points of interest marked in blue as considered in the simulation of this work. For instance, monitoring the maximum current or ampacity allowed through a transmission line is essential, as it is primarily limited by the cable's temperature. The system incorporates machine learning algorithms to intelligently monitor potential congestion and line faults by analyzing the dynamic line rating of OHTL. It utilizes weather forecasts to estimate the temperature around the transmission line, and the actual measurements via self-sufficient sensors are used to improve the reliability

of these forecasts. The temperature at a given current throughput of the line is closely linked to the outside temperature and the wind speed. These factors are not changing very fast, so the time between measurements can be quite large, so measurements from LoRa sensors every 5 minutes interval can fit the design requirement as a response for DLR to temperature change is usually up to 15 minutes [185].

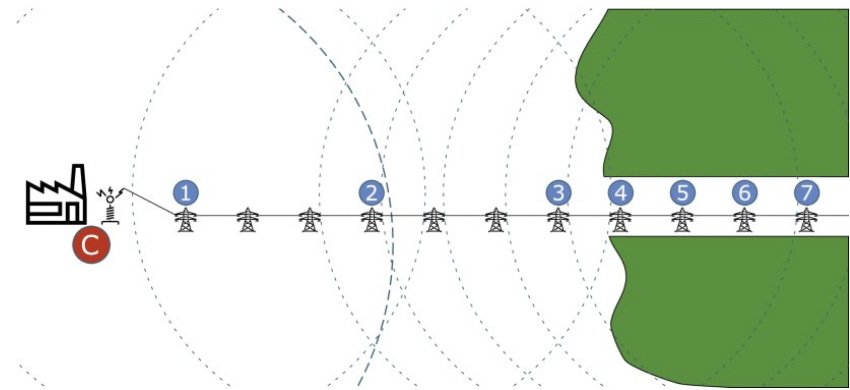


**Figure 10.1:** Example of a transmission line with points of interest and availability of network connection and electricity [193].

In areas with unreliable weather forecasts, like inside forests, more frequent measurements are taken. The system employs multi-hop connections to reach locations where direct communication is not possible, ensuring robust data transmission. However, challenges arise, such as nodes in the forest having connections to a central node, leading to a higher chance of collisions and unnecessary traffic. To mitigate these issues, optimized routing strategies and data filtering techniques may be employed to improve energy efficiency and reduce data redundancy.

The main points to remember from this situation are:

- **Limited internet connection:** Not all locations have access to the internet, which requires the transmission of data to a central location with internet connectivity.

- **No local energy source:** Many points of interest lack a local energy source to provide the required 5V DC for node operation.
- **Multi-hop connection:** Due to the geographical distribution of nodes, some nodes are out of reach from the central location with internet access, requiring multi-hop connections through neighboring nodes to establish communication.
- **Static network topology:** The network topology remains fixed, as all nodes have predetermined positions and will only change if a node fails.
- **Routing needed:** Some form of routing is essential to manage the number of transmissions, avoid collisions, and reduce energy consumption in the network.

### 10.1.2 Design choices

With the requirements from Section 10.1.1 in mind, an LPWAN mesh network was developed. The main goal was to enable monitoring structures with long but narrow shapes, that are hard to cover using networks with star topology due to their distribution from the control center. The data to be transmitted is assumed to be less than 100 bytes and the monitoring interval  $T_{mon}$  is not smaller than 5 minutes. The network will carry these packets over multiple hops towards a central gateway, that provides connectivity to a server, where the data can be evaluated as illustrated in Figure 10.1.

After evaluating all the requirements and their implications for the network, the network can be summarized as follows.

- **Topology:** The proposed topology is a mesh network divided into smaller cells, each managed by a central arbiter. This design aims to cover the entire area of interest while adhering to legal specifications and reducing energy consumption for sensor nodes located close to the central node.

- **Technology:**The chosen technology for the network is LoRa. LPWAN, which offers an open architecture (see Section 9.1.1 and Section 9.1.2).
- **Nodes:**There are two types of nodes: the central node, which acts as a gateway to the internet as well as an arbiter for each cell, and sensor nodes, which are battery-powered with energy harvesting capabilities. Protocol execution is concentrated at locations with continuous power to simplify sensor nodes, allowing them to be powered by batteries and solar panels.
- **Routing:**The routing method employed in the network is location-based routing (Section 9.3.3) with a central arbiter. The static configuration is determined at startup, and the distance to the central node serves as the primary criterion for packet relaying. As the nodes are stationary, support for dynamic networks is unnecessary.
- **Communication principle:**Communication among nodes follows a synchronized monitoring interval. Each node is assigned a sending slot, followed by additional transmission slots for administrative tasks. This setup allows nodes to enter sleep mode for the rest of the interval, conserving energy, and accommodating unplanned administrative operations.

## 10.2 Protocol Overview

### 10.2.1 Physical Layer (PHY)

The LoRa modulation technique from Semtech is utilized on the physical layer, offering excellent resistance to interference and long-range capabilities. Its main advantage is the ability to function independently of the LoRaWAN protocol stack. Each LoRa transceiver module provides access to transmission parameters of received packets, including signal-to-noise ratio (SNR) and received signal strength indicator (RSSI) after successful reception.

Since the network was partly tested at Karlsruhe Institute of Technology in Germany, and must comply with the fair-use policy governing the ISM bands in Europe. The same fair-use policy was adopted for Ethiopia, as there is no current regulation and standard for sub-GHz technologies. According to European norms EN 300 220-1 [186] and EN 300 220-2 [187], the policy limits each application to a one percent duty cycle, meaning it can only use the shared ISM spectrum actively for one percent of the observation interval  $T_{obs}$ . The duty cycle ( $DC$ ) can be calculated based on the cumulative transmission time ( $T_{on,com}$ ).

$$DC = \frac{T_{on,com}}{T_{obs}} \quad (10.1)$$

The timing of transmissions within  $T_{obs}$  is flexible, allowing the device to send consecutively at the beginning of  $T_{obs}$  and remain silent until the next observation interval starts. Assuming an observation interval  $T_{obs}$  of 1 day (86400 seconds), the maximum transmission time adhering to the fair-use policy can be determined as:

$$T_{on,com} = DC \cdot T_{obs} = 0.01 \times 86400s = 864s. \quad (10.2)$$

The central node in the network, which receives all the uplink packets, experiences the highest traffic. The air time  $t_{air}$  for each packet depends mainly on the spreading factor ( $SF$ ) and payload size, as described in Equation 9.6. Given a fixed monitoring interval  $I_{mon}$  and the assumption that each packet reaches the central node only once, the maximum number of nodes  $N_{c,max}$  for each cell can be calculated.

$$N_{c,max} < \frac{0.01 \times I_{mon}}{t_{air}} \quad (10.3)$$

Additionally, this equation can be utilized to determine the minimum monitoring interval when the number of nodes is fixed. In the design of the monitoring application, both the number of monitoring locations and the monitoring interval are crucial and should be assessed together. Figure 10.2 illustrates various design possibilities for different spreading factors with a bandwidth ( $B_c$  of 125 kHz, preamble size ( $N_{pre}$ ) set to 12 bytes, and  $N_{pay}$  (payload size) of 26 bytes.

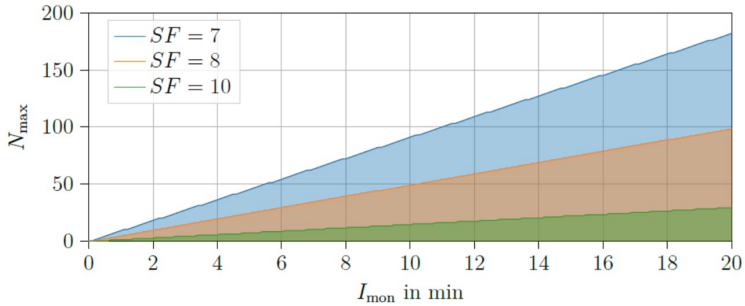


**Figure 10.2:** Area of valid application designs with  $SF = 7, 8$  and  $10$ ,  $B_c = 125$  kHz,  $N_{pre} = 12$  bytes and a payload of  $N_{pay} = 26$  bytes.

The network performance is heavily influenced by the spreading factor. For example, for  $SF = 7$ , up to 182 nodes can be connected, while for  $SF = 10$ , this number is reduced to only 29 nodes. However, it is crucial to note that these figures are theoretical optima and may be significantly lower in practice due to imperfections in the routing algorithm, where packets might be sent multiple times.

## 10.2.2 Medium Access Control (MAC)

The protocol operates without a dedicated MAC algorithm on the physical layer, employing the ALOHA principle for node communication. Nodes can transmit packets at any time, and when they have data to send and are not receiving, they initiate transmission immediately. The application layer will implement strategies to minimize collisions by coordinating the transmission times of the nodes.

## 10.2.3 Routing

A routing protocol is essential for the proposed mesh network due to its topology. A good routing algorithm reduces the number of transmissions, leading to lower

energy consumption for nodes and longer battery life for sensor nodes. Additionally, a decreased duty cycle allows for a higher number of nodes or more frequent measurements in the network. This dissertation work utilizes a location-based routing algorithm as the routing protocol. However, this approach requires precise knowledge of the current node's position and the positions of all neighboring nodes, which can be challenging with moving nodes but effective for static networks like the one described in this work.

The routing protocol is responsible for directing the packets towards their destination. The network uses a centralized location-based routing algorithm to direct packets to their destinations. Each cell in the network acts as an encapsulated subnetwork, and nodes are assigned a dynamic distance parameter relative to the central node. To avoid multiple transmissions and collisions, packets are assigned a unique packet-ID and a relay window is proposed, allowing packets to be re-transmitted within a specific time interval. The implementation prevents packets from circulating indefinitely and ensures efficient packet relay in the mesh network. The implementation of this routing algorithm is quite simple due to the static positions of the nodes, yet still effective.

Every node has a parameter called distance  $d_n$  that is representing its location in the cell relative to the central node. This distance is determined dynamically at the start-up of the network by a join procedure for all deployed nodes. The logic for this is implemented in the central node.

When all nodes have been assigned a distance, the setup needed for the routing protocol is complete. Now the nodes will relay packets that are from the same network. To improve the efficiency of the routing protocol, every packet is assigned a unique packet-ID called PID. When relaying a packet, this packet-ID is stored locally for a fixed amount of time. A packet whose PID is already stored locally will not be relayed, because this would lead to multiple transmissions of the same data. Furthermore, a fail-safe is implemented, by limiting the maximum number of times a packet can be relayed. This maximum number of hops,  $N_{h,max}$ , as well as the current number of hops,  $N_{h,cur}$ , is transmitted with each packet. When a packet is relayed, the current number of hops is increased by one. When  $N_{h,max} =$

$N_{h,cur}$  the packet is not relayed anymore. This prevents a packet from circulating around the network indefinitely and blocking other transmissions.

Another problem with relaying packets in a mesh network is the multiple re-transmission of the same packet, leading to collisions. To reduce the likelihood of this occurring, a relay window  $I_{rel}$  was proposed. Within,  $I_{rel}$  the packet can be re-transmitted at any time  $t_{trans}$ , with each start time being equally likely. It is then occupying the channel for the time  $t_{air}$  defined in equation (9.6). This means the transmission will occur within  $I_{rel} + t_{air}$ . Neglecting the propagation time from the sender to the receiving nodes, all receiving nodes randomly select a start time  $t_{trans}$  for relaying the packet. Such a scenario is depicted in Figure 10.3.



**Figure 10.3:** Exemplary relay interval for two nodes without a collision.

The key metric of interest in this scenario is the probability of collisions in the relay window. This probability can be calculated using the probability of intersecting intervals, representing the likelihood that  $n$  intervals with length  $\omega$  randomly placed in a range  $L \in [0; 1]$  do not overlap. The formula to compute this probability is:

$$P_{no,int} = [1 - (1 - n)\omega]^n \quad (10.4)$$

To calculate the likelihood of a collision-free transmission for a given relay window ( $I_{rel}$ ) and packet with airtime ( $t_{air}$ ), the formula can be simplified to:

$$P_{no,coll} = [1 - (1 - n)\omega]^n = [1 - (1 - n)\frac{t_{air}}{I_{rel} + t_{air}}]^n \quad (10.5)$$

where the relative interval length is  $\omega = \frac{t_{air}}{I_{rel} + t_{air}}$ . This probability is crucial in determining an appropriate value for  $I_{rel}$  to avoid excessive transmission times, which can negatively impact energy consumption.

In Figure 10.4, the probability of a collision-free relay window is assessed for  $n = 2, 3,$  and  $4$  nodes, depending on the relative interval length  $\omega$ .

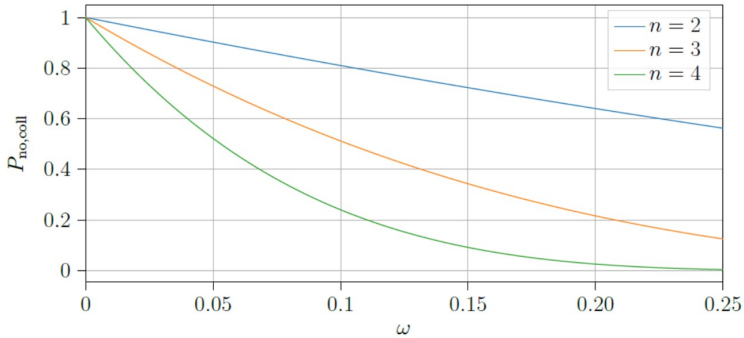


**Figure 10.4:** Probability of a collision-free transmission depending on the relative interval length  $\omega$ , evaluated for  $n = 2, 3, 4$  nodes.

A successful transmission is still possible even if some intervals intersect because they all transmit the same packet, and only one of the transmissions needs to be successful. Additionally, not all nodes are within the transmission range, so simultaneous transmissions might be received correctly by a node reachable only by one of the sending nodes. To ensure reliability, a probability threshold of  $P_{no,coll} \geq 0.5$  was chosen for selecting  $I_{rel}$ , resulting in a relative interval length of  $\omega = 0.05$ , as shown in Figure 10.4. Since the air time for each packet varies significantly with the selected spreading factor, the relay window size should be adjusted accordingly. The maximum packet air time  $t_{air,max}$ , calculated using Equation 9.6 and considering the maximum packet payload size  $N_{pay,max}$ , leads to the following definition of  $I_{rel}$ :

$$P_{no,int} = \left(\frac{1}{\omega} - 1\right) \cdot t_{air,max} \quad (10.6)$$

## 10.2.4 Transport and Application layer

The main purpose of the proposed network protocol is to monitor certain parameters of an infrastructure project. This is done periodically with the monitoring interval  $I_{mon}$ . Every interval lasts for  $I_{mon}$  and has the same structure. Synchronization of the nodes is needed to reduce the active time of the nodes while still allowing multi-hop connections. The nodes are only active for a time  $T_{act}$  at the beginning of the interval. For the rest of the interval, the nodes are in sleep mode to conserve the battery. This means that all communication must take place in the active part of the interval. This part is again split into two different paths. The first part is reserved for all scheduled data packets from the nodes. Every node is assigned a slot in which it is allowed to send. All slots have the same length,  $T_{slot}$  and thus the time required for all scheduled transmissions is  $T_{sched} = N_{con} \cdot T_{slot}$ , where  $N_{con}$  is the number of nodes connected to the central node of the cell. After the scheduled transmission window is finished, the second part of the active part of the interval is reserved for unplanned transmissions like commands. These can only be initiated by the central node and can be used for administration tasks. The length  $T_{ext}$  of this interval is fixed at the start of the network. After the windows for sending commands have ended, the nodes start sleeping. To ensure the nodes are awake at the beginning of the next interval, they wake up a bit earlier than needed. This buffer  $T_{buf}$  is defined at network start-up and is the same for all nodes. The structure of an exemplary interval with three connected nodes is shown in Figure 10.5.

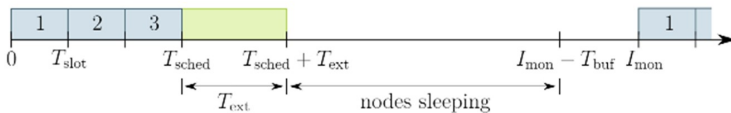


**Figure 10.5:** Structure of a monitoring interval with  $N_{con} = 3$  and the time relative to the interval  $t_{(int,start)}$ .

Setting up the network is done in three phases. First, the nodes are registering with the central node and join the cell. After this is completed, the monitoring interval

is synchronized with all nodes, and they are assigned their respective sending slot inside this interval. When all nodes have successfully adjusted to the interval, a command is broadcast to all nodes to start sending. The central node waits until it has received at least one data packet from each node. After it has done so, the network was successfully started, and monitoring can begin.

Once the network has been set up, the monitored data is sent to the central node. Because the nodes have a sending schedule, the successful reception can be checked. After  $t_{int,start} + T_{sched}$  a receive-check is executed, and it is checked if a packet was received from all nodes that are currently sending. If a packet is missing, the central node is sending a command to the node and requests the data to be sent again. These commands are sent inside the second part  $T_{ext}$  of the active part of the interval.

The transmissions in the network will be organized in packets. These packets consist of a fixed header and the actual payload. The header is also called overhead because it is not carrying any information that the user is interested in, but it is needed for routing and other application-specific tasks. The protocol implements different packet types for different actions the application needs to perform, for example, the join requests.

## 10.2.5 Packet structure

The LoRa transceivers from Semtech handle packets in bytes, resulting in byte-wise structured packets for the proposed network. The packet header has a fixed size of nine bytes, as shown in Figure 10.6.

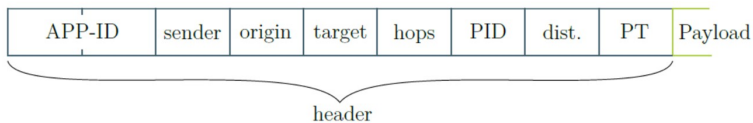


**Figure 10.6:** Byte-wise structure of a packet with a header.

The first two bytes of the header serve as the application identifier (APP-ID) for the network. This allows for distinguishing packets from external nodes, as the same ISM bands are used by other LoRa and LoRaWAN applications. The next three bytes represent the sender's node identifier (NID), the node where the packet originated, and the destination node's identifier. The destination can be a specific NID for direct communication or zero for broadcasting to all nodes in the cell.

The fifth byte stores the hop count, limited to a value of 16 to accommodate four bits. The first four bits represent the maximum hop count ( $N_{h,max}$ ), and the remaining bits indicate the current hop count ( $n_{h,cur}$ ).

The sixth byte is used for the packet identifier (PID), and the seventh byte stores the distance and direction of the last node that sent the packet. The first bit of the seventh byte indicates the packet direction (uplink or downlink), while the remaining seven bits represent the distance ( $d_n$ ) of the last node.

The eighth byte is reserved for the packet type, classifying the payload contents. All bytes after the ninth one are used for the payload, with the payload length for the proposed protocol denoted as  $N_{p,pay}$ . It is possible for a packet to have an empty payload.

## 10.2.6 Time synchronization

In order for the network to operate smoothly, all nodes must synchronize with each other. This synchronization is achieved by aligning all nodes with the interval cycle of the central node. Each monitoring interval has a length of  $I_{mon}$  and is divided into different phases, which must be synchronized with the sending interval of the nodes. This requires all nodes to start their intervals at the same time.

To achieve synchronization, a SET INTERVAL command is sent to every node, containing information to calculate the six timing variables of the nodes. The key parameter is  $t_{nls}$ , which represents the time until the next interval starts. Using this information along with  $T_{off}$ ,  $T_{act}$ , and  $I_{mon}$  from the network, the nodes can

calculate their local timing variables. Additionally, the transmission time  $t_{air}$  and the number of hops  $n_{h,cur}$  of the packet are used to estimate the time test when the packet was sent by the central node. With the estimated time test, the nodes can calculate three missing timing variables:  $t_{int}$ ,  $t_{start}$ ,  $t_{sleep}$ , and  $t_{send}$ .

Once the nodes have successfully calculated their timing variables and aligned their intervals with the central node, they send an ACK packet. Once all nodes have acknowledged the interval, the central node can proceed with starting the network.

To combat drift in the local real-time clock (RTC), the nodes periodically realign their intervals using RESYNC INTERVAL commands, which only contain the time until the start of the next interval  $t_{nis}$ . The nodes can re-align their local intervals using the calculations from the SET INTERVAL command. This process ensures that the network operates accurately and efficiently.

## 10.3 Simulation

A simulation program for LoRa nodes was created for quick testing of various protocol designs. A simulator was written in Python and the program was customized to suit the intended purpose and facilitate a detailed analysis of transmission failures.

The simulation operates on entities situated at specific positions within a two-dimensional world. Unlike event-based simulations, it uses a time-based approach, which may extend the simulation's runtime. However, this choice ensures smoother integration of the simulation code into real hardware in the future. Figure 10.7 shows the visualization of the simulation of the configuration from Figure 10.1. The simulation allows the possibility to visualize the scenario for a better understanding.

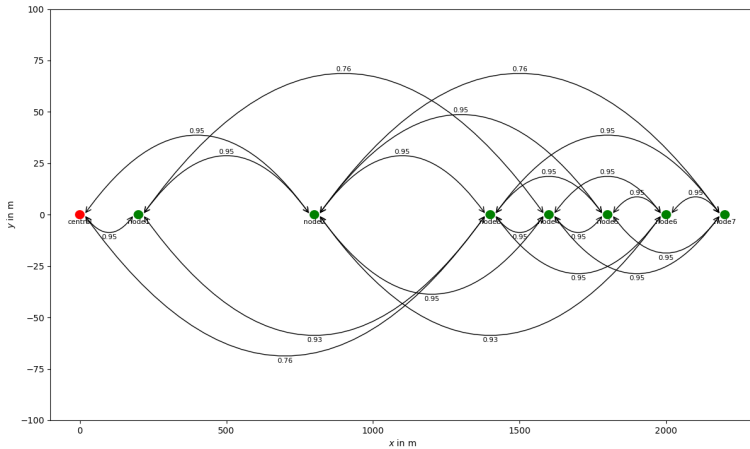


**Figure 10.7:** Automatically generated schematic for the example configuration with  $P_{c,static} = 0.05$ . The value next to the arrows indicates the probability of a successful transmission  $P_{succ}$  between these two nodes.

### 10.3.1 Simulation setup

The simulation proved to be highly beneficial for testing various protocol design points and enabled the gradual development of the network protocol. Initially, a simple flooding algorithm was used as a reference, resulting in a high packet delivery ratio (PDR) but an excessive number of sent packets. This negatively affected network size and energy consumption. However, through the simulation, the network protocol was refined to reduce the number of transmissions while maintaining a satisfactory PDR.

Another critical aspect investigated was the network's topology and the number of links each node possesses. This evaluation was essential for node placement outside the areas of interest, where nodes primarily serve as information relays to the central node. The simulation demonstrated that long chains of single links

lead to unreliable communication due to the accumulation of transmission error probability ( $P_{c,static}$ ) with each link.

### 10.3.2 Simulation result

The proposed protocol was evaluated through simulations, using distance-based and basic flooding as the routing algorithms. Each option was simulated ten times over a 24-hour period. The simulations measured the packet delivery ratio (PDR), collision rate ( $\gamma_{col}$ ) of packets at the nodes' transceiver modules, and the total number of packets ( $n_{air}$ ) in the air at the central node. The simulation results were analyzed and presented in Figure 10.8 using a box plot.

The simulations show that basic flooding performs poorly in terms of packet delivery ratio across all values of  $P_{c,static}$ . However, other relevant parameters need to be considered. For instance, the average collision rate in the network is high, with over half of the packets being wasted due to collisions. Additionally, the main drawback of using basic flooding as a routing parameter is the sheer number of packets sent. Even in a small scenario, the central node exceeds the fair use policy of approximately 15,000 packets/day for SF = 7 and a payload  $N_{pay} = 26$  bytes. In contrast, the proposed distance-based routing only reaches about two-fifths of that limit.

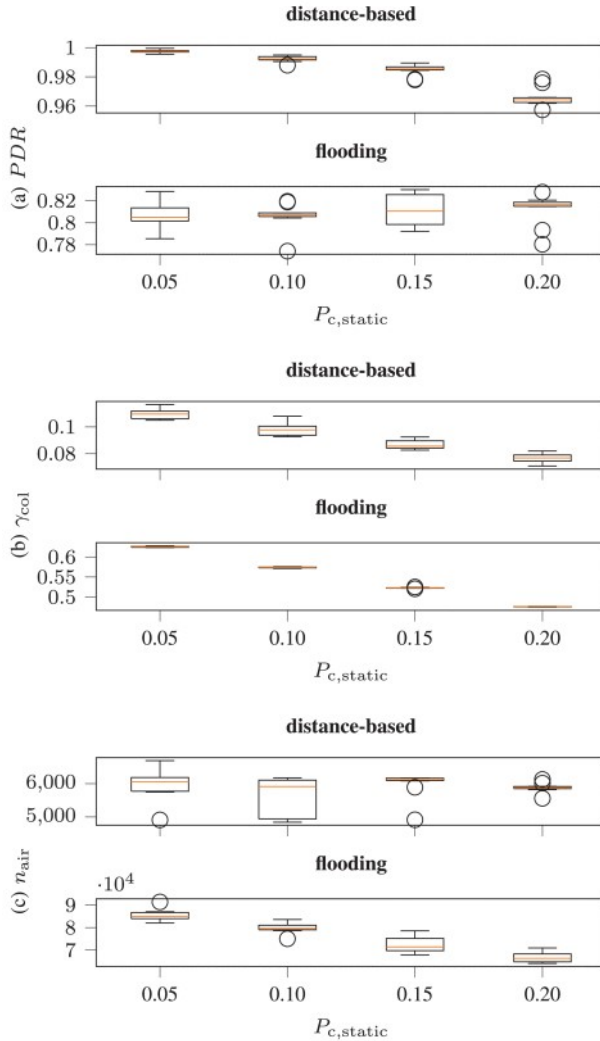


**Figure 10.8:** Simulation results of the example scenario with  $T_{mon} = 5$  min. Box-plot over 10 simulations for each value of  $P_{c,static}$ . Analyzing the packet deliver ratio PDR (a), averaged collisions rate  $\gamma_{col}$  overall transceivers (b) and number of packets on the channel at the central node  $n_{air}$  (c).

To analyze the impact of the number of nodes connected to the central node on the fair use policy, another set of simulations was carried out by doubling the length of the sensor chain to fourteen nodes. Figure 10.9 shows the PDR per node, and all results are available in Figure A.2 in the appendix for this scenario. The overall packet delivery ratio PDR of the longer scenario is only slightly lower when compared to the shorter sensor chain. When analyzing the PDR of each node individually, the far-off nodes have a slightly lower PDR. This is because these nodes require more hops to reach the central node and are thus more likely to be corrupted.

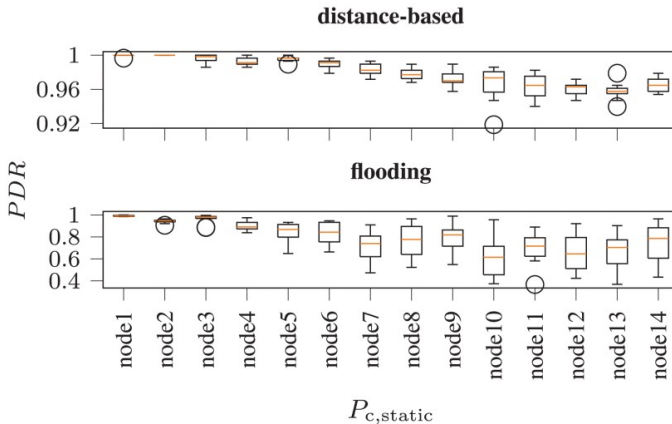


**Figure 10.9:** Number of packets on the channel at the central node for  $T_{mon} = 5$  min, analyzed for a sensor chain with 14 nodes.

## 10.4 Hardware measurement results

Once the network protocol was successfully developed and tested in simulations, the next step involved deploying it on real hardware for further validation. For the sensor nodes, Heltec LoRa 32 (V2) development boards were utilized [188], while a Raspberry Pi with a RAK811 LoRa module [189] was employed as

the central node. Both of these hardware options featured the SX1276 LoRa transceiver module from Semtech [190], ensuring smooth and compatible data transmissions.

### 10.4.1 Central node

The central node was created using a Raspberry Pi and a RAK811 LoRa transceiver module for LoRa communication. Leveraging Raspberry Pi's programming capabilities in Python, the simulation code could be easily adapted for real hardware, significantly speeding up the development time. Figure 10.10 shows the hardware setup of the central node.



**Figure 10.10:** Picture of the hardware used as the central node: RaspberryPi 3B with a RAK811 LoRa module connected over Serial.

The central node operates as a Linux service, continuously running in the background. Additionally, it hosts a website on the Pi, providing a simple user interface to control the network and display an estimated network topology. Users can send commands to the network through this interface. The central node also logs its operations in a text file for troubleshooting purposes. All received DATA packets

from the network are stored in an SQL database for later analysis, accessible through the website for quick evaluations. Figure 10.11 shows a screenshot of the website.

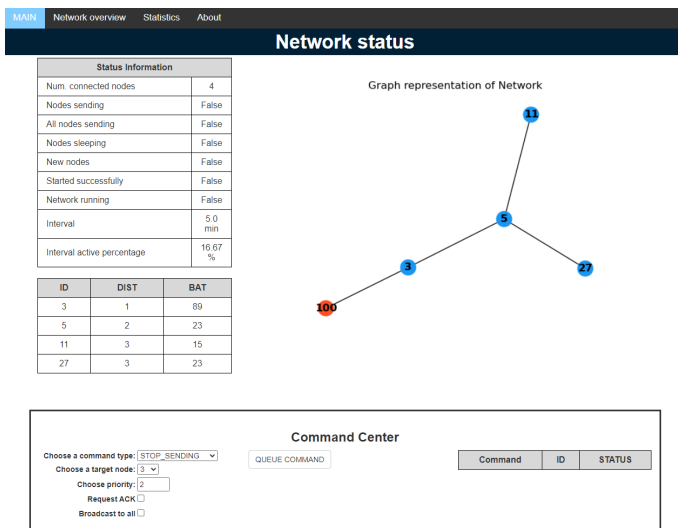


**Figure 10.11:** Screenshot of the website used to control the network.

## 10.4.2 Sensor node

The sensor nodes are constructed using the Heltec LoRa 32 (V2) development board, equipped with an ESP32 microcontroller, integrated USB to serial interface, and a charge controller for Li-Po batteries. The ESP32 microcontroller supports various sensors through standard interfaces like SPI and I2C. To test the network, the MPU6050 inertial measurement unit (IMU) was employed. This IMU allows the sensor node to measure acceleration in all three dimensions, providing information about its orientation. The collected data, including accelerometer readings, sensor temperature, and battery level, are transmitted in a DATA packet.

To supply the sensor nodes with power, 1200 mAh Li-Po battery was connected to the Heltec board. This enables the sensor node to run for a couple of days, due to the increased energy consumption compared to traditional LoRaWAN star networks. To increase the lifetime of the network, the batteries can be recharged using solar panels that can be connected to the TP4056 Li-Po charger chip already present on the Heltec board. Figure 10.12 shows the assembled sensor without the top of the case assembled.



**Figure 10.12:** Picture of the real sensor node without assembled top part of the case.

To facilitate outdoor testing of the network, a 3D-printable waterproof case was specifically designed to protect and shield the assembled sensor nodes from environmental elements. This allowed the network to be tested in real-world conditions, ensuring its functionality and reliability.

### 10.4.3 Range testing

The proposed network protocol was tested on the south campus of KIT. To begin the evaluation, suitable node placements were determined. A central node was placed at the ITIV institute, and its single-hop coverage was measured.

To assess the single-hop link quality, a NEO-6M GPS module was connected to one of the Heltec boards. The GPS module periodically sent the current location every 5 seconds once it obtained a valid position. The node with the GPS module was then moved around the campus to determine the coverage area. Whenever the central node received these GPS packets, it stored the received data, including the RSSI and SNR of the packet, in an SQL database. This process resulted in a collection of positions that had a direct communication link with the central node. The initial test was performed with  $SF = 7$ . The received locations and their corresponding RSSI values were plotted on a map of the campus, as shown in Figure 10.13.



**Figure 10.13:** Range testing for  $SF = 7$  using a GPS module in combination with the Heltec node, color coding the RSSI the packet was received with.

The theoretical values for the RSSI with the LoRa transceivers are in the range of  $-30$  dBm to  $-120$  dBm. These values were not reached during testing, as the minimum RSSI received was around  $-100$  dBm and the maximum was around  $-55$  dBm. The upper bound can be explained by the fact, that the GPS module was only working outside the building and the central node was located inside the department offices.

An analysis of the received positions revealed that most of them were within the line-of-sight (LOS) of the ITIV office building. This observation might be a consequence of using the lowest spreading factor  $SF = 7$ , which has the smallest transmission range. To investigate further, the test was repeated with  $SF = 10$ , and the results are presented in Figure 10.14.

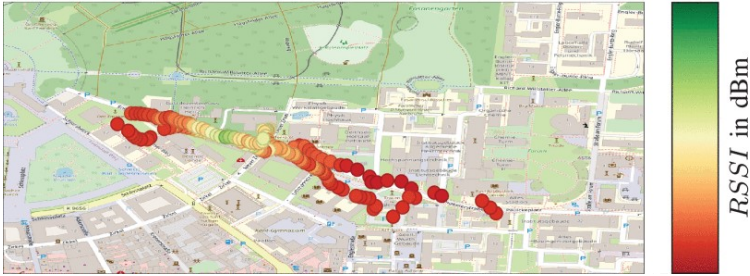


**Figure 10.14:** Range testing for  $SF = 10$  using a GPS module in combination with the Heltec node, color coding the RSSI the packet was received with.

In this test, the accuracy of the GPS connection suffered temporarily. One example of this is visible on the main street. But overall, the results were similar to  $SF = 7$ . This suggests that the spreading factor mainly affects the range in LOS transmissions over longer distances. Transmissions from lightly obstructed positions may come through, but they are hindered by normal-sized buildings. As the spreading factor does not significantly impact the transmission range in urban environments,  $SF = 7$  was chosen for testing to reduce the air time  $t_{air}$  of the packets.

## 10.5 Performance analysis

The sensor nodes on campus were strategically placed based on the results of the range test to assess the multi-hop communication capabilities of the developed network protocol. The chosen measurement locations were also designed to resemble the simulated example scenario. The positions of the sensor nodes on campus were marked with their respective node-IDs on the map in Figure 10.15.

In this test, the nodes were provisioned with node-IDs and placed at their designated locations on the campus. The central node then initiated the network re-configuration every 5 minutes ( $T_{mon}$ ) until all nodes were successfully connected within 20 minutes. The network remained stable for two days, experiencing rainy weather with occasional snow.

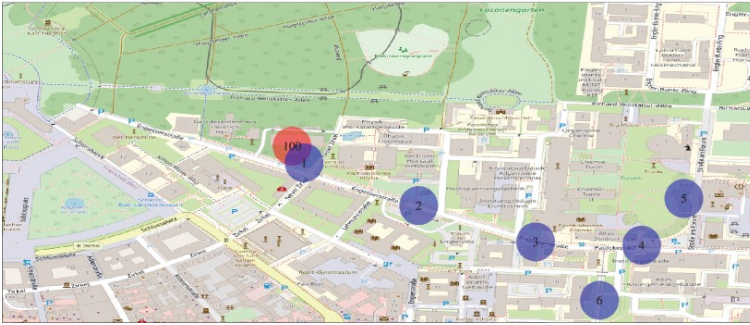


**Figure 10.15:** Placement and node-ID of the nodes at KIT campus south, red is the central node and blue is the sensor nodes.

During the two days, the network demonstrated an impressive overall PDR of 99.42%, surpassing the simulation results. This improvement could be attributed to a lower static packet error rate ( $P_{c,static}$ ) on the communication channel. As observed in the simulation, the communication link quality decreased with the chain length. Table 10.1 shows the PDR for each node.

**Table 10.1:** Packet delivery ratio (PDR) and distance  $d_n$  for each node.

Node	PDR in %	distance $d_n$
Node 1	100.0%	1
Node 2	100.0%	2
Node 3	100.0%	3
Node 4	99.5%	4
Node 5	98.0%	5
Node 6	99.0%	5

The communication link's quality in the Low Power Wireless Mesh Network (LPWMN) decreases with chain length, consistent with the findings from the simulation. However, the network's overall reliability remains sufficient for non-critical monitoring systems.

Another essential characteristic of the LPWMN is its energy efficiency, which was also evaluated in the field test. Battery levels of nodes 1, 3, and 4 were analyzed, as they were transmitted back to the central node with every DATA packet. The graph in Figure 10.16 displays the battery levels of these nodes.

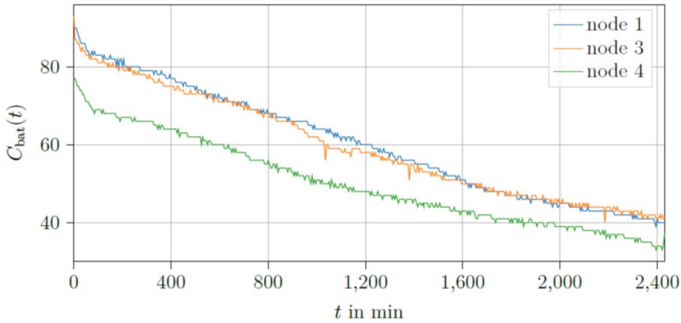


**Figure 10.16:** Charge level  $C_{bat}(t)$  of the batteries for nodes 1, 3, and 4.

Since the battery level was sent only after the nodes successfully joined the network, the graph does not start at 100%. Moreover, due to the measurement inaccuracies of the battery level, the exact time when the nodes received the ENABLE SLEEP command is less clear compared to the simulation. Nonetheless, the energy consumption observed in the field test allows the nodes to last for approximately four days, which aligns well with the simulated energy consumption.

## 10.6 Energy consumption

Continuous monitoring of nodes requires a reliable power source for battery recharge, and solar panels are commonly used for this purpose. In a network with four nodes, two nodes were equipped with solar panels while the other two were not. Figure 10.17 illustrates the battery level of these nodes over time, with nodes 1 and 2 having solar panels connected and nodes 3 and 4 without them.

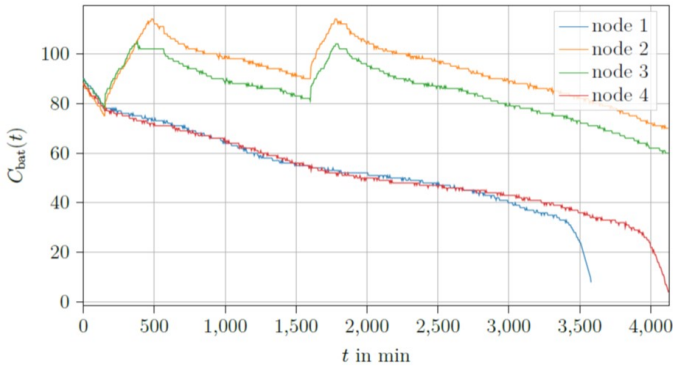


**Figure 10.17:** Charge level  $C_{bat}(t)$  of the batteries during the solar panel testing. Nodes 2 and 3 have a solar panel connected, whereas nodes 1 and 4 do not.

At approximately  $t = 150$  min, the ENABLE SLEEP command was sent to the nodes, resulting in a noticeable gradient change in the battery levels, as also observed in the simulation. Simultaneously, nodes 2 and 3 were connected to the solar panel, and the impact of the solar panel on the battery levels can be observed in the graph. The solar panel enables nodes 2 and 3 to recharge their batteries, ensuring the continued functionality of the network.

The battery level is estimated using voltage measurements across the battery terminals. With the solar panel charging the battery through the charge chip, there is a sudden jump in the battery level. This behavior is attributed to the measurement principle, which is based on the voltage between the battery's anode and cathode. The measured voltage is then linearly approximated within the operational voltages of the battery (3.7V to 4.2V) to estimate the charge status. This linear approximation works well for the first half of the battery capacity but deviates for the second half, as evident from the graph.

# **11 Intelligent sensors network for Power Grid Monitoring**

This dissertation section focuses on the development of frequency perturbation predictions and the creation of machine learning models to predict the current-carrying capacity of overhead lines based on weather conditions by employing a probabilistic non-parametric approach. Nevertheless, it is essential to integrate these models into a system that aligns with operational requirements to ensure their effective implementation for real-time monitoring and control.

## **11.1 Implementation of a distributed sensor network**

The LoRa wide mesh wide area network was presented in Chapter 10 for overhead transmission monitoring. An implementation of a distributed sensor network along an OHTL involves multiple sensors that are geographically distributed and interconnected to collect and exchange data for determining the current carrying capacity of different sections of an OHTL at various points in time. However, the placement of a sensor at every span of OHTL may not be economical and efficient.

The optimum placement of the sensor at the hotspot location is one of the fundamental tasks that has to be considered in DLR implementation for overhead transmission line monitoring. Identifying critical spans or segmenting overhead

transmission lines into critical and non-critical sections involves analyzing various factors such as temperature, wind speed, and current. The procedure involves calculating capacities for each span and identifying the spans with hotspots or with the minimum capacity. This information is then used to create a probability distribution function, which assesses the likelihood of encountering minimum current-carrying capacities at different parts of the overhead transmission line based on observed weather conditions. The histogram in Figure 11.1 shows hotspot distribution along the overhead transmission line and highlights regions with a high probability of becoming bottlenecks, where the conductor temperature frequently reaches its peak. Conversely, there are regions where the capacity rarely hits its minimum. To filter out less critical points, a threshold ( $t$ ) is set by the TSO, and any points below this threshold in the probability distribution function are disregarded from the list of hotspots along the line.

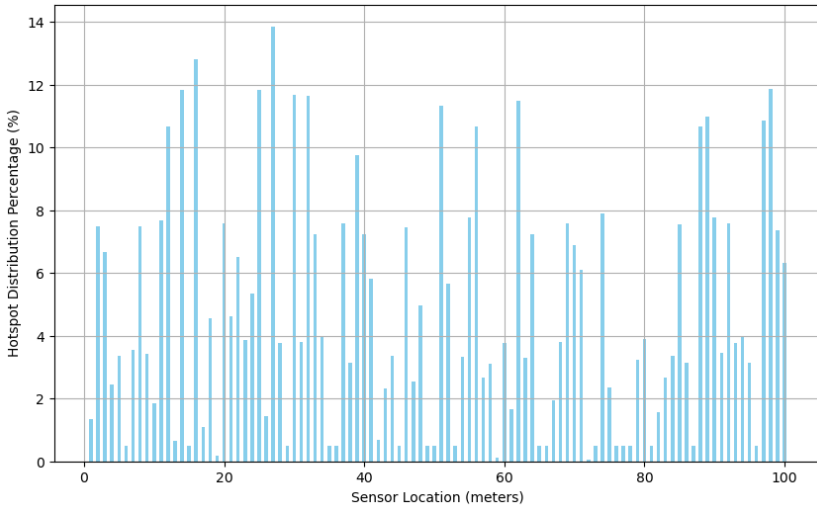


**Figure 11.1:** Simulation of a real case of a congested transmission network and positioning of minimum current-carrying capacities along the overhead line. The more frequently current-carrying capacity minima appear along the overhead line, the more likely it is that the specific line span will act as a bottleneck for capacity.

Figure 11.2 illustrates the hotspot filtering threshold (i. e, 5% percentiles) in which the probability distribution along the line is arranged in ascending order of probability. The hotspots at the left of the threshold point (or red dot on Figure 11.2) are considered negligibly. Consequently, these elements are rounded down to zero, retaining only the most probable hotspots. The unfiltered segments of the line are then rearranged and prioritized in descending order for sensor installation.

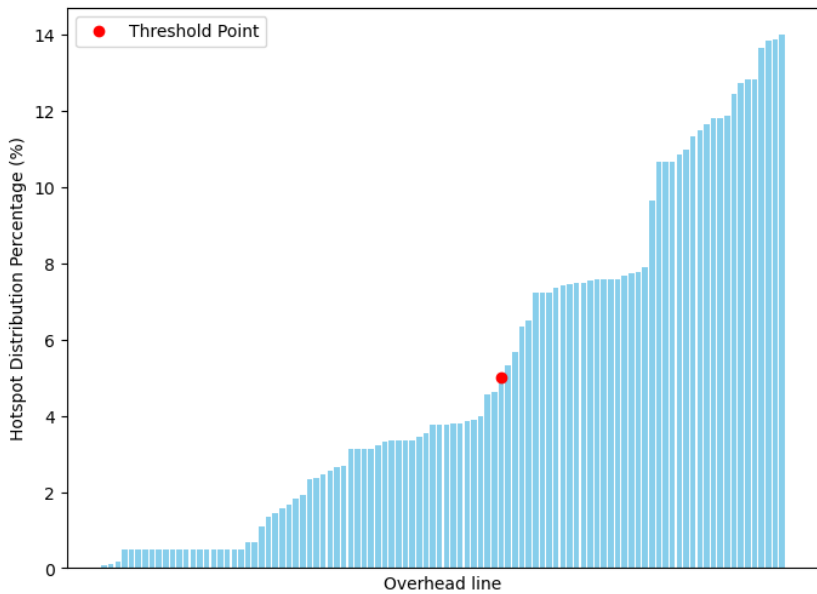


**Figure 11.2:** Example illustrates how to establish the filtering threshold for hotspot analysis. Specifically, it demonstrates using 5<sup>th</sup> percentile. Any values falling below this threshold are set to zero, focusing solely on higher probability locations.

Critical spans induce hot-spot temperature and are vital for determining line ampacity. Identifying these critical spans is crucial for utility providers overseeing expansive overhead transmission networks, as it enables them to pinpoint bottlenecks and optimize power transfer. The process involves determining the optimal

number and placement of sensors along the entire line, dividing it into non-uniform segments with spans considering various terrains. By identifying critical spans, providers can ascertain the maximum current carrying capacity, allowing for effective alleviation of transmission line congestion based on permissible vertical clearance to the ground.

The optimum sensor placement technique is crucial for the effective monitoring of transmission lines. The goal is to strategically position sensors to maximize coverage and detection capabilities while considering factors like line length, thermal constraints, budget constraints, etc. Once the hotspot span is identified and sorted from highest to lowest hotspot probabilities, the minimum number of required sensors is determined based on the constraints. After sensor installation, the current-carrying capacity is calculated. This capacity calculation relies on interpolating weather observations to the electrical towers. It's important to note that the implementation of a DLR system is a complex process that requires collaboration with experts in power systems, meteorology, and sensor technology. Additionally, local regulations and guidelines should be followed throughout the installation process.

## 11.2 Tools for system monitoring

The power grid monitoring tool aims to provide an interactive tool for operators to engage with grid information. It is designed to provide real-time situational awareness of power grid conditions and to help operators identify and respond to potential problems before they lead to outages or other disruptions. For an effective view of grid monitoring, an interactive website tool was developed and the first view of the website is shown in Figure 11.3. The software tool offers the capability to monitor the flow of electricity across the power grid and to respond to changes in supply and demand in real-time. The tool enables operators to observe updated data generation and active load consumption. Also, it provides the opportunity to trace back based on different timescale resolutions.



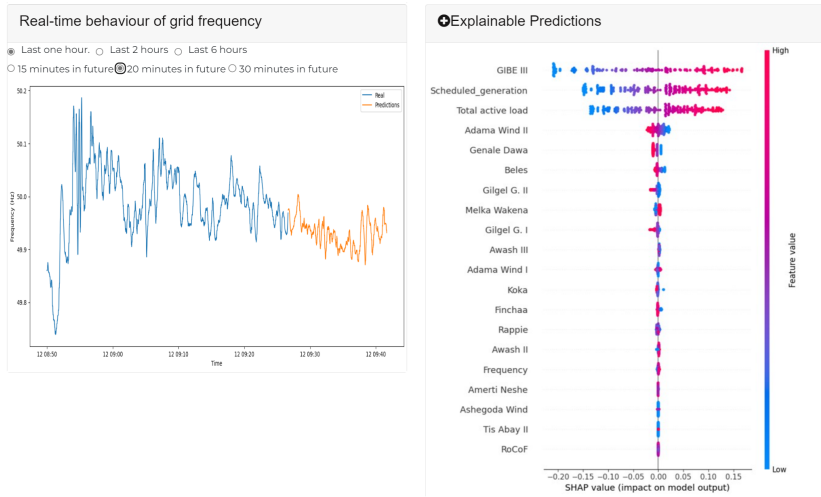


**Figure 11.4:** The example illustrates a grid frequency trajectory for the past 40 minutes and 20 minutes ahead predictions with explainable AI predictions.

Another view (Figure 11.6) on the website focuses on transient analysis. By considering current weather conditions and power flow through the conductor over time, it calculates changes in conductor temperature (see Section 7.1). Users can input current flow and analysis time, triggering a warning if the calculated temperature surpasses the safety limit, along with a notification of when this could happen. The ability to monitor short-term changes in conductor temperature allows system operators to manage short-duration congestion situations by leveraging the conductor’s slow thermal response. Usually, the thermal response time of the conductor occurs between 1 and 15 minutes, based on conductor type and weather conditions. This enables the transmission of more power than the current capacity without causing overheating in favorable weather conditions.

The grid monitoring software includes a tool to calculate how long an overhead line can handle extra power during congestion. It requires the Transmission System Operator (TSO) to input the electrical current for a brief period, and the tool predicts the duration this setting can operate based on current weather conditions. A user-interface example is illustrated in Figure 11.7. Short-term adjustments

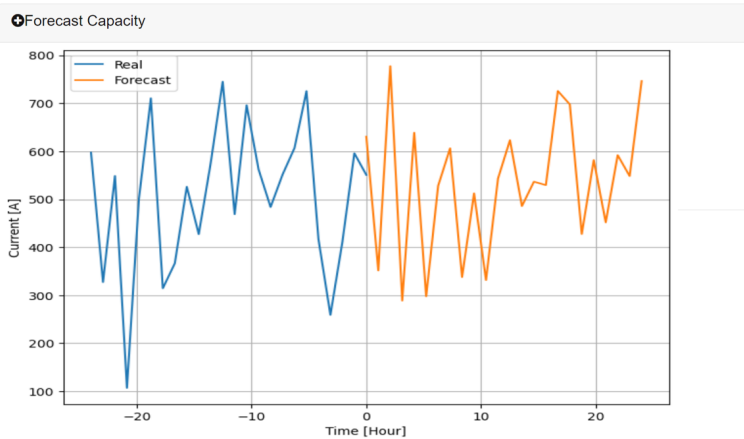


**Figure 11.5:** Grid monitoring software tool: view of the overhead line and its ampacity.

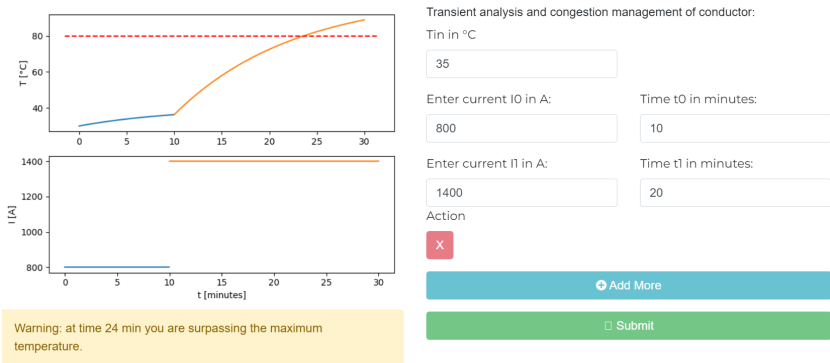


**Figure 11.6:** Grid monitoring software tool: Transient analysis of the conductor temperature under different loading schemes.

rely on a monitoring system and analysis tool. Redundant measurement systems, like combined weather stations and conductor temperature sensors, are strongly recommended to ensure overhead line longevity and system safety.

For instance, in a scenario with an ACSR Mallard overhead line experiencing sunny, windy, and cool conditions ( $980 \text{ W/m}^2$  solar radiation,  $2 \text{ m/s}$  wind speed perpendicular to the line,  $23 \text{ }^\circ\text{C}$  ambient temperature). Initially operated under

its capacity, the conductor's initial temperature registers at  $30\text{ }^{\circ}\text{C}$ . This provides a window to safely transmit additional power within the line's thermal constraints due to the gradual heating characteristics of the conductor. Figure 11.7 illustrates a short-time congestion measure.

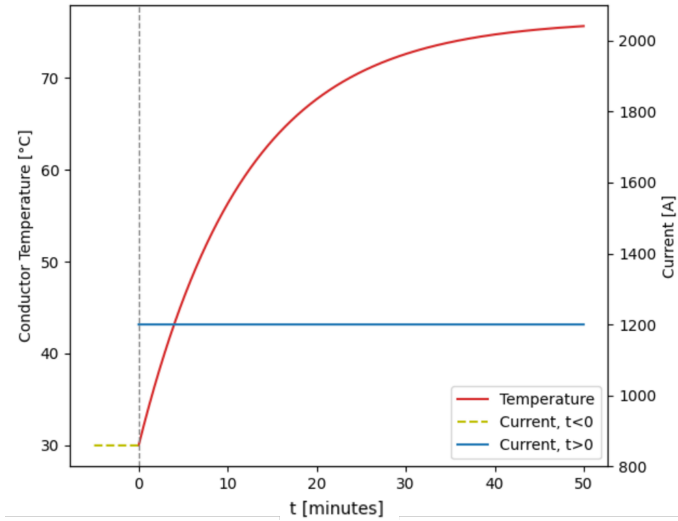


**Figure 11.7:** Grid monitoring software tool: Case of short time congestion management measure.

The need arises to increase power transmission due to congestion. When the current reaches the maximum transmission capacity, the conductor temperature reaches  $80\text{ }^{\circ}\text{C}$  in 50 minutes. To resolve congestion, the TSO suggests operating the line at 1.1 times the capacity for at least 5 minutes, confirmed safe by transient analysis, allowing over 11 minutes before reaching the maximum temperature.

# 12 Summary

## 12.1 Summary

This dissertation presented the development of machine learning models for predicting frequency deviation and probabilistic Dynamic line rating (DLR) forecasting of transmission grids. The system can help transmission system operators (TSOs) to avoid line congestion scenarios, which is a key point towards the flexible grid deployment.

Methodology for forecasting the frequency deviation of a power grid can provide operators with up-to-date information to assess the need for intervention to maintain the frequency within the stipulated limits. This was simulated and tested using the Ethiopian power grid frequency dataset and showed good performance compared to selected benchmarks. Further investigations revealed that the forecasting performance can be affected by the number of hidden layers, neurons, embedding window, prediction horizon, and learning rate. This methodology was also able to handle measurement errors and took 8 milliseconds of computation time for a single forecast, making it suitable for real-life applications.

DLR probabilistic forecasting has been analyzed and simulated for overhead lines located in the Ethiopian power grid. Quantile regression forest (QRF) is used to predict DLR as a function of environmental weather conditions for a simulated Aluminium conductor steel-reinforced cable (ACSR) overhead transmission line. The numerical testing for 220 KV transmission lines demonstrates the increase in line rating using this method. The risk analysis shows that the DLR can be safely integrated into grid monitoring and ampacity forecasting, by considering

probabilistic forecasts for quantiles below 50% (compared to point forecast benchmarks) to reduce overestimation and risk of overloading. Furthermore, the Mean Absolute Percentage Error (MAPE) is less than 20% for 0–2 hours, which will suit short-term congestion planning or overload monitoring.

For the data collection task of the transmission grid network, LoRa was chosen as the target technology. It is the Low-power WAN (LPWAN) technology with the most open architecture, both hardware and software. Only the LoRa modulation was used, and all LoRaWAN functionality was omitted and replaced by a custom protocol in this work. But the channel used will be in the same ISM bands around 868MHz as LoRaWAN, to allow the use of existing hardware as well as avoiding licensing costs. Therefore, LoRa-mesh offers a cost-effective and efficient alternative to manual inspection and monitoring techniques. It allows system operators to continuously monitor their infrastructure and receive timely alerts, enabling them to take necessary actions before possible failures. This work can easily extend to the distribution grid and transformer monitoring.

Simulation results indicated that a distributed sensor mesh network can effectively achieve a high packet delivery ratio (PDR) for monitoring purposes. Subsequent field tests at KIT on a university campus have further confirmed the efficacy of this network protocol. This suggests the potential use of the proposed network for monitoring transmission and distribution lines, thereby enhancing the stability of power grids in developing countries such as Ethiopia. Initial test outcomes provide a foundation for future comprehensive analysis and detailed investigation. A comparison between simulation and field test measurements underscores the need to implement the proposed system for intelligent grid monitoring.

The network consists of two types of nodes: a central gateway node with continuous power and internet access, and battery-powered sensor nodes without internet access placed at points of interest to measure the parameters in demand. Central nodes have more computing power and server connectivity. Most protocol implementation occurs on central nodes to reduce sensor node load, simplifying network control. The network is designed for remote, inaccessible locations for prolonged monitoring. Nodes have limited battery life, often just a few days. Solar

power is used to sustain nodes in remote areas, ensuring uninterrupted operation. The network consumes more energy than standard LoRaWAN networks but employs solar panels to offset energy usage, maintaining power without relying solely on batteries.

The network incorporates redundancy measures to prevent a solitary offline node from halting the entire system. Every node has multiple connections, boosting the network's dependability and ability to recover. The network's protocol is in line with LoRa modulation and works with Semtech's LoRa Transceivers, enabling smooth integration with existing technologies.

## 12.2 Outlook

This dissertation is part of the first steps toward a flexible electrical grid. Grid optimization mechanisms, such as active power balancing and dynamic line rating forecasting systems, offer a short-term solution to extend the need for the construction of new overhead lines. Machine learning algorithms showed the possibility of monitoring frequency dynamics and adjusting the current-carrying capacity of the transmission line conductor to the surrounding weather conditions.

The provided approach has been assessed and modeled using the Ethiopian transmission network, but it is adaptable to systems of varying scales. Thoroughly investigating load fluctuations over time and the electricity generation mix should also be taken into account for forecasting frequency anomalies.

The next step in the development of the forecasting model outlined in this dissertation involves implementing the system in a practical environment. Collecting weather data for a full year after installing the hardware is crucial for the results of this dissertation. Leveraging transfer learning techniques enables quick adaptations of pre-trained models in a short timeframe. Furthermore, continuous learning can be incorporated to ensure that models are regularly updated based on the latest measurements from the system.

Future developments include the integration of frequency prediction and DLR into control and protection systems. Integration of DLR and rate of change of frequency (RoCOF) into distance relay protection increases the reliability and security of the renewable-dominated power grid.

The developed LoRa mesh network protocol showed promising signs for implementing low-data rate monitoring tasks at remote locations. However, the energy consumption of the nodes is still too high to allow long-term monitoring. Thus, to extend the monitoring time, the nodes can use solar panels to recharge the batteries during the day. In addition, Wake-on-receive would allow the nodes to sleep for longer, as they could also sleep between the transmissions. Therefore, the development of more field tests in Ethiopia is one of the goals of future work.

Finally, the research presented in this dissertation can be expanded for various practical purposes. One potential extension involves utilizing soil sensors to closely monitor crop conditions, enabling farmers to optimize fertilizer and pesticide usage with greater precision. Furthermore, the study identifies promising domains like smart grids, smart cities, air quality management, environmental monitoring, and improved smart farming infrastructure for future applications.

# A Appendix

## A.1 Simulation results

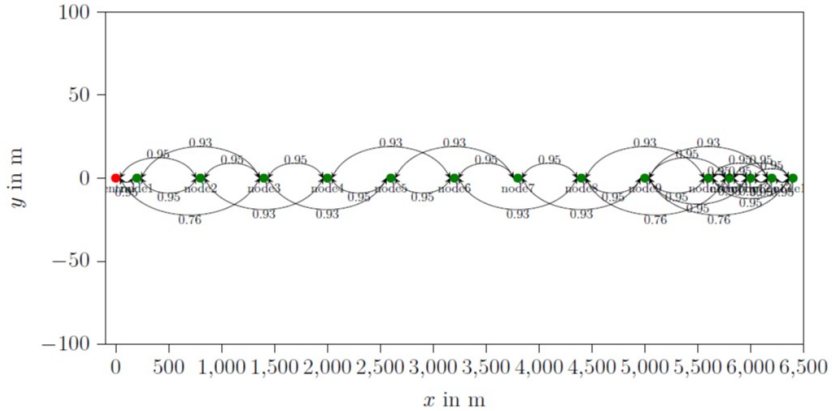


**Figure A.1:** Automatically generated schematic for the example configuration with double the sensor chain length with  $P_{c,static} = 0.05$ . The value next to the arrows indicates the probability of successful transmission of  $P_{succ}$  between these two nodes.

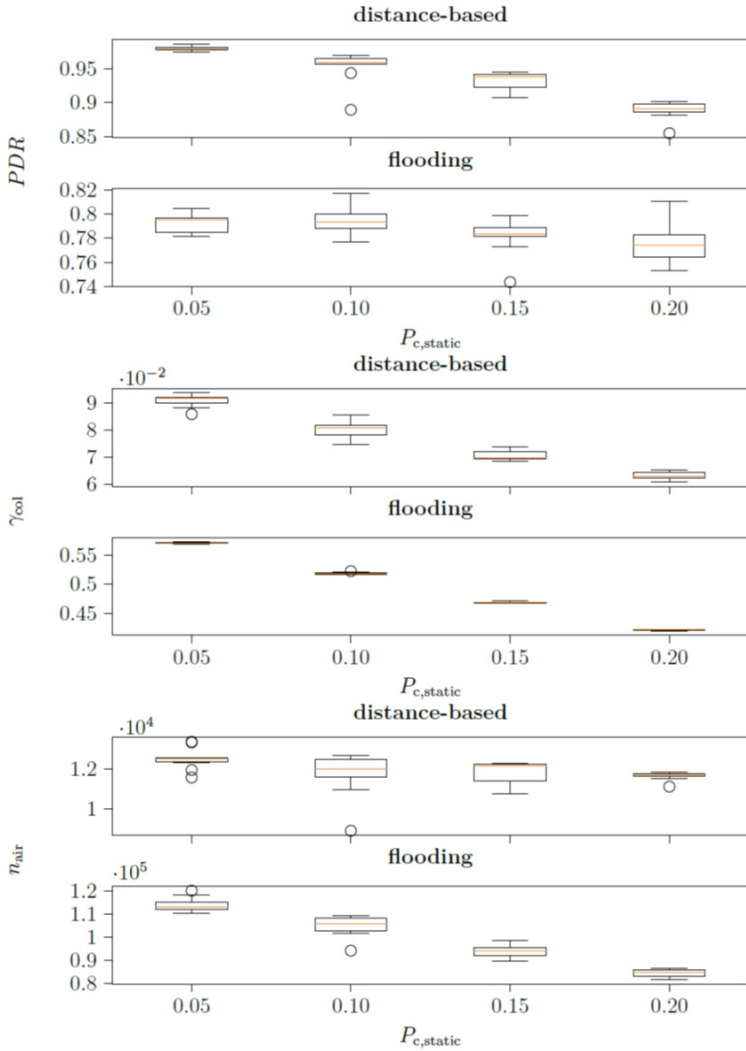


**Figure A.2:** Simulation results of the example scenario with double the chain length, with  $T_{mon} = 5$  min. Box-plot over 10 simulations for each value of  $P_{c,static}$ . Analyzing the packet deliver ration PDR. Averaged collisions rate  $\gamma_{col}$  overall transceivers and a number of packets on the channel at the central  $n_{air}$ .

# List of Figures

2.1	Electricity accessibility between high- and low-income nations. . . .	10
2.2	Geographical location of Ethiopia. . . . .	12
2.3	Trends of Ethiopia’s GDP growth from 1988 to 2028. . . . .	13
2.4	Energy supply in Ethiopia by type and sector. . . . .	14
2.5	Ethiopia’s share of installed capacity by source. . . . .	17
2.6	Geographical interconnection diagram of Ethiopian grid. . . . .	18
2.7	An example of transformer loading measurement result. . . . .	20
3.1	A high-level structure of modern power grid. . . . .	24
3.2	Active and reactive power transfer between a two-bus transmis- sion system. . . . .	25
3.3	Phases of blackout . . . . .	31
3.4	Mechanism of blackouts . . . . .	31
3.5	Dena Grid Study II Expansion and Annual Costs. . . . .	37
4.1	Indicative costs of electricity for on-grid, mini-grid, and off- grid technologies in sub-Saharan Africa. . . . .	42
4.2	Ranking of the top business environment obstacle for firms in Ethiopia. . . . .	46
5.1	Venn diagram of AI and its derivations. . . . .	48
5.2	The basic structure of an artificial neuron or perceptron structure. . .	63
5.3	Hidden layer of MLP network . . . . .	63
5.4	Effects of different learning rates . . . . .	66
5.5	Mostly used activation functions. . . . .	67
5.6	Basic architecture of Recurrent Neural Network . . . . .	69
5.7	LSTM network. . . . .	71
5.8	GRU network. . . . .	72
5.9	One-dimensional CNN network. . . . .	73
5.10	Quantile regression forest algorithm procedure flowchart . . . . .	74

5.11	A multidimensional binary decision tree . . . . .	75
6.1	Load trajectory of the electricity supply in Ethiopia on January 28, 2020. . . . .	81
6.2	Illustration of power-grid frequency fluctuates overtime. . . . .	82
6.3	Grid outage disturbance due to transmission line to Djibouti trip. . .	83
6.4	Flowchart of deep learning forecasting model development process. . .	84
6.5	Reconstruction matrix structure. . . . .	86
6.6	Training and validation loss plot. . . . .	88
6.7	10-step ahead prediction performance evaluation. . . . .	90
6.8	30-minute frequency forecast for 2-steps ahead prediction. . . . .	91
6.9	30-minute frequency forecast for 10-steps ahead prediction. . . . .	92
6.10	Factors for grid frequency perturbations. . . . .	93
6.11	Model bar plot. . . . .	95
6.12	Model summary plot. . . . .	96
7.1	Sample of current variation throughout the day for three different transmission lines. . . . .	98
7.2	Overhead Transmission Line Monitoring sensors. . . . .	106
8.1	Summary of machine learning forecast model. . . . .	110
8.2	High Voltage Grid layout of Ethiopia and study interest point. . . .	112
8.3	The main transmission network of central Ethiopia and Addis Ababa. .	113
8.4	PSS/E simulation for the transmission grid network. . . . .	114
8.5	The transmission grid network PSS/E simulation counter. . . . .	115
8.6	Trajectory of impedance during an unintended tripping. . . . .	116
8.7	A step change in the current and exponential curve for conductor temperature. . . . .	117
8.8	Summary of ampacity forecasting process. . . . .	119
8.9	Case study - selected weather stations from Addis Ababa and its area. .	121
8.10	Mean Absolute Percentage Error for 24-hour forecast model. . . . .	123
8.11	Structure of QRF forecasting development scheme. . . . .	124
8.12	Quantile of Ampacity forecast. . . . .	126
9.1	Schematic structure of LoRaWAN architecture. . . . .	129
9.2	LoRaWAN protocol architecture. . . . .	129
9.3	LoRaWAN packet format. . . . .	130
9.4	Chirp with bandwidth . . . . .	133
9.5	Modulation of data on a chirp . . . . .	133

9.6	Sample networks topology . . . . .	135
9.7	Schematic of flooding algorithm. . . . .	137
10.1	Example of transmission line . . . . .	143
10.2	Monitoring interval vs maximum number of nodes. . . . .	147
10.3	Exemplary relay interval for two nodes . . . . .	149
10.4	Probability of a collision-free transmission. . . . .	150
10.5	Exemplary relay interval for two nodes . . . . .	151
10.6	Byte-wise structure of a packet with header. . . . .	152
10.7	Automatically generated schematic for the example . . . . .	155
10.8	Simulation results of the example scenario . . . . .	157
10.9	Simulation results of the example scenario with double the chain length . . . . .	158
10.10	Hardware used as the central node. . . . .	159
10.11	Screenshot of the website used to control the network. . . . .	160
10.12	Hardware of sensor node. . . . .	161
10.13	Range testing for $SF = 7$ . . . . .	162
10.14	Range testing for $SF = 10$ . . . . .	163
10.15	Placement and node-ID of the nodes at KIT campus south. . . . .	164
10.16	Charge level of the batteries for nodes. . . . .	165
10.17	Charge level of the batteries during the solar panel testing. . . . .	166
11.1	Simulation of the positioning of minimum current-carrying ca- pacities along the overhead line. . . . .	168
11.2	Filtering threshold for hotspot analysis. . . . .	169
11.3	Grid monitoring software tool:Interactive real-time generation and active load. . . . .	171
11.4	Grid frequency trajectory for past 40 minutes and 20 minutes ahead predictions. . . . .	172
11.5	Grid monitoring software tool: view of the overhead line and its ampacity. . . . .	173
11.6	Grid monitoring software tool: transient analysis of the con- ductor temperature. . . . .	173
11.7	Grid monitoring software tool: Case of short time congestion management measure. . . . .	174
A.1	Automatically generated schematic of scenario with double the chain length . . . . .	179

A.2 Simulation results of scenario with double the chain length . . . . . 180

# List of Tables

2.1	An example of distribution network condition assessment result. . . .	20
2.2	Summary of detailed load assessment result. . . . .	21
4.1	Households power outage descriptive statistics. . . . .	41
4.2	Firms power outage descriptive statistics . . . . .	45
6.1	Frequency limits in the EEP transmission system. . . . .	80
6.2	Forecasting performance evaluation in terms of RMSE. . . . .	89
7.1	Surrounding weather conditions. . . . .	97
8.1	Specification of the typical Conductor under study. . . . .	124
10.1	Packet delivery ratio (PDR) and distance $d_n$ for each node. . . . .	164



# Bibliography

- [1] Landscape of climate finance in ethiopia. [Online]. Available: <https://www.climatepolicyinitiative.org/wp-content/uploads/2022/11/Landscape-of-Climate-Finance-in-Ethiopia.pdf>
- [2] A. A. Jenberu and T. G. Admasu, “Urbanization and land use pattern in arba minch town, ethiopia: driving forces and challenges,” *GeoJournal*, vol. 85, no. 3, pp. 761–778, 2020.
- [3] B. K. Terfa, N. Chen, D. Liu, X. Zhang, and D. Niyogi, “Urban expansion in ethiopia from 1987 to 2017: Characteristics, spatial patterns, and driving forces,” *Sustainability*, vol. 11, no. 10, p. 2973, 2019.
- [4] L. T. Abdisa, “Power outages, economic cost, and firm performance: Evidence from ethiopia,” *Utilities Policy*, vol. 53, pp. 111–120, 2018.
- [5] F. Carlsson, E. Demeke, P. Martinsson, and T. Tesemma, “Cost of power outages for manufacturing firms in ethiopia: A stated preference study,” *Energy Economics*, vol. 88, p. 104753, 2020.
- [6] S. R. Salkuti, “Congestion management using optimal transmission switching,” *IEEE Systems Journal*, vol. 12, no. 4, pp. 3555–3564, 2018.
- [7] N. Grass and A. Woelfel, “Optimization-algorithm addressing voltage and power quality in distributed grid control systems,” in *2017 IEEE International Telecommunications Energy Conference (INTELEC)*. IEEE, 2017, pp. 220–222.
- [8] P. CIGRE, “Guide for the selection of weather parameters for bare overhead conductor ratings,” *Technical Brochure*, vol. 299, 2006.

- [9] Z. Li and Z. Zhang, “Day-ahead and intra-day optimal scheduling of integrated energy system considering uncertainty of source & load power forecasting,” *Energies*, vol. 14, no. 9, p. 2539, 2021.
- [10] M. Numan, D. Feng, F. Abbas, S. Habib, and S. Hao, “Coordinated operation of reconfigurable networks with dynamic line rating for optimal utilization of renewable generation,” *International Journal of Electrical Power & Energy Systems*, vol. 125, p. 106473, 2021.
- [11] A. N. Akpolat, S. V. Nese, and E. Dursun, “Towards to smart grid: Dynamic line rating,” in *2018 6th International Istanbul Smart Grids and Cities Congress and Fair (ICSG)*. IEEE, 2018, pp. 96–100.
- [12] W. Bank. Enterprise survey 2015, ethiopia, 2015-2016. [Online]. Available: <https://doi.org/10.48529/xecs-m033>
- [13] V. Horban, “A multifaceted approach to smart energy city concept through using big data analytics,” in *2016 IEEE first international conference on data stream mining & processing (DSMP)*. IEEE, 2016, pp. 392–396.
- [14] W. Colglazier, “Sustainable development agenda: 2030,” *Science*, vol. 349, no. 6252, pp. 1048–1050, 2015.
- [15] I. A. Ibrahim, T. Ötvös, A. Gilmanova, E. Rocca, C. Ghanem, and M. Wanat, *International energy agency*. Kluwer Law International BV, 2021.
- [16] N. E. Benti, T. A. Woldegiyorgis, C. A. Geffe, G. S. Gurmesa, M. D. Chaka, and Y. S. Mekonnen, “Overview of geothermal resources utilization in ethiopia: Potentials, opportunities, and challenges,” *Scientific African*, p. e01562, 2023.
- [17] World bank. [Online]. Available: <https://data.worldbank.org/country/ethiopia?view=chart>
- [18] S. Benti, H. Terefe, and D. Callo-Concha, “Implications of overlooked drivers in ethiopia’s urbanization: curbing the curse of spontaneous urban

- development for future emerging towns,” *Heliyon*, vol. 8, no. 10, p. e10997, 2022.
- [19] M. O. Ozlu, A. Alemayehu, M. Mukim, S. V. Lall, O. T. Kerr, O. Kaganova, C. O. Viola, R. Hill, E. Hamilton, A. T. Bidgood *et al.*, “Ethiopia-urbanization review: urban institutions for a middle-income ethiopia,” *Washington DC: World Bank Group*, 2015.
- [20] A. C. Michalos, “Social indicators research,” *Policy Studies Journal*, vol. 6, no. 3, p. 393, 1978.
- [21] G. Mesfin, N. Dihel, and G. Zerihun, “The inescapable manufacturing–services nexus: Exploring the potential of distribution services,” *Addis Ababa: The World Bank*, 2018.
- [22] M. A. H. Mondal, E. Bryan, C. Ringler, and M. Rosegrant, “Ethiopian power sector development: Renewable based universal electricity access and export strategies,” *Renewable and Sustainable Energy Reviews*, vol. 75, pp. 11–20, 2017. [Online]. Available: <https://www.sciencedirect.com/science/article/pii/S1364032116306979>
- [23] IMF. Ethiopia: Gross domestic product (gdp) in current prices from 1988 to 2028(in billion u.s. dollars). [Online]. Available: <https://www.statista.com/statistics/455080/gross-domestic-product-gdp-in-ethiopia/>
- [24] AFDB. Ethiopia economic outlook-recent macroeconomic and financial development. [Online]. Available: <https://www.afdb.org/en/countries/east-africa/ethiopia/ethiopia-economic-outlook>
- [25] A. W. Yalaw, “The ethiopian energy sector and its implications for the sdgs and modeling,” *Renewable and Sustainable Energy Transition*, vol. 2, p. 100018, 2022.
- [26] (August 2019, Addis Ababa, Ethiopia) Energy balance 2017/18 - ministry of water, irrigation and energy ethiopia. [Online]. Available: [https://rise.esmap.org/data/files/library/ethiopia/Electricity%20Access/Ethiopia\\_Final%20Energy%20Balance%20of%202018%20final.pdf](https://rise.esmap.org/data/files/library/ethiopia/Electricity%20Access/Ethiopia_Final%20Energy%20Balance%20of%202018%20final.pdf)

- [27] D. H. Gebremeskel, E. O. Ahlgren, and G. B. Beyene, “Long-term evolution of energy and electricity demand forecasting: The case of ethiopia,” *Energy Strategy Reviews*, vol. 36, p. 100671, 2021.
- [28] EEU. Eeu profile at end of 2014 e.c fiscal year. [Online]. Available: <http://www.ethiopianelectricutility.gov.et/contents/profile>
- [29] macrotrends. Ethiopia electricity access 2000-2023. [Online]. Available: <https://www.macrotrends.net/countries/ETH/ethiopia/electricity-access-statistics>
- [30] E. consumption. Electricity consumption of private households by household size. [Online]. Available: <https://www.destatis.de/EN/Themes/Society-Environment/Environment/Material-Energy-Flows/Tables/electricity-consumption-households.html>
- [31] EEP. Ethiopian electric power. [Online]. Available: <https://www.eep.com.et/en/>
- [32] N. E. Benti, G. S. Gurmesa, T. Argaw, A. B. Aneseyee, S. Gunta, G. B. Kassahun, G. S. Aga, and A. A. Asfaw, “The current status, challenges and prospects of using biomass energy in ethiopia,” *Biotechnology for Biofuels*, vol. 14, no. 1, pp. 1–24, 2021.
- [33] G. Y. Senbato, C. Liu, and H. Wang, “Effect of geomagnetic induced current in ethiopian power grid,” *DEStech transactions on computer science and engineering (ICMSA)*, 2018.
- [34] T. H. Meles, A. Mekonnen, A. D. Beyene, S. Hassen, S. K. Pattanayak, S. Sebsibie, T. Klug, and M. Jeuland, “Households’ valuation of power outages in major cities of ethiopia: An application of stated preference methods,” *Energy Economics*, vol. 102, p. 105527, 2021.
- [35] T. H. Meles, “Impact of power outages on households in developing countries: Evidence from ethiopia,” *Energy Economics*, vol. 91, p. 104882, 2020.

- 
- [36] A. Tariku and G. Bekele, "Distribution transformer failure study and solution proposal in ethiopia," in *2020 IEEE PES/IAS PowerAfrica*. IEEE, 2020, pp. 1–5.
- [37] , *Data Collection Survey on Addis Ababa Transmission and Distribution System Final Report*. Addis Ababa: Japan International Cooperation Agency, NEWJEC Inc., 2017.
- [38] Ten year development plan a pathway to prosperity.2021-2030. [Online]. Available: [https://www.ircwash.org/sites/default/files/ten\\_year\\_development\\_plan\\_a\\_pathway\\_to\\_prosperity.2021-2030\\_version.pdf](https://www.ircwash.org/sites/default/files/ten_year_development_plan_a_pathway_to_prosperity.2021-2030_version.pdf)
- [39] V. Linga. Eia expects u.s. electricity generation from renewables to soon surpass nuclear and coal. [Online]. Available: <https://www.eia.gov/todayinenergy/detail.php?id=41533>
- [40] L. L. Delina and B. K. Sovacool, "Of temporality and plurality: an epistemic and governance agenda for accelerating just transitions for energy access and sustainable development," *Current Opinion in Environmental Sustainability*, vol. 34, pp. 1–6, 2018, sustainability Science. [Online]. Available: <https://www.sciencedirect.com/science/article/pii/S1877343517302725>
- [41] M. A. Bucher and G. Andersson, "Robust corrective control measures in power systems with dynamic line rating," *IEEE Transactions on Power Systems*, vol. 31, no. 3, pp. 2034–2043, 2015.
- [42] D. Divan and H. Johal, "Distributed facts-a new concept for realizing grid power flow control," in *2005 IEEE 36th Power Electronics Specialists Conference*. IEEE, 2005, pp. 8–14.
- [43] F. Erden, M. C. Kisacikoglu, and O. H. Gurec, "Examination of ev-grid integration using real driving and transformer loading data," in *2015 9th International Conference on Electrical and Electronics Engineering (ELECO)*. IEEE, 2015, pp. 364–368.

- [44] E. Veldman and R. A. Verzijlbergh, “Distribution grid impacts of smart electric vehicle charging from different perspectives,” *IEEE Transactions on Smart Grid*, vol. 6, no. 1, pp. 333–342, 2014.
- [45] D. Van Hertem, J. Verboomen, R. Belmans, and W. L. Kling, “Power flow controlling devices: An overview of their working principles and their application range,” in *2005 International Conference on Future Power Systems*. IEEE, 2005, pp. 6–pp.
- [46] L. Gyugyi, C. D. Schauder, and K. K. Sen, “Static synchronous series compensator: a solid-state approach to the series compensation of transmission lines,” *IEEE Transactions on power delivery*, vol. 12, no. 1, pp. 406–417, 1997.
- [47] B. Fardanesh, “Optimal utilization, sizing, and steady-state performance comparison of multiconverter vsc-based facts controllers,” *IEEE Transactions on Power Delivery*, vol. 19, no. 3, pp. 1321–1327, 2004.
- [48] S. Y. Hadush and L. Meeus, “Dso-tso cooperation issues and solutions for distribution grid congestion management,” *Energy Policy*, vol. 120, pp. 610–621, 2018.
- [49] P. Kundur, N. J. Balu, and M. G. Lauby, *Power System Stability and Control*, 7th ed. New York, NY, USA: McGraw-Hill, 1994.
- [50] P. Kundur, *Power System Stability and Control*. New York, NY, USA: The EPRI Power System Engineering Series, McGraw-Hill, 2004.
- [51] M. Anvari, G. Lohmann, M. Wächter, P. Milan, E. Lorenz, D. Heinemann, M. R. R. Tabar, and J. Peinke, “Short term fluctuations of wind and solar power systems,” *New Journal of Physics*, vol. 18, no. 6, p. 063027, jun 2016. [Online]. Available: <https://dx.doi.org/10.1088/1367-2630/18/6/063027>
- [52] J. Machowski, Z. Lubosny, J. W. Bialek, and J. R. Bumby, *Power system dynamics: stability and control*. John Wiley & Sons, 2020.

- 
- [53] L. L. Grigsby, *Power system stability and control*, 3rd ed. Boca Raton, FL, USA: CRC Press, 2012.
- [54] L. Bird, M. Milligan, and D. Lew, “Integrating variable renewable energy: Challenges and solutions,” National Renewable Energy Lab.(NREL), Golden, CO (United States), Tech. Rep., 2013.
- [55] P. Meibom, H. V. Larsen, R. Barth, H. Brand, A. Tuohy, and E. Ela, “Advanced unit commitment strategies in the united states eastern interconnection,” National Renewable Energy Lab.(NREL), Golden, CO (United States), Tech. Rep., 2011.
- [56] M. Anvari, L. R. Gorjão, M. Timme, D. Witthaut, B. Schäfer, and H. Kantz, “Stochastic properties of the frequency dynamics in real and synthetic power grids,” *Physical review research*, vol. 2, no. 1, p. 013339, 2020.
- [57] J. Kruse, B. Schäfer, and D. Witthaut, “Exploring deterministic frequency deviations with explainable ai,” in *2021 IEEE International Conference on Communications, Control, and Computing Technologies for Smart Grids (SmartGridComm)*. IEEE, 2021, pp. 133–139.
- [58] H. Bevrani and J. Raisch, “On virtual inertia application in power grid frequency control,” *Energy Procedia*, vol. 141, pp. 681–688, 2017, power and Energy Systems Engineering. [Online]. Available: <https://www.sciencedirect.com/science/article/pii/S1876610217355029>
- [59] S. Kamali and T. Amraee, “Blackout prediction in interconnected electric energy systems considering generation re-dispatch and energy curtailment,” *Applied Energy*, vol. 187, pp. 50–61, 2017. [Online]. Available: <https://www.sciencedirect.com/science/article/pii/S0306261916316257>
- [60] P. Henneaux, P.-E. Labeau, J.-C. Maun, and L. Haarla, “A two-level probabilistic risk assessment of cascading outages,” *IEEE Transactions on Power Systems*, vol. 31, no. 3, pp. 2393–2403, 2016.

- [61] W. Lu, Y. Bésanger, E. Zamaï, and D. Radu, “Blackouts: Description, analysis and classification,” in *Proceedings of the 6th WSEAS International Conference on Power Systems, Lisbon, Portugal*. WSEAS, 2006, p. 14.
- [62] N. I. Voropai and D. N. Efimov, “Analysis of blackout development mechanisms in electric power systems,” in *2008 IEEE Power and Energy Society General Meeting - Conversion and Delivery of Electrical Energy in the 21st Century*, 2008, pp. 1–7.
- [63] M. Schneider, A. Hoffrichter, and R. Puffer, “Theoretical potential of dynamic line ratings for congestion management in large-scale power systems,” in *2019 IEEE Milan PowerTech*. IEEE, 2019, pp. 1–6.
- [64] M. Gupta, V. Kumar, G. K. Banerjee, and N. Sharma, “Mitigating congestion in a power system and role of facts devices,” *Advances in Electrical Engineering*, vol. 2017, 2017.
- [65] F. Mohammadi, G.-A. Nazri, and M. Saif, “A new topology of a fast proactive hybrid dc circuit breaker for mt-hvdc grids,” *Sustainability*, vol. 11, no. 16, p. 4493, 2019.
- [66] P. Glaum and F. Hofmann, “Leveraging the existing german transmission grid with dynamic line rating,” *Applied Energy*, vol. 343, p. 121199, 2023.
- [67] F. Qiu and J. Wang, “Distributionally robust congestion management with dynamic line ratings,” *IEEE Transactions on Power Systems*, vol. 30, no. 4, pp. 2198–2199, 2014.
- [68] D. Szabó and B. Németh, “A novel methodology for critical span identification for dynamic line rating system implementation,” *Energy Reports*, vol. 7, pp. 242–249, 2021.
- [69] N. Viafora, K. Morozovska, S. H. H. Kazmi, T. Laneryd, P. Hilber, and J. Holbøll, “Day-ahead dispatch optimization with dynamic thermal rating of transformers and overhead lines,” *Electric Power Systems Research*, vol. 171, pp. 194–208, 2019.

- 
- [70] dena, “dena grid study ii — integration of renewable energy sources in the german power supply system from 2015-2020 with an outlook to 2025,,” 2010.
- [71] W. Chen, M. Alharthi, J. Zhang, and I. Khan, “The need for energy efficiency and economic prosperity in a sustainable environment,” *Gondwana Research*, 2023.
- [72] M. A. Tikuneh and G. B. Worku, “Identification of system vulnerabilities in the ethiopian electric power system,” *Global Energy Interconnection*, vol. 1, no. 3, pp. 358–365, 2018.
- [73] W. Bank. National electrification program (nep) 2.0: Integrated planning for universal access, 2019. [Online]. Available: <https://ppp.worldbank.org/public-private-partnership/library/national-electrification-program-nep-2-0-integrated-planning-universal-access-2019>
- [74] IEA, *Africa Energy Outlook - A focus on energy prospects in sub-Saharan Africa*. Paris: International Energy Agency: World Energy Outlook Special Report, 2014.
- [75] P. Collier and A. J. Venables, “Greening africa? technologies, endowments and the latecomer effect,” *Energy Economics*, vol. 34, pp. S75–S84, 2012.
- [76] B. Eifert, A. Gelb, and V. Ramachandran, “The cost of doing business in africa: Evidence from enterprise survey data,” *World development*, vol. 36, no. 9, pp. 1531–1546, 2008.
- [77] M. A. Cole, R. J. Elliott, G. Occhiali, and E. Strobl, “Power outages and firm performance in sub-saharan africa,” *Journal of Development Economics*, vol. 134, pp. 150–159, 2018.
- [78] M. O. Oseni and M. G. Pollitt, “A firm-level analysis of outage loss differentials and self-generation: Evidence from african business enterprises,” *Energy Economics*, vol. 52, pp. 277–286, 2015.

- [Online]. Available: <https://www.sciencedirect.com/science/article/pii/S0140988315003035>
- [79] X. Zeng and L. Long, "Introduction to artificial intelligence," in *Beginning Deep Learning with TensorFlow: Work with Keras, MNIST Data Sets, and Advanced Neural Networks*. Springer, 2022, pp. 1–45.
- [80] T. M. Mitchell and M. Learning, "Mcgraw-hill science," *Engineering/Math*, vol. 1, p. 27, 1997.
- [81] L. Breiman, "Random forests," *Machine learning*, vol. 45, pp. 5–32, 2001.
- [82] G. Bontempi, S. Ben Taieb, and Y.-A. Le Borgne, "Machine learning strategies for time series forecasting," *Business Intelligence: Second European Summer School, eBISS 2012, Brussels, Belgium, July 15-21, 2012, Tutorial Lectures 2*, pp. 62–77, 2013.
- [83] S. B. Taieb, A. Sorjamaa, and G. Bontempi, "Multiple-output modeling for multi-step-ahead time series forecasting," *Neurocomputing*, vol. 73, no. 10-12, pp. 1950–1957, 2010.
- [84] S. B. Taieb, R. J. Hyndman *et al.*, *Recursive and direct multi-step forecasting: the best of both worlds*. Department of Econometrics and Business Statistics, Monash Univ., 2012, vol. 19.
- [85] A. Sorjamaa, J. Hao, N. Reyhani, Y. Ji, and A. Lendasse, "Methodology for long-term prediction of time series," *Neurocomputing*, vol. 70, no. 16-18, pp. 2861–2869, 2007.
- [86] N. H. An and D. T. Anh, "Comparison of strategies for multi-step-ahead prediction of time series using neural network," in *2015 International Conference on Advanced Computing and Applications (ACOMP)*. IEEE, 2015, pp. 142–149.
- [87] D. M. Kline, "Methods for multi-step time series forecasting neural networks," in *Neural networks in business forecasting*. IGI Global, 2004, pp. 226–250.

- 
- [88] G. Bontempi, “Long term time series prediction with multi-input multi-output local learning,” *Proc. 2nd ESTSP*, pp. 145–154, 2008.
- [89] G. Bontempi and S. B. Taieb, “Conditionally dependent strategies for multiple-step-ahead prediction in local learning,” *International journal of forecasting*, vol. 27, no. 3, pp. 689–699, 2011.
- [90] H. Tong, *Threshold models in non-linear time series analysis*. Springer Science & Business Media, 2012, vol. 21.
- [91] L. C. Jain *et al.*, “Recurrent neural networks: design and applications,” Crc Press, Tech. Rep., 2000.
- [92] L. Medsker and L. C. Jain, *Recurrent neural networks: design and applications*. CRC press, 1999.
- [93] S. B. Taieb, G. Bontempi, A. Sorjamaa, and A. Lendasse, “Long-term prediction of time series by combining direct and mimo strategies,” in *2009 International Joint Conference on Neural Networks*. IEEE, 2009, pp. 3054–3061.
- [94] C. A. Micchelli and M. Pontil, “On learning vector-valued functions,” *Neural computation*, vol. 17, no. 1, pp. 177–204, 2005.
- [95] J. M. Matías, “Multi-output nonparametric regression,” in *Portuguese Conference on Artificial Intelligence*. Springer, 2005, pp. 288–292.
- [96] T. Januschowski, J. Gasthaus, Y. Wang, D. Salinas, V. Flunkert, M. Bohlke-Schneider, and L. Callot, “Criteria for classifying forecasting methods,” *International Journal of Forecasting*, vol. 36, no. 1, pp. 167–177, 2020.
- [97] S. Moritz and T. Bartz-Beielstein, “imputets: time series missing value imputation in r.” *R J.*, vol. 9, no. 1, p. 207, 2017.
- [98] L. J. Tashman, “Out-of-sample tests of forecasting accuracy: an analysis and review,” *International journal of forecasting*, vol. 16, no. 4, pp. 437–450, 2000.

- [99] F. Takens, “Detecting strange attractors in turbulence,” in *Dynamical Systems and Turbulence, Warwick 1980: proceedings of a symposium held at the University of Warwick 1979/80*. Springer, 2006, pp. 366–381.
- [100] M. B. Kennel, R. Brown, and H. D. Abarbanel, “Determining embedding dimension for phase-space reconstruction using a geometrical construction,” *Physical review A*, vol. 45, no. 6, p. 3403, 1992.
- [101] I. Aljarah, H. Faris, and S. Mirjalili, “Optimizing connection weights in neural networks using the whale optimization algorithm,” *Soft Computing*, vol. 22, pp. 1–15, 2018.
- [102] H. Wu, Y. Zhou, Q. Luo, and M. A. Basset, “Training feedforward neural networks using symbiotic organisms search algorithm,” *Computational intelligence and neuroscience*, vol. 2016, 2016.
- [103] S. Mirjalili, S. Z. M. Hashim, and H. M. Sardroudi, “Training feedforward neural networks using hybrid particle swarm optimization and gravitational search algorithm,” *Applied Mathematics and Computation*, vol. 218, no. 22, pp. 11 125–11 137, 2012.
- [104] V. K. Ojha, A. Abraham, and V. Snášel, “Metaheuristic design of feedforward neural networks: A review of two decades of research,” *Engineering Applications of Artificial Intelligence*, vol. 60, pp. 97–116, 2017.
- [105] Train/val accuracy. [Online]. Available: <https://cs231n.github.io/neural-networks-3/#accuracy>
- [106] S. Hochreiter and J. Schmidhuber, “Long short-term memory,” *Neural computation*, vol. 9, no. 8, pp. 1735–1780, 1997.
- [107] I. Sutskever, O. Vinyals, and Q. V. Le, “Sequence to sequence learning with neural networks,” *Advances in neural information processing systems*, vol. 27, 2014.

- 
- [108] S. Siami-Namini, N. Tavakoli, and A. S. Namin, “The performance of lstm and bilstm in forecasting time series,” in *2019 IEEE International Conference on Big Data (Big Data)*. IEEE, 2019, pp. 3285–3292.
- [109] K. Cho, B. Van Merriënboer, C. Gulcehre, D. Bahdanau, F. Bougares, H. Schwenk, and Y. Bengio, “Learning phrase representations using rnn encoder-decoder for statistical machine translation,” *arXiv preprint arXiv:1406.1078*, 2014.
- [110] J. Chung, C. Gulcehre, K. Cho, and Y. Bengio, “Empirical evaluation of gated recurrent neural networks on sequence modeling,” *arXiv preprint arXiv:1412.3555*, 2014.
- [111] N. Gruber and A. Jockisch, “Are gru cells more specific and lstm cells more sensitive in motive classification of text?” *Frontiers in artificial intelligence*, vol. 3, p. 40, 2020.
- [112] W. Zheng, J. Yu, and Y. Zou, “An experimental study of speech emotion recognition based on deep convolutional neural networks,” in *2015 international conference on affective computing and intelligent interaction (ACII)*. IEEE, 2015, pp. 827–831.
- [113] O. Abdeljaber, O. Avci, S. Kiranyaz, M. Gabbouj, and D. J. Inman, “Real-time vibration-based structural damage detection using one-dimensional convolutional neural networks,” *Journal of Sound and Vibration*, vol. 388, pp. 154–170, 2017.
- [114] Y. LeCun, L. Bottou, Y. Bengio, and P. Haffner, “Gradient-based learning applied to document recognition,” *Proceedings of the IEEE*, vol. 86, no. 11, pp. 2278–2324, 1998.
- [115] N. Meinshausen and G. Ridgeway, “Quantile regression forests.” *Journal of machine learning research*, vol. 7, no. 6, 2006.
- [116] T. Hastie, R. Tibshirani, J. H. Friedman, and J. H. Friedman, *The elements of statistical learning: data mining, inference, and prediction*. Springer, 2009, vol. 2.

- [117] A. Adadi and M. Berrada, “Peeking inside the black-box: a survey on explainable artificial intelligence (xai),” *IEEE access*, vol. 6, pp. 52 138–52 160, 2018.
- [118] R. Roscher, B. Bohn, M. F. Duarte, and J. Garcke, “Explainable machine learning for scientific insights and discoveries,” *Ieee Access*, vol. 8, pp. 42 200–42 216, 2020.
- [119] T. Ahmad, D. Zhang, C. Huang, H. Zhang, N. Dai, Y. Song, and H. Chen, “Artificial intelligence in sustainable energy industry: Status quo, challenges and opportunities,” *Journal of Cleaner Production*, vol. 289, p. 125834, 2021.
- [120] J. L. Cremer, I. Konstantelos, and G. Strbac, “From optimization-based machine learning to interpretable security rules for operation,” *IEEE Transactions on Power Systems*, vol. 34, no. 5, pp. 3826–3836, 2019.
- [121] A. Das and P. Rad, “Opportunities and challenges in explainable artificial intelligence (xai): A survey,” *arXiv preprint arXiv:2006.11371*, 2020.
- [122] A. B. Arrieta, N. Díaz-Rodríguez, J. Del Ser, A. Bennetot, S. Tabik, A. Barbado, S. García, S. Gil-López, D. Molina, R. Benjamins *et al.*, “Explainable artificial intelligence (xai): Concepts, taxonomies, opportunities and challenges toward responsible ai,” *Information fusion*, vol. 58, pp. 82–115, 2020.
- [123] S. M. Lundberg, G. G. Erion, and S.-I. Lee, “Consistent individualized feature attribution for tree ensembles,” *arXiv preprint arXiv:1802.03888*, 2018.
- [124] S. M. Lundberg and S.-I. Lee, “A unified approach to interpreting model predictions,” *Advances in neural information processing systems*, vol. 30, 2017.
- [125] S. M. Lundberg, G. Erion, H. Chen, A. DeGrave, J. M. Prutkin, B. Nair, R. Katz, J. Himmelfarb, N. Bansal, and S.-I. Lee, “From local explanations

- to global understanding with explainable ai for trees,” *Nature machine intelligence*, vol. 2, no. 1, pp. 56–67, 2020.
- [126] M. A. Tikuneh and G. B. Worku, “Analysis of the power blackout in the ethiopian electric power grid,” *Circuits, Systems and Signal Processing*, vol. 8, no. 2, pp. 53–65, 2019.
- [127] T. Krontiris, A. Wasserrab, and G. Balzer, “Weather-based loading of overhead lines—consideration of conductor’s heat capacity,” in *2010 Modern Electric Power Systems*. IEEE, 2010, pp. 1–8.
- [128] A. Michiorri, H.-M. Nguyen, S. Alessandrini, J. B. Bremnes, S. Dierer, E. Ferrero, B.-E. Nygaard, P. Pinson, N. Thomaidis, and S. Uski, “Forecasting for dynamic line rating,” *Renewable and sustainable energy reviews*, vol. 52, pp. 1713–1730, 2015.
- [129] L. Staszewski and W. Rebizant, “The differences between ieee and cigre heat balance concepts for line ampacity considerations,” in *2010 Modern electric power systems*. IEEE, 2010, pp. 1–4.
- [130] J. Iglesias, G. Watt, D. Douglass, V. Morgan, R. Stephen, M. Bertinat, D. Muftic, R. Puffer, D. Guery, S. Ueda *et al.*, *Guide for thermal rating calculations of overhead lines*. CIGRE, Paris, France, 2014.
- [131] T. Sterc, B. Filipovic-Grcic, B. Franc, and K. Mesic, “Methods for estimation of ohl conductor temperature based on ann and regression analysis,” *International Journal of Electrical Power & Energy Systems*, vol. 151, p. 109192, 2023.
- [132] W. Black and R. Rehberg, “Simplified model for steady state and real-time ampacity of overhead conductors,” *IEEE Transactions on Power Apparatus and Systems*, no. 10, pp. 2942–2953, 1985.
- [133] S. D. Foss and R. A. Maraiio, “Dynamic line rating in the operating environment,” *IEEE Transactions on power Delivery*, vol. 5, no. 2, pp. 1095–1105, 1990.

- [134] —, “Evaluation of an overhead line forecast rating algorithm,” *IEEE transactions on power delivery*, vol. 7, no. 3, pp. 1618–1627, 1992.
- [135] S. Jupe, M. Bartlett, and K. Jackson, “Dynamic thermal ratings: The state of the art,” in *21st Int. Conf. on Electricity Distribution*, 2011.
- [136] C. R. Black and W. A. Chisholm, “Key considerations for the selection of dynamic thermal line rating systems,” *IEEE Transactions on Power Delivery*, vol. 30, no. 5, pp. 2154–2162, 2014.
- [137] L. Ren, J. Xiuchen, and S. Gehao, “Research for dynamic increasing transmission capacity,” in *2008 International Conference on Condition Monitoring and Diagnosis*. IEEE, 2008, pp. 720–722.
- [138] J. Raniga and R. Rayudu, “Stretching transmission line capabilities—a trans-power investigation,” in *Proceeding of Annual IPENZ Conference*, 1999.
- [139] —, “Dynamic rating of transmission lines—a new zealand experience,” in *2000 IEEE Power Engineering Society Winter Meeting. Conference Proceedings (Cat. No. 00CH37077)*, vol. 4. IEEE, 2000, pp. 2403–2409.
- [140] J. Engelhardt and S. Basu, “Design, installation, and field experience with an overhead transmission dynamic line rating system,” in *Proceedings of 1996 transmission and distribution conference and exposition*. IEEE, 1996, pp. 366–370.
- [141] L. Rácz, D. Szabó, G. Göcsei, and B. Németh, “Distributed thermal monitoring of high-voltage power lines,” *Sensors*, vol. 23, no. 5, p. 2400, 2023.
- [142] Conductor monitoring - dynamic line rating. [Online]. Available: <https://microtronics.com/partnerloesungen/emo-leiterseilmonitoring-dynamic-line-rating/>
- [143] Gridpulse. [Online]. Available: <https://www.mosdorfer.com/en/produkte/line-management-otlm/>
- [144] Grid monitoring solutions. [Online]. Available: <https://www.ampacimon.com/en/>

- 
- [145] Fraunhofer. Astrose – power line monitoring. [Online]. Available: [https://www.izm.fraunhofer.de/en/abteilungen/rf---smart-sensor-systems/key\\_research\\_areas/autarkic-sensor-systems/Astrose.html](https://www.izm.fraunhofer.de/en/abteilungen/rf---smart-sensor-systems/key_research_areas/autarkic-sensor-systems/Astrose.html)
- [146] Smartline. [Online]. Available: <https://lindsey-usa.com/dynamic-line-rating/>
- [147] R. Adapa, “Increased power flow guidebook: Increasing power flow in transmission and substation circuits,” in *EPRI Technical Report*. EPRI, 2005.
- [148] M. Nick, O. A. Mousavi, R. Cherkaoui, and M. Paolone, “Integration of transmission lines dynamic thermal rating into real-time optimal dispatching of power systems,” in *2015 50th International Universities Power Engineering Conference (UPEC)*. IEEE, 2015, pp. 1–6.
- [149] C. J. Wallnerström, Y. Huang, and L. Söder, “Impact from dynamic line rating on wind power integration,” *IEEE Transactions on Smart Grid*, vol. 6, no. 1, pp. 343–350, 2014.
- [150] Y. Yaqoob, “Uncertainty analysis of transmission line with fuzzy dynamic thermal rating,” in *2021 IEEE International Future Energy Electronics Conference (IFEEC)*. IEEE, 2021, pp. 1–6.
- [151] D. L. Alvarez, F. F. da Silva, E. E. Mombello, C. L. Bak, J. A. Rosero, and D. L. Ólason, “An approach to dynamic line rating state estimation at thermal steady state using direct and indirect measurements,” *Electric Power Systems Research*, vol. 163, pp. 599–611, 2018.
- [152] A. Babs, “Weather-based and conductor state measurement methods applied for dynamic line rating forecasting,” in *2011 International Conference on Advanced Power System Automation and Protection*, vol. 1. IEEE, 2011, pp. 762–765.
- [153] E. Fernandez, I. Albizu, G. Buigues, V. Valverde, A. Etxegarai, and J. G. Olazarri, “Dynamic line rating forecasting based on numerical weather prediction,” in *2015 IEEE Eindhoven PowerTech*. IEEE, 2015, pp. 1–6.

- [154] D.-M. Kim and J.-O. Kim, "Prediction of transmission-line rating based on thermal overload probability using weather models," *European transactions on electrical power*, vol. 20, no. 4, pp. 534–544, 2010.
- [155] R. Dupin, A. Michiorri, and G. Kariniotakis, "Optimal dynamic line rating forecasts selection based on ampacity probabilistic forecasting and network operators' risk aversion," *IEEE Transactions on Power Systems*, vol. 34, no. 4, pp. 2836–2845, 2019.
- [156] M. M. Alam, H. Leite, N. Silva, and A. da Silva Carvalho, "Performance evaluation of distance protection of transmission lines connected with vsc-hvdc system using closed-loop test in rtds," *Electric Power Systems Research*, vol. 152, pp. 168–183, 2017.
- [157] G. WMO, "Guide to meteorological instruments and methods of observation," 1996.
- [158] A. Michiorri, P. Taylor, and S. Jupe, "Overhead line real-time rating estimation algorithm: description and validation," *Proceedings of the Institution of Mechanical Engineers, Part A: Journal of Power and Energy*, vol. 224, no. 3, pp. 293–304, 2010.
- [159] M. Alexiadis, P. Dokopoulos, and H. Sahsamanoglou, "Wind speed and power forecasting based on spatial correlation models," *IEEE Transactions on Energy Conversion*, vol. 14, no. 3, pp. 836–842, 1999.
- [160] D. A. Bechrakis and P. D. Sparis, "Correlation of wind speed between neighboring measuring stations," *IEEE Transactions on Energy Conversion*, vol. 19, no. 2, pp. 400–406, 2004.
- [161] S. Hsu, E. A. Meindl, and D. B. Gilhousen, "Determining the power-law wind-profile exponent under near-neutral stability conditions at sea," *Journal of Applied Meteorology and Climatology*, vol. 33, no. 6, pp. 757–765, 1994.
- [162] G. Molinar, L. T. Fan, and W. Stork, "Ampacity forecasting: an approach using quantile regression forests," in *2019 IEEE Power & Energy Society*

- 
- Innovative Smart Grid Technologies Conference (ISGT)*. IEEE, 2019, pp. 1–5.
- [163] N. Doban, “Building predictive models for dynamic line rating using data science techniques,” 2016.
- [164] K. Mekki, E. Bajic, F. Chaxel, and F. Meyer, “A comparative study of lpwan technologies for large-scale iot deployment,” *ICT express*, vol. 5, no. 1, pp. 1–7, 2019.
- [165] B. S. Chaudhari and M. Zennaro, *LPWAN Technologies for IoT and M2M Applications*. Academic Press, 2020.
- [166] Semtech. Sx1272/3/6/7/8: Lora modem designer’s guide. [Online]. Available: [https://www.openhacks.com/uploadsproductos/loradesignguide\\_std.pdf](https://www.openhacks.com/uploadsproductos/loradesignguide_std.pdf)
- [167] A. Augustin, J. Yi, T. Clausen, and W. M. Townsley, “A study of lora: Long range & low power networks for the internet of things,” *Sensors*, vol. 16, no. 9, p. 1466, 2016.
- [168] L. Alliance, “Lora alliance technical committee regional parameters workgroup,” 2018.
- [169] J. Kim, J. Song *et al.*, “A dual key-based activation scheme for secure lorawan,” *Wireless Communications and Mobile Computing*, vol. 2017, 2017.
- [170] A. Berni and W. Gregg, “On the utility of chirp modulation for digital signaling,” *IEEE Transactions on Communications*, vol. 21, no. 6, pp. 748–751, 1973.
- [171] T. Attia, M. Heusse, B. Tourancheau, and A. Duda, “Experimental characterization of lorawan link quality,” in *2019 IEEE Global Communications Conference (GLOBECOM)*. IEEE, 2019, pp. 1–6.
- [172] L. Vangelista, A. Zanella, and M. Zorzi, “Long-range iot technologies: The dawn of lora™,” in *Future Access Enablers for Ubiquitous and Intelligent*

- Infrastructures: First International Conference, FABULOUS 2015, Ohrid, Republic of Macedonia, September 23-25, 2015. Revised Selected Papers 1.* Springer, 2015, pp. 51–58.
- [173] Semtech corporation. an1200.22: Lora modulation basics. 2015. [Online]. Available: <https://www.frugalprototype.com/wp-content/uploads/2016/08/an1200.22.pdf>
- [174] K. Hung, W. Lee, V. Li, K. Lui, P. Pong, K. Wong, G. Yang, and J. Zhong, “On wireless sensors communication for overhead transmission line monitoring in power delivery systems,” in *2010 First IEEE International Conference on Smart Grid Communications*. IEEE, 2010, pp. 309–314.
- [175] K. Mazur, M. Wydra, and B. Ksiezopolski, “Secure and time-aware communication of wireless sensors monitoring overhead transmission lines,” *Sensors*, vol. 17, no. 7, p. 1610, 2017.
- [176] T. Brito, M. Zorawski, J. Mendes, B. F. Azevedo, A. I. Pereira, J. Lima, and P. Costa, “Optimizing data transmission in a wireless sensor network based on lorawan protocol,” in *Optimization, Learning Algorithms and Applications: First International Conference, OL2A 2021, Bragança, Portugal, July 19–21, 2021, Revised Selected Papers 1.* Springer, 2021, pp. 281–293.
- [177] U. Raza, P. Kulkarni, and M. Sooriyabandara, “Low power wide area networks: An overview,” *ieee communications surveys & tutorials*, vol. 19, no. 2, pp. 855–873, 2017.
- [178] M. Magno, F. A. Aoudia, M. Gautier, O. Berder, and L. Benini, “Wulora: An energy efficient iot end-node for energy harvesting and heterogeneous communication,” in *Design, Automation & Test in Europe Conference & Exhibition (DATE), 2017*. IEEE, 2017, pp. 1528–1533.
- [179] L. Li and J. Y. Halpern, “Minimum-energy mobile wireless networks revisited,” in *ICC 2001. IEEE International Conference on Communications*.

- 
- Conference Record (Cat. No. 01CH37240)*, vol. 1. IEEE, 2001, pp. 278–283.
- [180] M. H. Anisi, A. H. Abdullah, S. A. Razak, and M. A. Ngadi, “An overview of data routing approaches for wireless sensor networks,” *Sensors*, vol. 12, no. 4, pp. 3964–3996, 2012.
- [181] D. Bhattacharyya, T.-h. Kim, and S. Pal, “A comparative study of wireless sensor networks and their routing protocols,” *sensors*, vol. 10, no. 12, pp. 10 506–10 523, 2010.
- [182] E. Ancillotti, R. Bruno, and M. Conti, “Reliable data delivery with the ietf routing protocol for low-power and lossy networks,” *IEEE Transactions on Industrial Informatics*, vol. 10, no. 3, pp. 1864–1877, 2014.
- [183] P. Thubert and M. Richardson, “Routing for RPL (Routing Protocol for Low-Power and Lossy Networks) Leaves,” RFC 9010, Apr. 2021. [Online]. Available: <https://www.rfc-editor.org/info/rfc9010>
- [184] T. Tsvetkov, “Rpl: Ipv6 routing protocol for low power and lossy networks,” *Sensor nodes—operation, network and application (SN)*, vol. 59, no. 2, 2011.
- [185] entsoe. Dynamic line rating (dlr). [Online]. Available: <https://www.entsoe.eu/Technopedia/techsheets/dynamic-line-rating-dlr>
- [186] European telecommunications standards institute. short range devices (srd) operating in the frequency range 25 mhz to 1 000 mhz: Part 1: Technical characteristics and. 2017-02. [Online]. Available: [https://www.etsi.org/deliver/etsi\\_en/300200\\_300299/30022001/03.01.01\\_60/en\\_30022001v030101p.pdf](https://www.etsi.org/deliver/etsi_en/300200_300299/30022001/03.01.01_60/en_30022001v030101p.pdf)
- [187] European telecommunications standards institute. short range devices (srd) operating in the frequency range 25 mhz to 1 000 mhz: Part 2: Harmonised standard for access to radio spectrum. 2018-06. [Online]. Available: [https://www.etsi.org/deliver/etsi\\_en/300200\\_300299/30022002/03.02.01\\_60/en\\_30022002v030201p.pdf](https://www.etsi.org/deliver/etsi_en/300200_300299/30022002/03.02.01_60/en_30022002v030201p.pdf)

- [188] Heltec automation. wifi lora 32 (v2). ed. by heltec automation. [Online]. Available: <https://heltec.org/project/wifi-lora-32/>
- [189] Rak wireless. rak811 wisduo lpwan module datasheet. ed. by rak wireless. [Online]. Available: <https://dl-docs.rakwireless.com/api/render/?emulateScreenMedia=false&pdf.format=legal&url=https%3A%2F%2Fdocs.rakwireless.com%2FProduct-Categories%2FWisDuo%2FRAK811-Module%2FDatasheet%2F>
- [190] (May 7, 2020) Semtech corporation. sx1276/77/78/79: Sx1276/77/78/79 - 137 mhz to 1020 mhz low power long range transceiver.

# List of Publications

## Journal articles

- [191] D. B. Gemedá, M. Lehner, and W. Stork, “Design and evaluation of condition monitoring of distribution transformers for developing countries,” *Mathematical Statistician and Engineering Applications*, vol. 71, no. 3s2, pp. 1939–1950, 2022.

## Conference contributions

- [192] D. B. Gemedá and W. Stork, “Probabilistic ampacity forecasting of dynamic line rating considering tsos risk-averse,” in *2022 6th International Conference on Green Energy and Applications (ICGEA)*. IEEE, 2022, pp. 176–181.
- [193] D. B. Gemedá, M. Lehner, P. Rauh, and W. Stork, “Lora mesh network for overhead transmission line monitoring,” in *2022 International Conference on Information and Communication Technology for Development for Africa (ICT4DA)*. IEEE, 2022, pp. 121–126.